A STUDY ON BOILING HEAT TRANSFER OF NON-METALLIC NANOPARTICLES IN WATER-BASED NANOFLUID POOL BOILING

Muhamad Zuhairi Bin Sulaiman

A thesis submitted in partial fulfillment
of the requirements for the degree of
Doctor of Philosophy (Mechanical Engineering)

To the

Department of Mechanical Engineering and Intelligent Systems
Graduate School of Informatics and Engineering
The University of Electro–Communications
Tokyo, Japan

June 2018

A STUDY ON BOILING HEAT TRANSFER OF NON-METALLIC NANOPARTICLES IN WATER-BASED NANOFLUID POOL BOILING

A thesis submitted in partial fulfillment
of the requirements for the degree of
Doctor of Philosophy (Mechanical Engineering)

Approved by:

Chair of Committee: Professor Tomio Okawa, Advisor
Department of Mechanical and Intelligent Systems
Graduate School of Informatics and Engineering
The University of Electro–Communications

Committee Members: Professor Hiroshi Maekawa
Professor Miyazaki Takeshi
Professor Kazuto Masamoto
Associate Professor Hans-Georg Matuttis

Dedication

To my kind parents

and

To my patient spouse
who have encouraged and inspired me during this project

非金属粒子を縣濁させた水ベースナノ流体のプール沸騰熱伝達に関する研究

ムハマド　ズハイリ　ビン　スライマン

概要

非金属ナノ粒子を縣濁させた水ベースのナノ流体中における沸騰伝熱特性を系統的に調べた。3 種類の実験装置を用いて、伝熱面姿勢、ナノ粒子材料、ナノ粒子濃度、ナノ粒子分散状態、ナノ粒子層形成時の熱流束の影響を検討した。伝熱面姿勢としては、上向き面と下向き面で実験を実施し、限界熱流束(CHF)の絶対値は伝熱面姿勢によって異なるが、いずれの条件においてもナノ流体中の CHF は純水中の値の約 2 倍となることを示した。次に、ナノ流体中の沸騰熱伝達率は、ナノ粒子の材質および濃度により大きく異なり得ることを示した。ナノ粒子の材質として、本研究では TiO_2、Al_2O_3、SiO_2 を使用したが、Al_2O_3 では伝熱促進、SiO_2 では伝熱劣化が生じるのに対して、TiO_2 では低粒子濃度で劣化、高粒子濃度で向上する結果となった。一方、ナノ流体中における粒子の分散状況は、本実験で調べた範囲内において、沸騰熱伝達に及ぼす影響は顕著ではなかった。また、各実験条件で沸騰曲線を描いたところ、Al_2O_3 ナノ流体では水の場合と類似の沸騰曲線が得られたのに対して、TiO_2 と SiO_2 では、高熱流束条件で壁面過熱度が大きく増加するという独特の振る舞いを呈する場合があった。ただし、計測された CHF 値は 1.7～2.1MW/m^2 の範囲にあり、純水中の CHF よりも顕著に増大するものの、ナノ粒子の材質、濃度、分散状態による明確な影響は認められなかった。これに対して、伝熱面上にナノ粒子層を形成する際の熱流束は、CHF 値に多大な影響を及ぼした。すなわち、高熱流束条件では、ナノ粒子層を形成する際の沸騰時間が短くても顕著な CHF 増大を実現できるのに対して、低熱流束条件では十分な CHF 向上を達成する伝熱面状態とするのにきわめて長いナノ粒子層形成時間を要した。特に、本研究で用いた最低熱流束条件では、ナノ流体中で沸騰状態を 1 時間継続した場合でも、十分な CHF 向上効果を発現するには至らなかった。本研究では、純水中にナノ粒子を添加した後の熱伝達率の時間変化を様々な条件で調べたが、ナノ粒子の添加直後では、熱伝達率が向上する場合が多かった。そこで、ナノ流体中における熱伝達率変化のメカニズムについて知見を得るため、透明容器を用いた可視化実験を実施して、ナノ粒子天下の前後における沸騰気泡の生成状況の差異を検討した。この結果、ナノ粒子を加えた直後、より多数の発泡核で気泡生成が生じることが観察された。これより、伝熱面上にナノ粒子層が形成される際に、そのいくつかの部分が気泡生成核となり、核沸騰熱伝達の促進に寄与することを示した。

A STUDY ON BOILING HEAT TRANSFER OF NON-METALLIC NANOPARTICLES IN WATER-BASED NANOFLUID POOL BOILING

Muhamad Zuhairi Bin Sulaiman

ABSTRACT

Heat transfer characteristics in boiling systems are significantly important, especially in high-density cooling, for instance, the application of In-Vessel Retention (IVR) during the Loss of Coolant Accident (LOCA) in a Nuclear Reactor. In the present study, the performance of nanofluids in a boiling system, namely, non-metallic water-based nanofluids has been explored. The parametric effects of the nanofluids in nucleate pool boiling with various configurations have been tested. Three main experimental setups were prepared separately to investigate the effect of heater orientations: material, concentration, and dispersion as well as heat flux density, respectively. Additional research was performed by using a separate experimental apparatus in order to elucidate a possible nucleate boiling mechanism occurring in nanofluids.

Conclusively, the Critical Heat Flux (CHF) was improved significantly in the nanofluid nucleate boiling, compared to pure water. The orientation effects showed similar magnitudes of enhancement, up to 200 percent in both upward-facing and downward-facing heaters. Several parameters related to the CHF enhancement rate, such as concentration and boiling time in nanofluids, were simultaneously investigated. The CHF enhancement rates are considerably high in a higher concentration of TiO_2 nanofluid and vice versa. In addition, the CHF enhancement for the downward-facing heater orientation is only half of that for the upward-ward facing heater. Surface wettability measurements were also being conducted to explore the relationship between surface properties and the CHF enhancement.

Separately, the effects of nanoparticle materials, concentrations and dispersion conditions on the heat transfer coefficient and CHF were elucidated. The boiling heat transfer characteristics observed were significantly different depending on the nanoparticles' material as well as on the difference in the concentration. The higher concentration of TiO_2 and Al_2O_3 showed higher heat transfer enhancements (except for the low concentration of TiO_2), whereas for SiO_2 the heat transfer deteriorated for all concentrations in the time-variation of wall superheat. However, no noticeable effects of

the dispersion condition was observed. Some peculiar boiling curves (BCs) were observed in TiO_2 and SiO_2 at the high heat flux compared to the simple BCs in Al_2O_3. The CHF enhancement was found to be within the range of 1.7 up to 2.1 MW/m^2 for all materials.

The effects of different heat flux density on the CHF enhancements were also investigated. The enhancement rate of CHF greatly depended on the heat flux density; the heat flux at the higher densities had shown considerably higher CHF enhancements rate to compare to lower heat flux density. The CHF enhancement still did not reach the asymptotic CHF value after boiling for 1 hour at the lowest heat flux in the present experimental investigation. Both the dimensionless CHF enhancement value respective to the dimensionless heat flux, concentration and boiling time were correlated. The trend showed a linearity in the high heat flux, especially for 450 and 600 kW/m^2. Nevertheless, for lower heat flux, non-linear trends were observed especially at heat flux densities of 300 kW/m^2 and more obvious at 150 kW/m^2.

In conclusion, nanofluids showed an enhanced CHF both for upward-facing and downward-facing conditions. However, the heat transfer characteristic (HTC) performances was stochastic depending on materials and concentration of nanofluids, and nearly no noticeable dispersion condition was observed. The heat flux density affected the rate of CHF enhancements, where the high heat flux resulted in high enhancement rates, but nominal enhancements in the lowest heat flux.

Acknowledgements

I would like to express my sincere acknowledgments to my supervisor, Professor Tomio Okawa at The University of Electro-Communications for his consistent direction, advisement and encouragement in this study. His open and broad-minded view impressed me greatly and will benefit me all my life. Thank you to Dr. Enoki Koji for assisting my study, motivation and support. Special appreciation to Associate Professor Hans-Georg Matuttis for his insightful comments and suggestions that allowed me to greatly improve the quality of the thesis.

I am also grateful to all members of my dissertation committee for their feedback and valuable comments.

I am thankful to Malaysian Government, which granted me with the financial aid for the study. I owe too much to my wife (Siti Rohaya Nordin), my children (Aimuni, Ahmad Muizzuddin, Ahmad Azimuddin, Azzahra and Ahmad Arhamuddin) and my parents who give me support, confidence and power to complete the study.

Finally, I want to express my affect and thanks to many friends and fellow students who helped and encouraged me (without being able to list all their names here).

List of Tables

List of Figures

Variable Nomenclature

k	thermal conductivity [W m^{-1} K^{-1}]
g	gravity [m s^{-2}]
d_b	bubble departure diameter [m]
T_{SAT}	saturation temperature [K]
a_l	thermal diffusivity [m^2 s^{-1}]
c_{pl}	heat capacity of the liquid [kJ kg^{-1} K^{-1}]
C_{sf}	surface factor constant in Rohsenow correlation
s	surface factor constant in Rohsenow correlation
h_{fg}	latent heat of vaporization [J kg^{-1}]
Pr	Prandtl number
q_W	heat flux [W m^{-2}]
q_{CHF}	critical heat flux [W m^{-2}]
R_q	root mean square of the heater surface [μm]
ΔT_W	wall superheat [K]
C	nanoparticle concentration [kg m^{-3}]
t_b	boiling time of nucleate boiling [minutes]
t_{us}	excitation time in the ultrasonic bath [hour]
d_{sm}	Sauter mean diameter [m]
d_p	primary particle diameter [m]
d_{agg}	aggregation diameter [m]
T_1	copper block temperature at 5 mm below the heated surface [K]
Q	heater power [W]
q_c^*	dimensionless CHF enhancement
q_c	critical heat flux of coated heater surface [W m^{-2}]
q_{c0}	critical heat flux of uncoated heater surface [W m^{-2}]
$q_{C,asy}$	asymptotic CHF value [W m^{-2}]
q_W^*	dimensionless applied heat flux density
q_{hf}	heat flux density applied during surface preparation [W m^{-2}]

q_{max}	maximum heat flux density applied during surface preparation [W m^{-2}]
ΔT_{BW}	bottom wall superheat temperature of the glass heater [K].

Greek letters

α	heat transfer coefficient [W m^{-2} K^{-1}]
ρ_l	density of liquid [kg m^{-3}]
ρ_v	density of vapor [kg m^{-3}]
σ	surface tension [N m^{-1}]
β_o	contact angle of the vapor bubbles [degrees]
μ	dynamic viscosity [Pa s]
β_r	receding contact angle [degrees]
ϕ	heater surface angle with horizontal [degrees]
θ	static contact angle [degrees].

Subscripts

hf	heat flux
max	maximum
c	critical
asy	asymptotic
o	pure water
SAT	saturation
W	wall
l	liquid
v	vapor
g	gas
s	surface
CHF	critical heat flux.

Abbreviations

NPP	nuclear power plant
CHF	critical heat flux
BHT	boiling heat transfer
HTC	heat transfer coefficient
LOCA	loss of coolant accident
ESBWR	economic simplified boiling water reactor
PCS	passive cooling systems
PCCS	passive containment cooling system
GDCS	gravity driven cooling system
RPV	reactor pressure vessel
IC	isolation condenser
ICS	isolation condenser system
ONB	onset of nucleate boiling
DNB	departure of nucleate boiling
IVR	in-vessel retention
LWR	light water reactor
TEM	transmission electron microscope
BC	boiling curve
DC	Direct current
ITO	indium tin oxide
DLS	dynamic light scattering.

CHAPTER 1 INTRODUCTION

1.1 Background

Nucleate boiling is known as a superior mode of heat transfer due to the latent heat transport during the phase-change. To date, when the advancement of modern technologies demands high heat flux removal, this mode of heat transfer has been widely integrated into a variety of engineering applications. Examples are high-density micro-electronics cooling systems, heat exchanger system, as well as the emergency cooling systems in nuclear power plants (NPPs).

Although extensive research has been performed on boiling heat transfer, the understanding of the responsible mechanisms involved in nucleate boiling is still in its infancy due to its non-equilibrium character. Therefore, researchers adopted semi-empirical correlations based on experimental data and used such correlations to simplify the calculation of the complex variables in nucleate boiling, especially during the design of applications. This approach has been reasonably successful. Also, the heat transfer characteristics of boiling systems became even more complicated to deal with the integration of nano-meter sized particles.

The nano-meter sized particles dispersed in the base-fluid called nanofluid have been conceived by Choi et al. [1]. This new type base-fluid has been extensively researched and had been proven to have superior thermo-physical properties. For instance, the thermal conductivity was increased significantly without significant changes in the physical properties. These features have attracted researchers to integrate the nanofluids in both pool and flow boiling systems. Since the integration, some plausible critical heat flux (CHF) enhancement has been found despite some inconsistencies, which had been reported concerning the boiling heat transfer characteristic.

Nucleate boiling studies concerning nanofluids have dramatically evolved within a decade since the introduction of nanofluids. In 2003, You et al. [2] performed the pioneering work to integrate Al_2O_3 nanofluids into the boiling system. They reported significant improvements on the CHF. A separate study conducted in the same year by

Das et al. [3] on the boiling heat transfer (BHT) reported that the heat transfer coefficient (HTC) deteriorated. Since then, an increasing number of publications have appeared in this field.

In nucleate boiling with nanofluids, investigators have focused predominantly on two parameters the HTC and the CHF. Both parameters are exceedingly significant and represent the performance of the integration of nanofluids into the boiling system. Information on HTC and CHF are valuable in designing applications that make use of nanofluid boiling.

1.2 Motivation

High-performance cooling systems are in high demand, especially in cooling for nuclear reactors. In particular, improvements in the safety margins are desirable to avoid a hypothetical severe accident. In the situation of a loss of coolant accident (LOCA) in a nuclear reactor, Buongiorno et al. [4] initially suggested to anticipate the insertion of the nanofluid into the in-vessel retention (IVR) to enhance the CHF in order increase the safety margin, which could avoid the subsequent fatal accident.

Nanofluids can be assimilated into a vast spectrum of applications. For instance, in recent design of NPPs called economic simplified boiling water reactor (ESBWR), the nanofluid can be integrated into the passive coolant systems (PCSs) in either the isolation condenser system (ICS) or the passive containment cooling system (PCCS) or in both.

In the ESBWR design, the cooling systems by passive method is extensively integrated and equipped with multiple safety management strategies to avoid a loss of coolant accidents (LOCAs) and to mitigate further damage to the system. The systems configuration are shown in the schematics in Fig. 1.1.

During the moderate LOCA, passive safety features in ESBWR is activated to allow the steam flows to the ICS inside the water pool above the containment and remove the heat. The ICSs are designed to continuously operate for 72 hours. During the process, the heat transferred from the steam in ICSs pool by the convection mode especially via nucleate boiling as shown in Fig. 1.2(a). Here by integrating with suitable nanofluids as a base coolant, the heat dissipation could significantly improve.

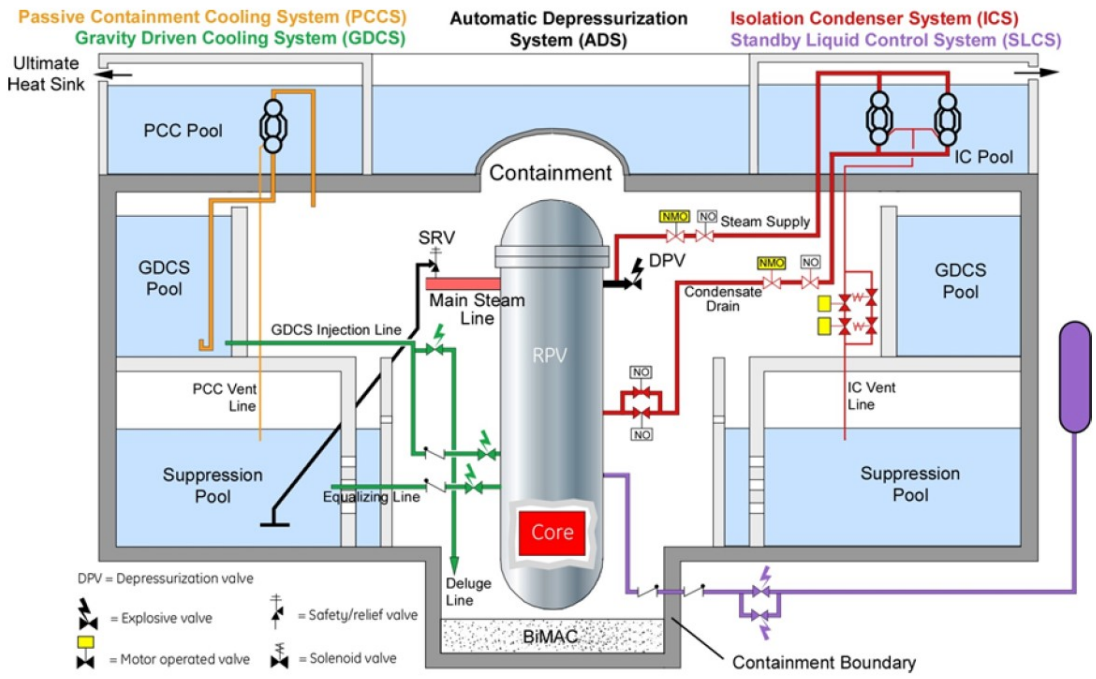

Fig. 1.1: Safety system configuration of an ESBWR [5]

However in the case of severe LOCA, another passive safety system (PCS) named as a passive containment cooling system (PCCS) together with a gravity driven cooling system (GDCS) could be initiated. In this safety management, the reactor pressure vessel (RPV) will be flooded to cool down the RPV temperature especially during the hypothetical large break in LOCA cases and the conditions is shown in Fig. 1(b). In this case, the lower surface of RPV surface is in the downward facing orientation and it is experiencing the lowest possible heat that could be transferred (known as CHF) compared to the other surface. Here, increasing the CHF at this region could significantly improve the safety margin. In parallel to that, the nanofluid has been proven to improve the CHF in many cases and the integration of this base liquid could increase higher safety margin especially during severe LOCA.

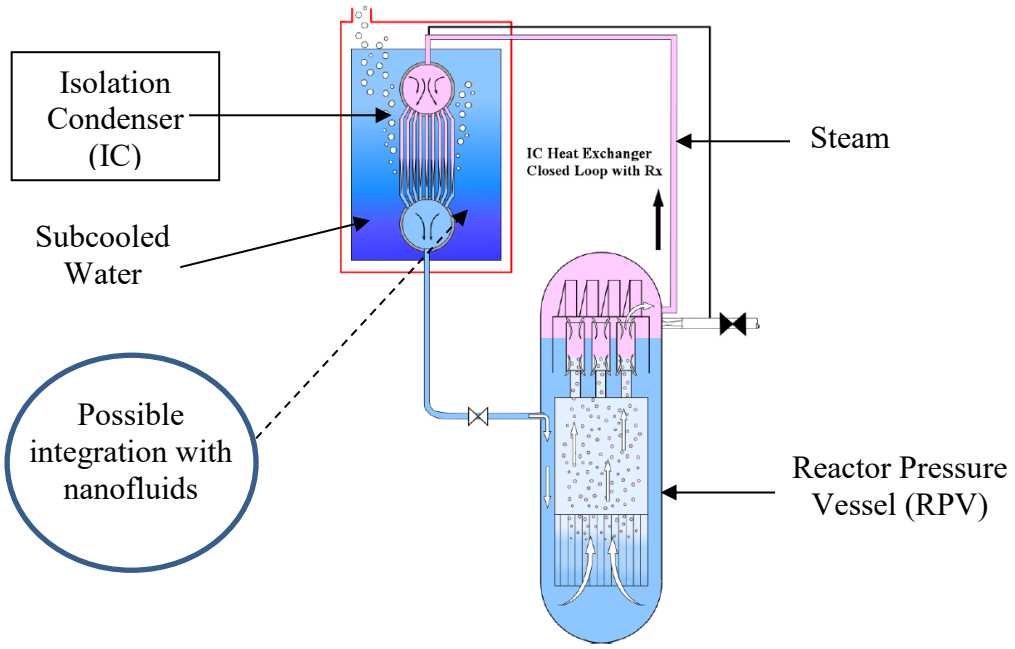

(a) Isolation condenser system (ICS)

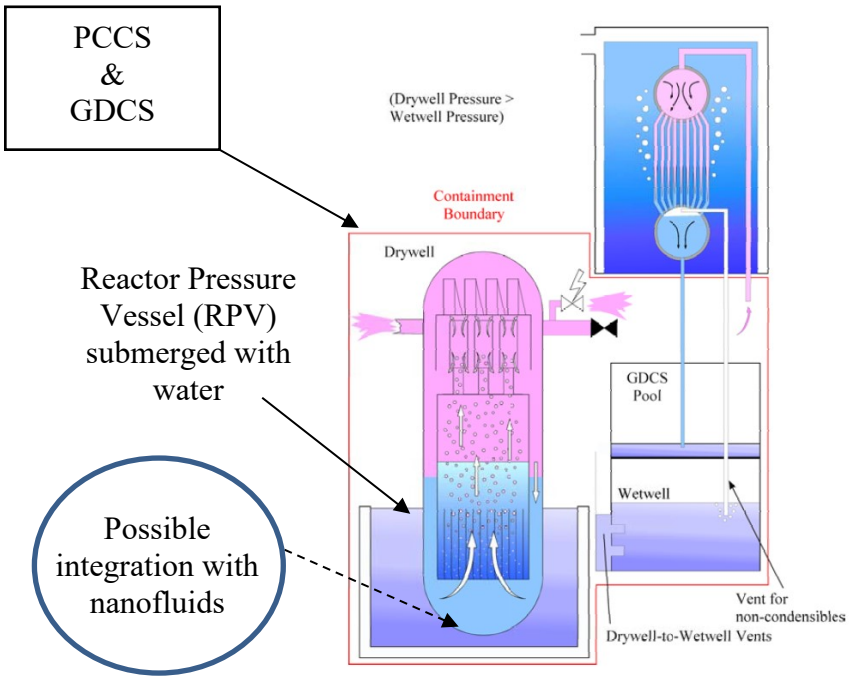

(b) Passive containment cooling systems (PCCS) and Gravity Driven Cooling System (GDCS)

Figs. 1.2: Passive cooling systems in ESBWR [5]

1.3 Technical objective

Given the lack of information concerning the boiling heat transfer in nanofluids, namely the HTC and CHF, the present study is designed to explore the performance of nucleate boiling in water-based nanofluids. The exploratory work is conducted to elucidate the parameters which influence the boiling performance. The objectives of the research are presented next.

The first objective is to explicate the effect of nanofluids under different heater orientations. This objective aims to identify the effect of heater orientation (upward-facing of down-ward facing) concerning the CHF performance. These experimental findings are be hugely beneficial during the flooding of the outer surface of the reactor pressure vessel (RPV) and the activation of PCCS in ESBWR.

Bearing in mind the inconsistency of the HTC and CHF characteristics reported by many investigators, the second objective is to explore the effect of nanoparticle-materials, concentrations and dispersion conditions of nanofluids. The study is expected to be useful and crucial for nanoparticle selection for optimum HTC and CHF performance.

The third objective is directed towards investigating the heat flux effects on the CHF enhancement at a different deposition rate of nanoparticles. Where, for the case of a hypothetical accident, the effects of the heat flux on the CHF enhancement is significant as the rate of CHF enhancement determines the time frame that is available for maximum enhancement during the activation of PCCS.

Finally, from the observed HTC reduction in the most with the addition of nanofluids in a small heater, further investigations are performed with a larger and transparent heater to explore the possible mechanism of the BHT.

1.4 Thesis outline

This paper consists of eight chapters, and the content of each chapter is as follows: Chapter 2 discusses the fundamental theorem on the nucleate boiling heat transfer and assessment on the available and reported literature of nanofluids.

Chapter 3 explains the experimental methodology and the nanoparticle characterizations in the present experiment.

Chapter 4 demonstrates and discusses the experimental work on the effect of heater orientation on the CHF namely, upward- and downward-facing copper heaters. Further, CHF enhancement in the downward-facing and upward-facing heaters, as well as the relation with nanofluid concentration and boiling time are discussed.

Chapter 5 includes a detailed discussion of the parametric investigations of the effects of nanoparticle-materials, concentrations, and dispersion conditions of nanofluids. The influence of those parameters on the HTC performance is reported, which also reveals some peculiarities in the boiling curve.

Chapter 6 explains the effects of different heat flux density on the CHF enhancement, from low to high heat flux, when the heated surface is prepared with a defined concentration. The time variation of wall superheat, and the surface wettability are also investigated. The boiling curves at the particular boiling time and heat flux are discussed as well.

Chapter 7 demonstrates the possible mechanism when the nanofluid is added to the boiling system. Given the findings concerning the HTC enhancement in several cases studied, the visualization was performed using a larger and transparent glass heater in the separate test vessel. The findings are reported and discussed in detail.

Finally, in Chapter 8 the conclusions obtained in this dissertation are summarized.

CHAPTER 2 LITERATURE REVIEW

2.1 Nucleate boiling heat transfer

2.1.1 Boiling curves

Nukiyama [6] was the first to introduce boiling curves for nucleate boiling in 1934, followed by several well known works by Bergles [7], Rohsenow et al. [8] Kutateladze [9], Katto [10], Berenson [11], Kandlikar [12] and Dhir [13]. The three boiling regimes in the curve classify nucleate boiling, transition boiling and film boiling. These classifications are based on the bubble condition, representing the mode and intensity of the heat transfer. Among these boiling regimes, the nucleate boiling regime exhibits the highest heat transfer rate.

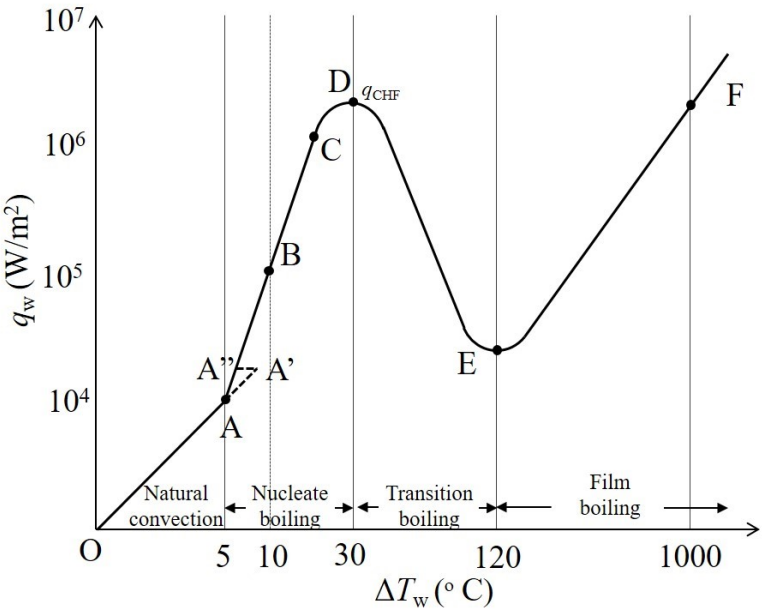

Fig. 2.1: Pool boiling curve for water at atmospheric pressure

Fig. 2.1 depicts the boiling curve relation between the heat flux, q_W and the wall superheat, ΔT_{SAT}. The boiling curve consists of several regions differentiated by the

bubble conditions. In the boiling curve, the region indicated by O to A is classified as natural convection, where no boiling occurs. The next region is the nucleate boiling region, which ranges from A to D. In this region, the curve from A to A' indicates that the bubble nucleation was initiated at the vicinity of the surface, which known as the onset of nucleate boiling (ONB). At later stage, from A' to A", bubbles were nucleated and the wall superheat later reduced but maintained at the similar heat flux. This region is called the inception of boiling region. In the region from A" to C, the bubble nucleation grows and departs more rapidly as the heat flux increases. As the applied heat flux increases, more nucleation sites will be activated, and the bubble behavior deviates from weak boiling until vigorous boiling conditions. The bubbling bubbles in this region differ depending on the heat flux intensities, i.e., discrete bubbles, vapor columns and mushrooms types. Later, in the region C to D, the intense evaporation underneath the vigorous bubble leads to periodic dry patches at the vicinity of the heater surface due to the reduction in the fluid rewetting process by the surrounding fluid. Consequently, the heat transfers stemming from the latent heat transfer start to decrease. The nucleate boiling at the highest heat flux intensity (point D) is referred to as critical heat flux (CHF). At a later stage, the liquid rewetting onto the heater surface decreases, leading to the formation of dry patches covering the heater surface region called transition boiling. At this point, insufficient liquid is supplied to cool the surface and to reduce the heat flux. These eventually decrease the heat flux and increase the wall temperature up to point E, where the heat flux reached a minimum called the Leindfrost point. At this stage, the surface is entirely covered with a tiny vapor blanket. As the heat flux is further increased, the temperature reaches point F, the film boiling region. Through experimental investigation, Nukiyama (1934) observed that the high temperature following the CHF point leads to physical burnout of nichrome wires, while platinum wires were able to withstand the higher temperatures.

2.1.2 Heat transfer coefficient (HTC)

The heat transfer coefficient α represents the heat transfer performance in nucleate boiling. It is modeled from Newton's law of cooling

$$q_{\mathrm{W}} = \alpha \left(T_{\mathrm{W}} - T_{\mathrm{SAT}} \right) \tag{2.1}$$

where q_{W} is the heat flux, α is the HTC, T_{W} is the wall temperature (usually the heat wall temperature) and T_{SAT} is the bulk liquid.

2.1.3 Correlations on boiling heat transfer

The complexity of nucleate boiling heat transfer had led many researchers to develop semi-empirical correlation equations. Most of the correlations were based on experimental results from pure liquids and were only capable of predicting the performance of boiling heat transfer for most of the pure substances. The most well-known correlations are summarized in the following.

Stephen-Abdelsalam correlation

The Stephan and Abdelsalam correlation [14] is used to estimate the ideal heat transfer coefficient in various types of pure fluid. The correlation is as follows:

$$\alpha = 0.23 \frac{k_{\mathrm{l}}}{d_{\mathrm{b}}} \left(\frac{q_{\mathrm{W}} d_{\mathrm{b}}}{k_l T_{\mathrm{SAT}}} \right)^{0.674} \left(\frac{\rho_{\mathrm{v}}}{\rho_{\mathrm{l}}} \right)^{0.297} \left(\frac{h_{\mathrm{fg}} {d_{\mathrm{b}}}^2}{a_{\mathrm{l}}^2} \right)^{0.371} \left(\frac{a_{\mathrm{l}}^2 \rho_{\mathrm{l}}}{\sigma d_{\mathrm{b}}} \right)^{0.35} \left(\frac{\left(\rho_{\mathrm{l}} - \rho_{\mathrm{v}} \right)}{\rho_{\mathrm{l}}} \right)^{-1.73} \tag{2.2}$$

where k_{l} is the thermal conductivity of the liquid, d_{b} is the bubble departure diameter T_{SAT} is the saturation temperature a_{l} is the thermal diffusivity and α is the heat transfer coefficient.

The departure bubble diameter d_{b} is given by

$$d_{\mathrm{b}} = 0.851 \beta_0 \sqrt{\frac{2\sigma}{g\left(\rho_{\mathrm{l}} - \rho_v \right)}}, \tag{2.3}$$

where β_{o} is the contact angle of the vapor bubbles. For water, $\beta_{\mathrm{o}} = 45°$ was used and the mean absolute mean error was within 11.3 percent.

The boiling curve drawn from Stephen-Abdelsalam (S-A) in Fig. 2.2 is widely used to estimate the value of wall superheat versus heat flux in the nucleate boiling region for various fluids.

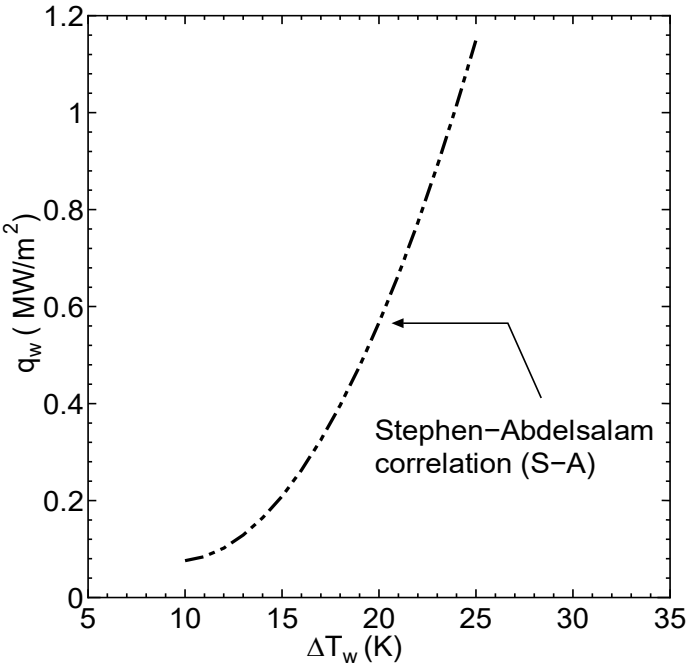

Fig. 2.2: Boiling curve drawn from Stephen-Abdelsalam correlation for water

Rohsenow correlation

Boiling is evaporation process associated with the development of vapor bubbles in the liquid. Based on the postulate that the nucleate boiling heat flux is associated with the pumping and removing the bubbles from the heated surface, Rohsenow et al. [15] obtained a correlation of nucleate pool boiling in the form

$$q_{\mathrm{W}} = \mu_{\mathrm{l}} h_{\mathrm{fg}} \left[\frac{g\left(\rho_{\mathrm{l}} - \rho_{v}\right)}{\sigma} \right]^{0.5} \left(\frac{C_{\mathrm{pl}} \Delta T_{\mathrm{W}}}{C_{\mathrm{sf}} h_{\mathrm{fg}} \, \mathrm{Pr}_{\mathrm{l}}^{\mathrm{s}}} \right)^{3}, \tag{2.4}$$

where h_{fg} is the latent heat of vaporization of the fluid, σ is the surface tension, ρ_{l} and ρ_{g} are the liquid and vapor densities respectively, g is the gravitational acceleration, and Pr_{l} is the Prandtl number defined as $\mu c_{\mathrm{pl}}/k_{\mathrm{l}}$ in which k_{l}, μ_{l}, and c_{pl} are the thermal

conductivity, viscosity and heat capacity of the liquid, respectively. C_{sf} and s are constants and their conventionally used values for copper-water (surface-fluid) combination are 0.013 and 1. The boiling curve drawn from Rohsenow correlation is shown in Fig. 2.3.

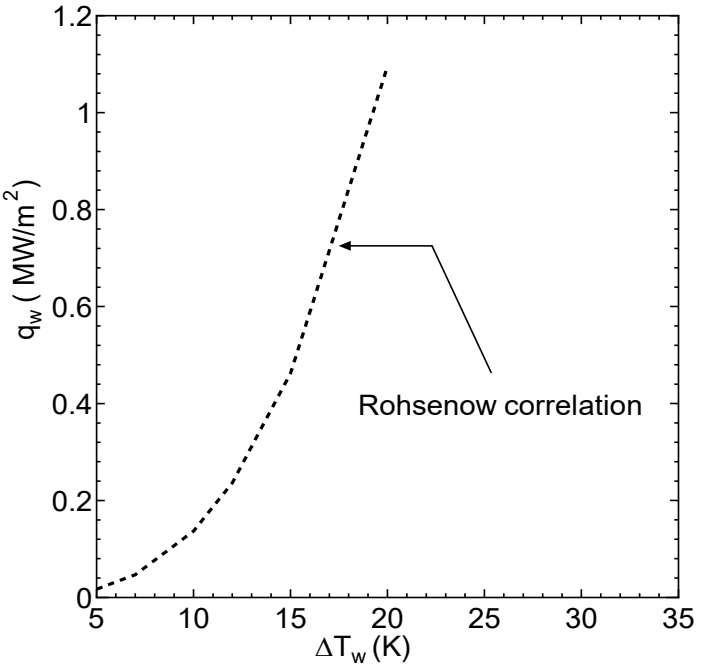

Fig. 2.3: Boiling curve drawn from Rohsenow correlation for copper-water combination

2.1.4 Correlations on critical heat flux

The critical heat flux is defined as the maximum point of the nucleate boiling region, where the heat flux is at the highest rate. This point is also referred to as a departure of nucleate boiling (DNB) or the burnout heat flux. After this stage, the capability of removing high heat flux is reduced and the wall superheat continues to increase to the transition boiling regime and later reaches film boiling. Several well known researchers have reported in the literature to predict the CHF which have been widely used in the heat transfer applications design. The details of these correlations are further explained below:

Zuber-correlation on hydrodynamics boundary-layer model

The most imperative correlation on the CHF is developed by Zuber [16] to predict the critical heat flux based on the hydrodynamic boundary-layer model of the burnout crisis. This work is further supported by Kutateladze [9] and Tien [17]. At present, this correlation equation has been reasonably successful in predicting the CHF for various pure liquids. The equation for the Zuber correlation as [18]

$$q_{\mathrm{CHF}} = 0.131 h_{\mathrm{fg}} \rho_v^{0.5} \left[\sigma g \left(\rho_{\mathrm{l}} - \rho_v \right) \right]^{0.25}. \tag{2.5}$$

For pure water, the CHF value for Zuber correlation is 1.1 MW/m^2 and the calculated value is drawn in Fig. 2.4.

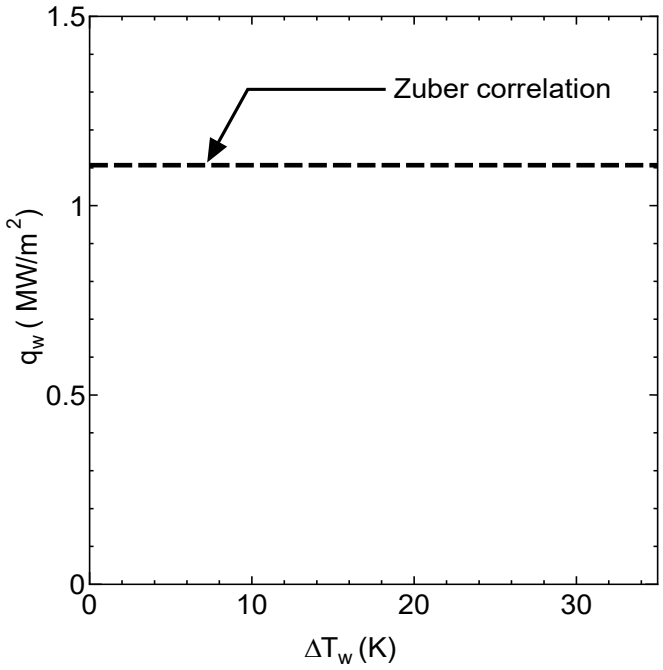

Fig. 2.4: CHF drawn from Zuber correlation

However, this correlation does not take into account the heating surface properties, and could not explain the CHF enhancement in nanofluids' boiling. Based on this equation, the influencing parameters for CHF values are the heat of vaporization (h_{fg}), the density of the vapor (ρ_{v}) and liquid (ρ_{l}). It should be noted that the density values of

nanofluids for heat vaporization are nearly the same as for pure water since the mass concentration of nanoparticles is insignificantly small. As the nanoparticles are colloidal, the deposition on the heated surface during the bubble nucleation is unavoidable. They dramatically modify the surface morphology. One of the most significant changes observed is the modification of the surface wettability.

Kandlikar Correlation

In connection with the previous section, Kandlikar [19] has introduced an improvement that takes into account the effect of the surface condition

$$q_{\mathrm{CHF}} = h_{\mathrm{fg}}\rho_{\mathrm{v}}^{0.5}\left(\frac{1+\cos\beta_r}{16}\right)\left[\frac{2}{\pi}+\frac{\pi}{4}\left(1+\cos\beta_{\mathrm{r}}\right)\cos\phi\right]^{0.5}\left[\sigma g\left(\rho_{\mathrm{l}}-\rho_{\mathrm{v}}\right)\right]^{0.25}, \tag{2.6}$$

where β_{r} is the receding contact angle of the heater surface and ϕ is the angular orientation of the heater, corresponding to the horizontal orientation as shown in Fig. 2.5.

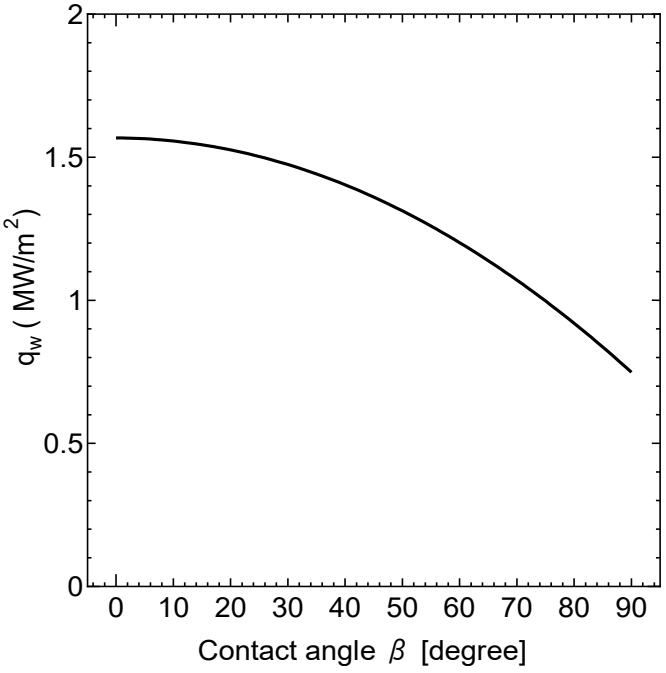

Fig. 2.5: CHF enhancement respective to the contact angle drawn from Kandlikar correlation for copper-water combination

Specifically, he takes into account the heater surface morphology and the wettability which dramatically influences the mechanism of bubbling during the nucleation. It is in excellent agreement with many experimental studies on the effect of reduction of the contact angle respective to the CHF as

Ramilison Correlation

As a result of more detailed studies on the surface properties to the CHF, Ramilison et al. [20] have proposed another correlation which takes into account another vital surface property, the surface roughness and contact angle into his correlation. The equation is

$$q_{\mathrm{CHF}} = 0.0366\left(\pi - \beta_{\mathrm{r}}\right)^{3.0} R_{\mathrm{q}}{}^{0.125} \frac{\pi}{4}\left[\rho_{\mathrm{v}}{}^{1/2} h_{\mathrm{fg}}\left[\sigma g\left(\rho_{\mathrm{l}} - \rho_{\mathrm{v}}\right)\right]^{0.25}\right], \tag{2.7}$$

where R_{q} is the root mean square surface roughness of a heater and β_{r} is the receding contact angle. Measurement of the contact angle and the surface roughness are required for this correlation.

2.2 Properties of the nanofluids

2.2.1 Thermo-physical properties

Nanofluids have been reported to have improved thermo-physical properties in a number of articles [1,21–30]. In particular, the thermal conductivity became a primary research interest. The thermal conductivity was shown to improve with the dilution of the nanofluids in various base fluids, i.e., aluminum oxide (Al_2O_3), titanium oxide (TiO_2) and silicon oxide (SiO_2) as well as carbon nanotubes (CNT). These were the nanofluids that have been tested and most commonly used for various applications. The enhancement of the thermal conductivity varies depending on the materials, concentrations, size and chemical characteristics. The improvement of the thermal conductivity usually ranges

from about 10 to 300 percent, as discussed by Wang et al. [31]. The details of the respective effect on the pertinent parameters of particle volume concentration, material, size, shape, base fluid material, temperature, additive, and acidity were considered individually by various research groups, and the results were summarized in a review by Yu et al. [32].

Apart from thermal conductivity, another important parameter usually considered by many researchers is the viscosity, i.e., the viscosity of the base fluid after the addition of nanoparticles. It has been reported that the viscosity is significantly influenced by parameters such as temperature, particle size, and shape as well as volume fractions, for which a detailed reviewed has been given by Mahbubul et al. [33]. The significant enhancement in the thermal conductivity of nanofluids was also observed in experimental studies of natural and forced convection. However, the relations of these characteristics to the boiling heat transfer are still unclear due to the non-linearity phenomena in boiling system. Thus, to reveal the possible mechanism of the heat transfer performance in boiling systems, these parameters should not be neglected.

2.2.2 Dispersion condition in fluid

The preparation of the nanofluid is the crucial step in the experimental studies related to nanofluids and has been treated by many researchers [26,34–38]. Nanofluids are not merely any liquid-solid mixtures. For a technical application as coolants, several special requirements are essential, such as even and stable suspension, durable suspension, the negligible agglomeration of particles, and an absence of any chemical change of the fluid [31]. It was found that agglomeration could lead to different structures after deposition onto the heater surface, which could produce different sizes of micro-cavities that promote the nucleation of bubbles. Haddad et al. [39] had reviewed how various techniques that were used by investigators to obtain a good dispersion condition. In general, to obtain stable dispersions, ultrasonic vibrators, adjusting the pH value and the addition of surfactants are the most commonly used techniques. However, in some cases, the addition of chemical stabilizers such as surfactants could lead to inconsistencies in experimental results, especially in studies related to heat transfer. Apart of that, study on

nanofluid stability of several types of aluminium oxide also has been reported in detail by Andersson [40].

2.3 Nucleate boiling in nanofluids

Two characteristics which are crucial in nucleate boiling are the heat transfer coefficient (HTC) and critical heat flux (CHF). To date, many researchers have published their experimental work in the study of nucleate pool boiling heat transfer in nanofluids [3,41–54]. However, the coefficient of the heat transfer is still elusive due to the complexity of the phenomena related to nucleate boiling.

Several arguments among researchers on the enhancement and the deterioration of nucleate boiling heat transfer characteristics, especially in nanofluids pool boiling have been reported. However, for the CHF results, most researchers have reported enhancements from their studies [3,46,55–68].

Research on pool boiling with nanofluids was initially conducted in the early 21st century pioneered by You et al. [2] and Das et al. [3]. Since then, numerous studies have focused on pool boiling and related areas, such as HTC. Such studies have been conducted by Vassallo et al. [69], Bang and Chang [42], Park and Jung [43], Soltani et al. [44] and Huang et al. [45]; CHF studies were performed by H. Kim et al. [70], H. Kim et al. [71], Hegde et al. [72] and Kwark et al. [73]. Morerover, Jeong et al. [74] and Peng et al. [75] focused on the surfactant addition.

A more in-depth understanding of both of these critical characteristics is an essential key to design cooling devices with optimum heat dissipation capabilities.

2.3.1 Review of the heater orientation effects

Buongiorno et al. [4] proposed the use of nanofluids to enhance the in-vessel retention (IVR) capability as a management strategy in the case in severe accidents in light-water reactors (LWRs). By IVR, in the case of severe accidents, the core melts and relocates to the lower head of the reactor vessel, these consequences can be mitigated by flooding the reactor cavity with cooling water from a water storage tank and nanofluids

stored in separate storage tanks. Thus, the decay heat from the molten core is removed by conduction through the reactor vessel wall and boiling on the outer surface of the vessel. Since the heat flux at the outer surface of the reactor vessel during severe accidents tends to increase the core power density while the CHF limits the possible decay heat removal. Thus, the use of nanofluids is expected to increase the safety margin. Moreover, in the newer design of nuclear power plants such as the economic boiling water reactor (ESBWR) [5], passive coolants have been integrated to a significant degree.

Till today, the effects of the heater orientation have been less widely addressed by researchers, especially in the case of pool boiling for nanofluids. However, prior to the CHF in the pool boiling of nanofluids studies, Howard and Mudawar et al. [76] have reported findings on the effect of the heater orientation (change from upward to downward orientation) together with the CHF performance using pure water. In their study, it was reported that the CHF values decreased approximately by half for the downward-facing condition in Fluorinert liquid (FC-72).

In the case of pool boiling of nanofluids, investigation results were reported by using different types of heaters, either for wire or flat plate heaters [2,45,70,77]. The reported information was mainly on the upward-facing flat heaters and nearly no information was available on the orientation effect. Also, for cylindrical heaters due to the wiring, the orientation effect could not be investigated. This setup is impracticable to reveal the information about the CHF with respect to the orientation of the heater. To obtain management strategy in severe loss of coolant accidents, a deeper understanding of the influence of the heater orientation on the CHF, especially in the case of downward-facing heaters, is needed. Hence, the study on effects of the orientation is crucial to elucidate the CHF characteristics in both upward- and downward-facing nano-coated heaters.

In the literature, the CHF of pure water in pool boiling was found to decrease as the heater orientations was changed from upward to downward-facing [76]. Parallel to the application of nanofluids in the severe management strategy, a better understanding of the influence of heater surface orientation, especially for downward-facing heaters to critical heat flux became necessary. Therefore, in the present study, an attempt was made to investigate effects of the orientation with respect to critical heat flux in both upward-

and downward-facing heaters in nanofluid nucleate pool boiling and will be discussed in Chapter 4.

2.3.2 Review on the effect of the particles' material, concentration and dispersion condition

Until now, many experimental investigations have been conducted since the study of pool boiling of water-based nanofluids by You et al. [2] revealed enhancement of the critical heat flux (CHF) by up to 200 percent. Also, a number of reports can be found for pool boiling with nanofluids which indicate CHF enhancement and the dependence on surface properties in particular, surface wettability, roughness, porosity and capillarity [19,48,70,78–82]. The deposition of the nanoparticles due to microlayer evaporation in nucleate boiling has been shown to improve the surface wettability and the porous structure along with the changes in roughness and capillarity and to contribute to a dramatical enhancement of the CHF. However, Kim et al. [71] reported that the CHF values obtained by using nanofluids with a nano-coated heater surface and pure water are lower than those for nanofluids. CHF values observed under different conditions depended on the particles' material. Similarly, the boiling heat transfer characteristics have been extensively studied by an immense number of researchers [41,52,57,58,83–85] and great variations were reported. There is still no agreement on the cause for these contradictions. However, in the boiling heat transfer of nanofluids, it was reported that the heater surface structure (characterized by wettability, roughness, and nanoparticles-layer thickness) is not the sole the reason for these inconsistencies, but there is also an effect from the suspended nanofluids' physical properties (nanofluid materials, concentration, dispersion condition and shape) and thermo-physical properties (viscosity and thermal conductivity). How this could affect the bubbles dynamic has been discussed thoroughly by Wen D. [84]. Accordingly, one could conjecture the important parameters that consequently affect the boiling heat transfer performance in many ways and represented them by a complex time-variation of the wall superheat [86]. On the other hand, one could infer that the conflicting reports in the literature on boiling heat transfer are most probably due to the combined effects of the parameters listed above. These

effects may be either be self-attenuating or cancel depending on the material, size and dispersion conditions. In addition, an extensive review by Haddad et al. [39] on various preparation techniques showed a distinctive dispersion of the nanofluids, which depends on sonication time, volume fraction, nanoparticle size and type, base fluids, surfactants and the nanofluids production methods. In nanofluid nucleate boiling, it should be noted that varying the dispersion conditions leads to a different morphology of the heater surface microstructure. These significantly influence the bubbling activity due to an increase in the density of nucleation sites during nucleate boiling, as reported by Barber et al. [87] and Kamatchi et al. [88]. The complex time-variation of the boiling heat transfer in nanofluids [86] would be also one of the reasons for the inconsistency between investigations by different groups. The literatures above revealed the effects of several vital parameters on the boiling heat transfer characteristics. However, the effects of other parameters, such as the material and dispersion condition of nanoparticles on the CHF are yet to understood sufficiently. To date, no systematic experimental information is available in the literature for boiling heat transfer in a nanofluid. Thus, the present study is also aimed at investigating the effects of the nanoparticle-material, the concentration and the dispersion condition of nanofluids. The detailed discussion will be presented in Chapter 5.

2.3.3 Review on the different heat flux density on the boiling heat transfer and critical heat flux

The heat flux density is the most decisive parameter in high power cooling systems. In nuclear systems, the heat is continuously generated inside the core, transferred through the pressure vessel and dissipated at the outer surface. During this process, the amount of transferred heat is controlled by the elevation of the control rod bundles in the reactor vessel. However, during loss of coolant accidents (LOCAs), the amount of heat flux represented by the heat transfer coefficient (HTC) is unpredictable, uncontrollable and fluctuates depending on the severity of the accident. It is limited only by the maximum heat transfer capability of the system called the critical heat flux (CHF). Consequently, this has led to the introduction and adoption of in-vessel retention (IVR) in the design for

LOCAs in 1989. After that, progressive research on IVR has been reported in the literature [89–91]. Realizing the unique properties achieved, nanofluids have also been introduced in IVR for Light Water Reactors (LWRs) by Buongiorno et al. [4] to mitigate the consequences of a hypothetical severe accident.

To the best knowledge of the author, so far only a few studies have been conducted on the effect of heat flux on the CHF enhancement and the boiling heat transfer (BHT) characteristics can be found in the literature. From the available reported literature, most of the work in nanofluid boiling was performed in the quasi-equilibrium in BHT experiments with subsequent CHF measurement. Here, the heat flux effect at a particular fraction of the CHF could not be quantified as the heater surface had already been altered by the previous boiling process with nanofluids due to heat flux in quasi-equilibrium. Therefore, the applied elevated quasi-equilibrium heat flux is not applicable for research on the IVR condition. Conversely, Okawa et al. [86] had investigated CHF and HTC performance in constant heat flux and found that the CHF enhancement also depends on the boiling time and concentration; however, for the HTC their characteristics were somewhat random, with increases and decreases in HTC for a relatively high concentration. On the other hand, Kwark et al. [52] showed a decrease of the HTC in Al_2O_3 in quasi-equilibrium nucleate boiling experiments for a specified period and suggested that the responsible factors are the increased thickness of the deposition. Suriyawong et al. [92] also observed degradation of the HTC in TiO_2 quasi-equilibrium experiments.

Apart from that, it can also be noted that nucleate boiling is known to be the most efficient heat removal method due to the latent heat in the vaporization. Since the nucleate boiling system consists of at least three regions [93] which can behave differently depending on the nucleation size density, bubble departure diameter, bubble frequency, bubble coalescence and also the heat transfer mode in natural convection at low heat flux. It is expected that nanofluids could remarkably influence the boiling system characteristics which are at present poorly known. Differences in heat flux could affect the parameters that govern nanofluid nucleate boiling differently, and the changes are essential for successful IVR with nanofluid.

In short, numerous investigations have been conducted on pool boiling with nanofluids, with limited emphasis on the heat flux effect. Also, a sufficient understanding

on the performance of the HTC and the degree of the CHF enhancement after nanofluid injection is necessary. Therefore, the current study is expected to provide several noteworthy contributions to the success of IVR integration with nanofluids to improve the safety margins. The present work also attempts to explore experimentally the effects of heat flux applied during nanofluid boiling on the CHF and their HTC in nucleate pool boiling by using titanium oxide nanofluids, an extension to the previous study in Ref. [86]. A detailed discussion will be presented in Chapter 5.

2.3.4 On the possible mechanism of the boiling heat transfer (BHT) improvement

As the BHT-data were inconsistent among various research groups, it is challenging to identify the mechanism involved in the BHT characteristic. In most cases, the boiling curve measurements were performed using a base fluid that had been diluted with nanoparticles prior to pouring it into the vessel. Based on the detailed discussion in Chapter 5, the time variation of the wall superheat could be used to extract crucial information of the nucleate boiling condition at a particular heat flux. However, the limitation to observe bubbles using the small size copper heater and limited visibility of the nanofluid in the present experimental work was the primary constraint to observe the behavior of the bubble. Evidently, the finding in the current study by using the copper heater shows the heat transfer coefficient (HTC) to increase in most cases at the initial stage of the nanofluid addition for all concentrations and nanoparticle-materials (except in some cases indicated in the discussion in Chapter 5). The observed enhancement can be attributed to the ability of nanofluids to promote the addition of nucleation sites which eventually increases the HTC at the initial stages of the nanofluid injection.

Based on the hypothesis that the nucleation site density increased upon the addition of the nanofluid into the test vessel at the initial stage of the time variation of wall superheat, a preliminary observation was conducted to observe the bubbling behavior. The visualization of nucleate boiling was performed by using another experimental apparatus. The details are further described in Chapter 7.

2.4 Bubble nucleation in nanofluid pool boiling

In nanofluid boiling systems, the most significant feature is the deposition of nano-particles due to bubbling. The deposition modifies the heater surface morphology, and the changes in morphology lead to the changes of several properties such as surface wettability, roughness, and porosity.

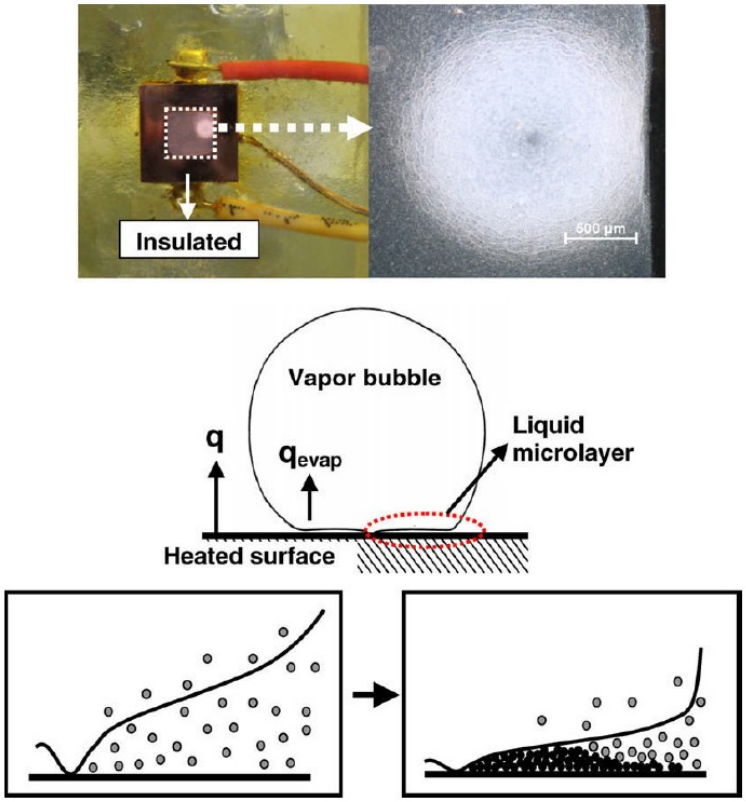

Fig. 2.6: Deposition of nanoparticles at the nucleation site region [94]

These properties are closely related to the availability of micro-cavities for bubble nucleation that could alter nucleation site density, bubble departure diameter, and frequency. Consequently, it is widely believed these are the primary causes of the changed heat transfer performance. Fig. 2.2 shows the surface modification during the nanofluid pool boiling.

The study conducted by You et al. [2] reported an increase of the bubble size and a decrease in the frequency after the addition of the nanofluid. The photograph in Fig 2.3 shows sample pictures of the bubbles' condition between the bare and the nanofluid boiling system.

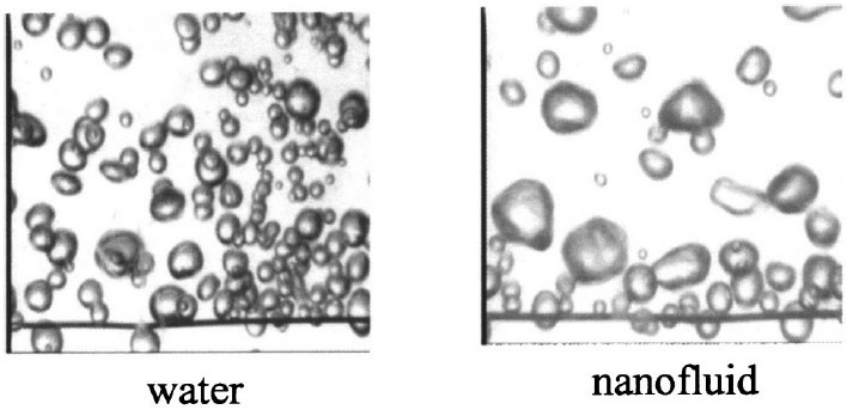

Fig. 2.7: Sample pictures of bubbling from a wire heater [2]

CHAPTER 3 EXPERIMENTAL SETUP

In this chapter, the selected nanoparticles, experimental procedures, experimental apparatus and equipment are described in detail.

3.1 Nanoparticle materials

Three different types of nanoparticles are selected for the nanofluid preparation and used in the experiments. In the present study, two types of nanofluids are used, one prepared using a two-step method and one using the one-step method. The nanoparticles are purchased in powder form and later dispersed in the liquid ("two-step method", "Type I"), while the second type is a nanofluid purchased in liquid form and later diluted into a larger volume of the base fluid ("one-step method", "Type II").

The properties of the three different nanoparticle materials used in this research are summarized in Table 3.1 and 3.2.

Table 3.1: Nanoparticle-materials and description

Item	Nanoparticles	Original form	Size d_p [nm]	Type	Manufacturer
1	Titanium Oxide (TiO_2)	Particles	21	Type I	Aerosil Corporation (Aeroxide TiO_2 P25)
2	Alumnium Oxide (Al_2O_3)	Particles	13	Type I	Aerosil Corporation (Aeroxide Alu C)
3	Silicon Oxide (SiO_2)	Particles	20	Type I	Aerosil Corporation (Aerosil 90)
4	Titanium Oxide (TiO_2)	Slurry	21	Type II	Aerosil Corporation Aeroxide (AERO DISP W740 X, 40 wt. %)

Table 3.2: Nanoparticles properties

Molecular formula	TiO_2	Al_2O_3	SiO_2
Melting point [°C]	1850	1750	1713
Appearance	White solid	White solid	Transparent solid
Density [g/cm^3]	3.8	3.89	2.33
Thermal conductivity [W/m.K]	11.8	35	1.4

3.2 Experimental equipment

Four different experimental test setups are designed and used in the present study to achieve the specific technical objectives. The four different test vessels used are described in detail in the following section.

3.2.1 Test vessel I (Upward-facing heater)

Fig. 3.1 shows the schematic diagram of the experimental apparatus for the upward-facing heater experiment. The system is composed of a copper block, cartridge heaters, a test vessel, a cover plate, an external thermocouple to measure the liquid temperature, a series of thermocouples embedded in the copper block, and a thermal insulator. The heating device is mounted at the bottom of the cylindrical stainless steel vessel of 160 mm diameter and 200 mm height as shown in the figure. The side wall of the vessel is covered with an insulation material.

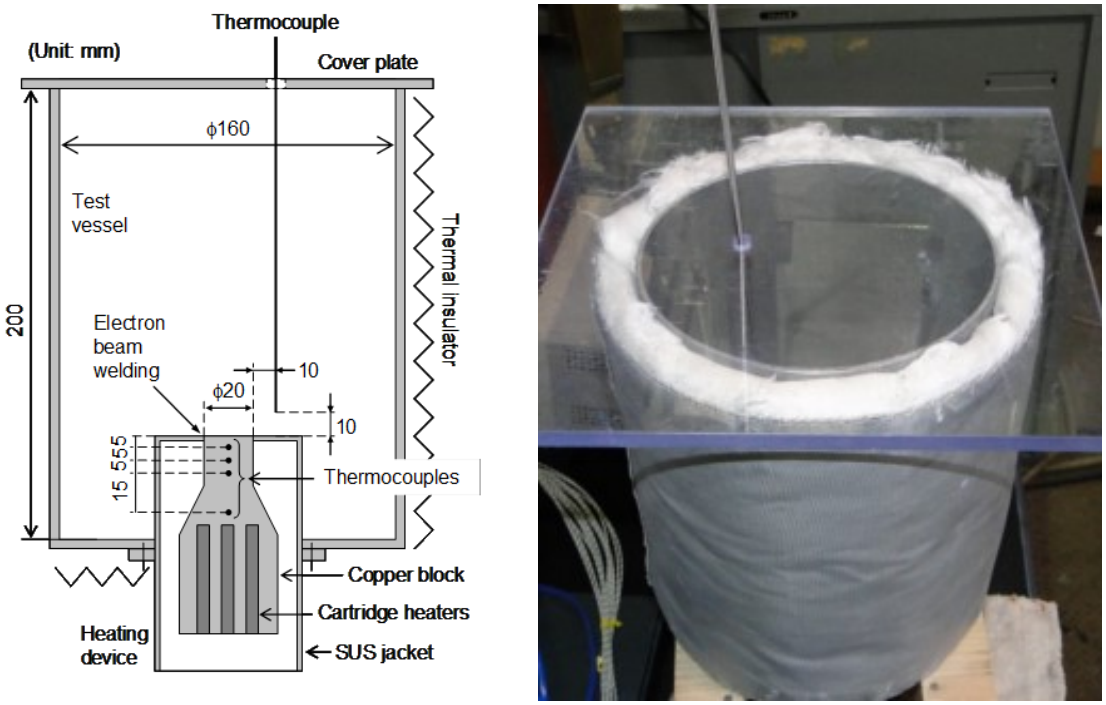

(a) (b)

Fig. 3.1: Experimental apparatus for upward-facing experiment; (a) schematic diagram and (b) photo

3.2.2 Test Vessel II (Downward-facing heater surface)

Fig. 3.2 shows the schematic diagram of the experimental apparatus for the downward-facing heater experiment. The components are similar to those in upward-facing heater except that the heating device is mounted on the top of the stainless steel bracket attached to the vessel of 160 mm diameter and 200 mm height as shown in Fig. 3.2. The side wall of the vessel is covered with insulation material. At the bottom, the auxiliary heater is used to supply heat to keep the water at saturation temperature.

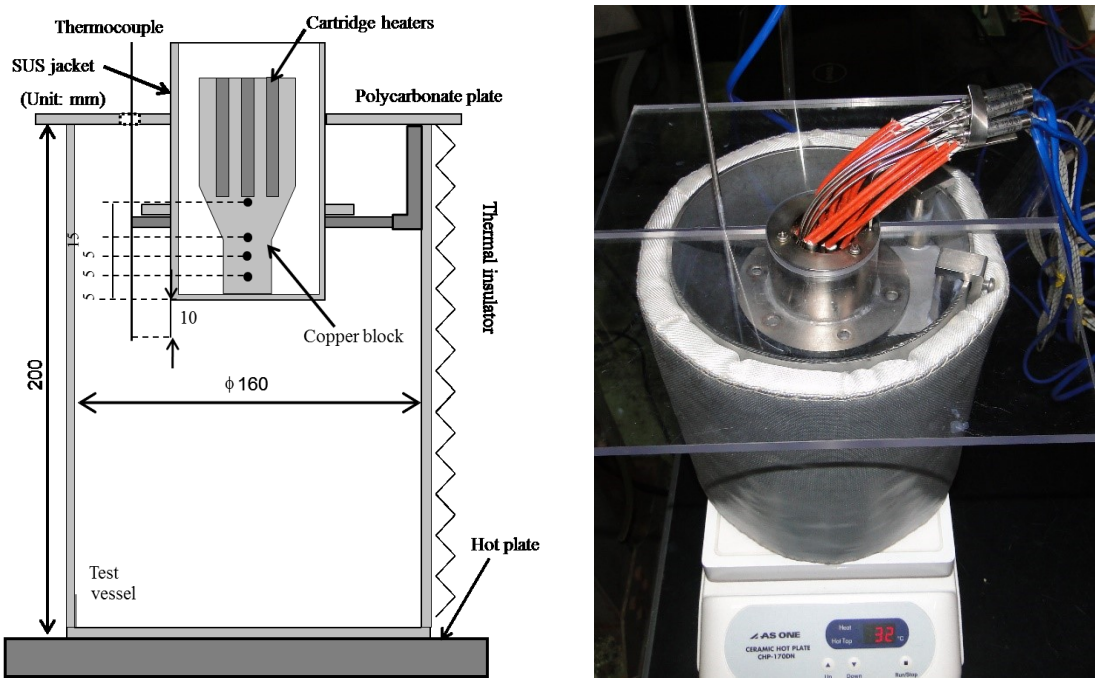

(a) (b)

3.2.3 Test Vessel III (Transparent vessel)

The schematic diagram and the picture of the experimental apparatus for test Vessel II are shown in Figs. 3.3 (a) and (b), respectively. The test vessel mainly consisted of a polycarbonate circular tube as a side wall, a stainless steel bottom plate, and a polycarbonate top plate. The inner diameter and height of the vessel are 144 and 170 mm, respectively, and the side wall of the vessel is covered with a thermal insulator. The heating device is mounted concentrically at the bottom of the test vessel as shown in Fig. 3.3. An immersion heater with 1 kW power is arranged in the lower part of the vessel to keep the bulk liquid temperature at saturation temperature. A water-cooled reflux condenser is mounted in the top plate to prevent vapor release from the test vessel. Since the top of the condenser is not closed, the pressure inside the vessel can be assumed to be equal to atmospheric pressure. A type-K thermocouple is positioned 10 mm above the center of the heated surface to ensure that the bulk liquid is maintained in saturation. The top plate was designed with a 15 mm diameter hole to inject the nanofluid with a syringe into the vessel containing boiling water. The hole was always kept closed with a silicone rubber plug except during the nanofluid injection.

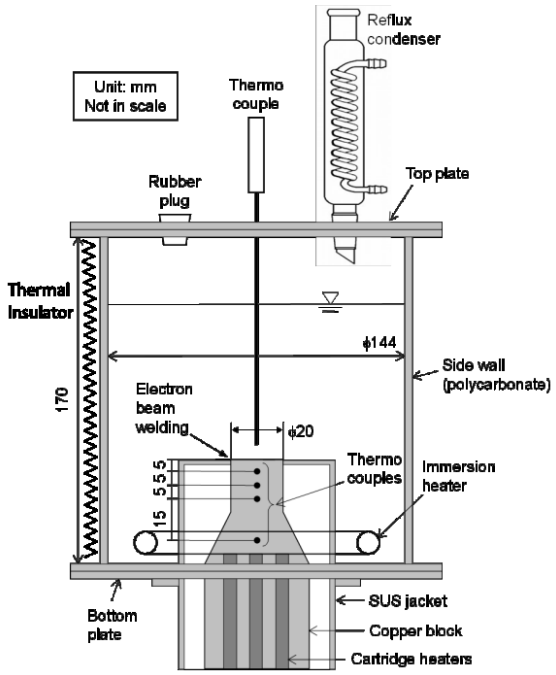

(a) Schematic diagram

(b) Photo

Fig. 3.3: Schematic diagram and photograph of the experimental apparatus

3.2.4 Test Vessel IV (Transparent Heater and Transparent Vessel)

The vessel is made of polycarbonate with the internal dimensions of 20 mm width, 230 mm length and 98 mm depth, as shown in Fig. 3.4.

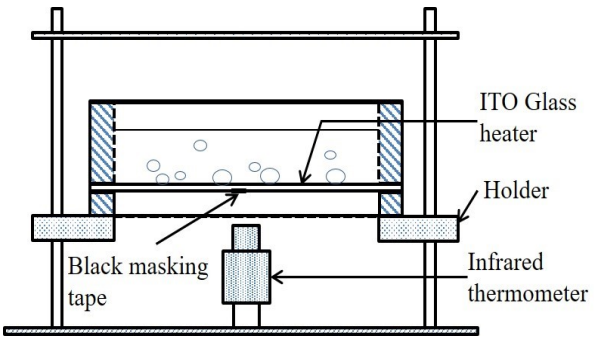

(a) Schematic diagram

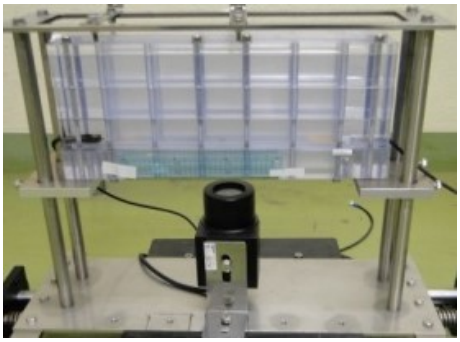

(b) Photo

Fig. 3.4: Schematic diagram and photograph of the experimental apparatus

3.2.5 Copper block heater

The one end of a copper block was machined into a cylindrical shape of 20 mm diameter, and its end face was used as the heating surface. Nine heating cartridges with 900 W power in total were embedded into the opposite end of the copper workpiece. The calculated maximum heat flux for this arrangement is 2.86 MW/m^2. Whereas four type-K thermocouples with an accuracy of ± 1.5 K were positioned along the central axis of the copper cylinder to measure the heat flux, q_W and the wall superheat, ΔT_W and also to shut down the system when the critical heat flux condition is reached. The copper block is placed in a stainless steel jacket of 2 mm in thickness to reduce the heat loss from the side wall of the block. The copper block and the jacket are bonded smoothly by electron-beam welding to avoid leakage and to eliminate the possibility of any significant vapor bubble generation at the bond part.

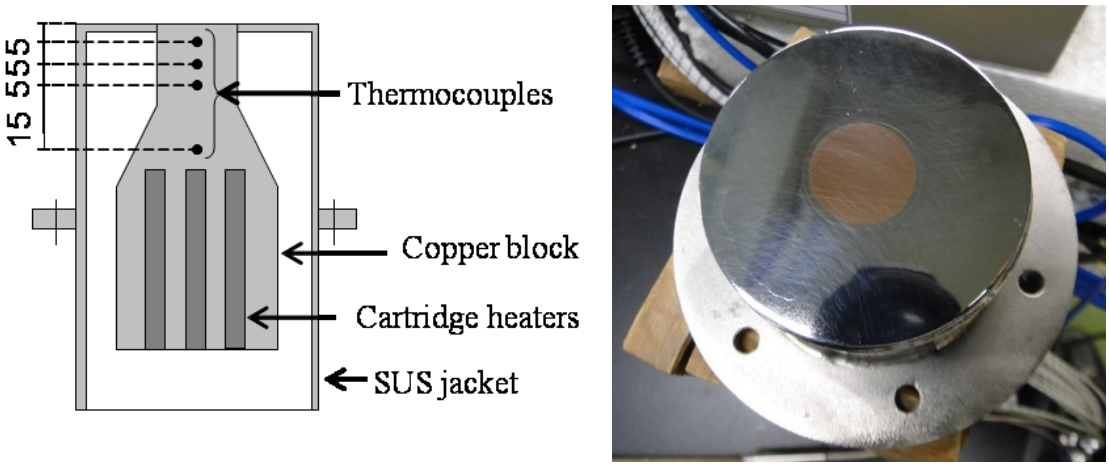

(a) Schematic diagram (b) Photo

Fig. 3.5: Schematic diagram and photograph of the heater block

3.2.6 ITO Quartz glass heater

The heater surface has a dimension of 10 mm width and 170 mm length (Fig. 3.6) and the surface is heated ohmically using a DC power supply. An ITO film-deposited glass plate forms the bottom face of the experimental vessel and the vessel is fixed to the

holder as shown schematically in Fig. 3.4. A small stripe of black tape is placed at the center of the underside surface of the glass plate. The superheat temperature, ΔT_{BW} of the glass plate is then measured using an infrared thermometer.

(a)

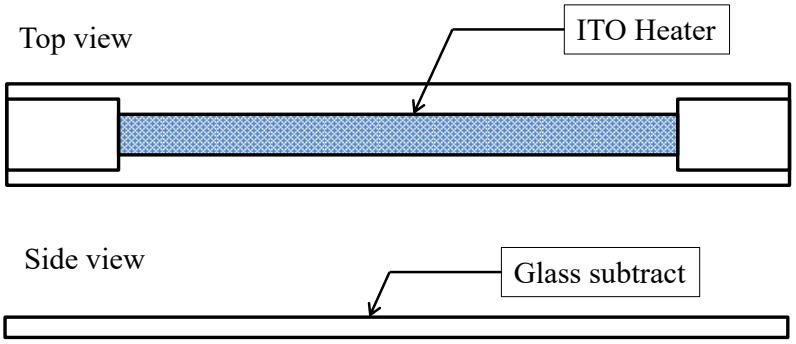

(b)

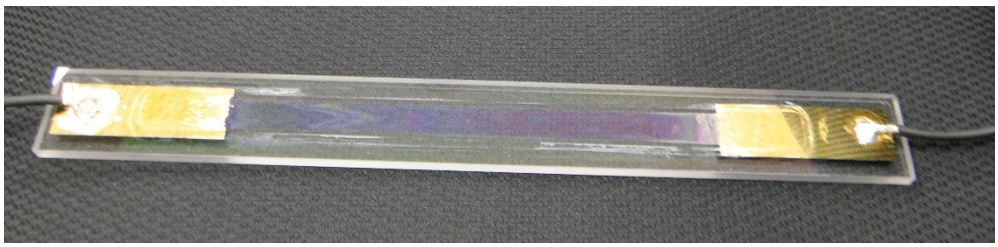

Fig. 3.6: ITO Quartz glass heater (a) Schematic diagram (b) Photo

3.3 Instrumentation and Equipment

Ultrasonic bath device

In order to obtain a finer dispersion of nanofluid, an ultrasonic bath as shown in Fig. 3.7 is used to break the agglomeration of the nanoparticles into smaller agglomerates. The sonication time t_{us} used in this study was between 1 to 8 hours. The detail description is given in Table 3.3.

Fig. 3.7: Ultrasonic bath

Table 3.3: Descriptions of the ultrasonic bath

Manufacturer	BRANSON
Model	CPX2800H-J
Specification	Voltage：110W Frequency：40kHz

Scale

The nanoparticles were weighted with the high-resolution scale in Fig. 3.8 with the detailed specifications of the scale in Table 3.4.

Fig. 3.8: Scale used for the experiment

Table 3.4: Detail description of the scale

Manufacturer	AS ONE
Model	ASP213
Specification	Minimum Display：0.001g Accuracy：±0.002g Stabilizing time：3 second

Contact angle measurement device

The PG-X (FIBRO system AB) instrument (Fig. 3.9) is used to measure the contact angle for the surface wettability. The integrated micropump is designed for a

standard liquid where the droplet size can be set in steps of 0.5 μL. Degassed and distilled water is injected into a small tube to develop a single drop of water on a copper surface. The digital image of the droplet profile is obtained and analyzed to derive the static contact angle.

Fig. 3.9: Contact angle measurement device

Condenser

In order to retain the fluid and prevent it from evaporating into atmosphere (outside of the vessel), two condensers are used to prevent the changes in the concentration caused by evaporation. The specification is shown in Table 3.5.

Table.3.5: Detailed description of the condenser device

Manufacturer	Shibata Scientific Technology Co. Ltd.
Product name	SPC Cooler rod (a) Dimroth condenser rod (b)
Model	030730-15200(a) 006680－24500(b)
Specification	(a) Height：200mm Diameter：30mm Rubber cap：8mm (b) Height：500mm Diameter：34mm Rubber cap：10mm

Cartridge heater

Cartridge heaters are attached to the copper block to supply heat. The specification is shown in Table.3.6

Table 3.6: Description of the cartridge heater

Manufacturer	Daiki Industrial Co. Ltd.
Name	Cartridge Heater
Specification	Diameter：7.3mm Length：45mm Power：100W

Voltage controller

Slider type voltage controllers supply the electrical power to the heater. Two controllers are used, one to regulate the heat for the immersion heater and one for the copper block heater as shown in Fig. 3.10. The specifications are given in Table 3.7.

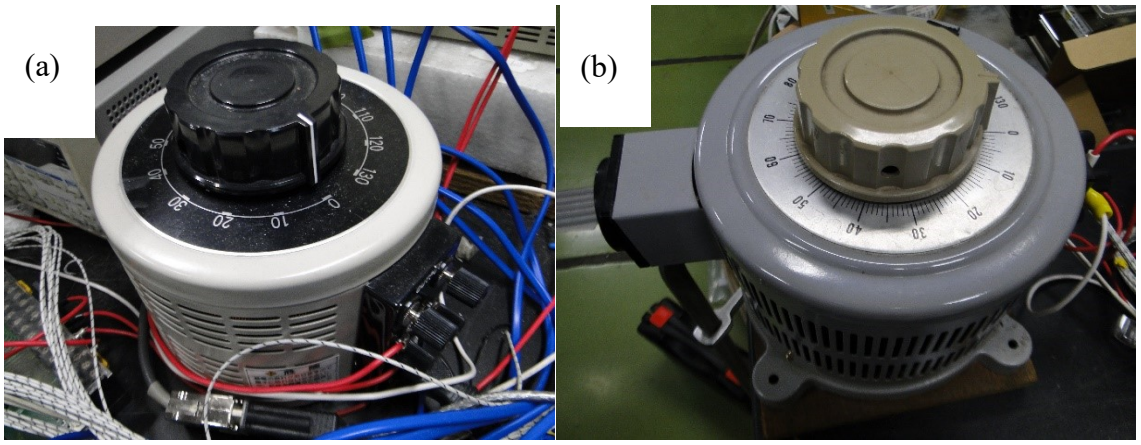

Fig. 3.10: Voltage controller for the copper block heater (a) and the one used for the immersion heater in (b).

Table 3.7: Description of the voltage controller

Manufacturer	Yamabishi Electric Co. Ltd.
Product name	Voltage controller (Slider type)
Model	S-130-10(a) N-130-10M(b)
Specifications	(a) & (b) Output：0~130V Input：100V Maximal current：10A

Digital multimeter

The digital multimeter shown in Fig. 3.11 is used to measure the supplied input current to the copper block. The specifications of the meter are given in Table 3.8.

Fig 3.11: Digital multimeter

Table 3.8: Description of the digital multimeter

Manufacturer	Advance Ltd.
Product name	Digital multimeter
Model	R6452A
Specification	Resolution：Voltage 0.01V， Current 0.1mA Measurement accuracy：±0.1V， ±2.3mA

Thermocouples

The thermocouples used in the experiment are the K-type thermocouples. Four units of thermocouples are used; three units is attached to the copper block heater and one for the temperature measurement of the bulk fluid.

Data logger

The data logger in Fig. 3.12 with a capability of recording data in intervals of 1 s is used to measure the temperature and voltage during the experiment. The specification of the logger is given in Table 3.9.

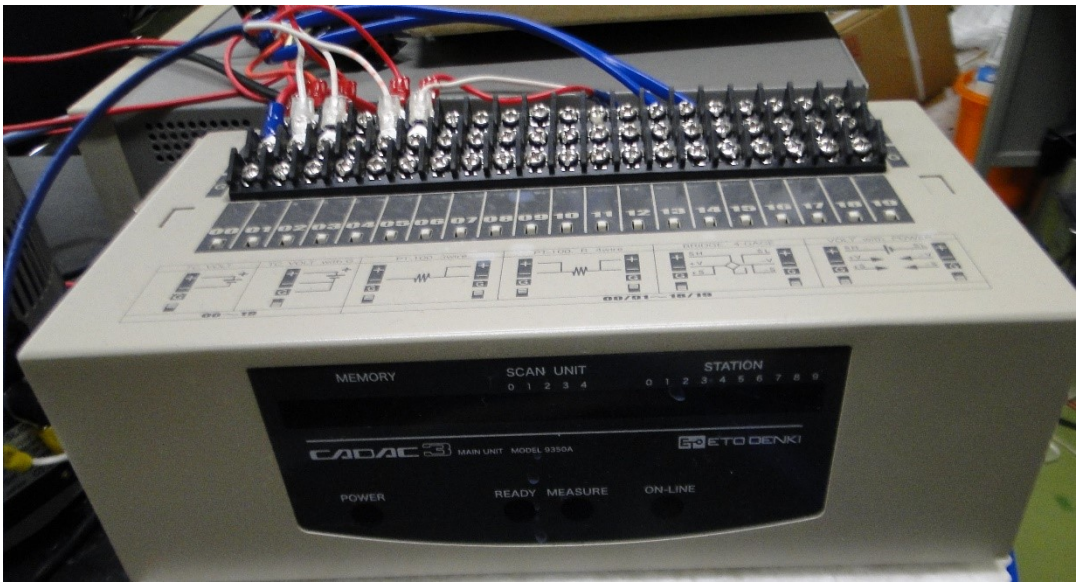

Fig. 3.12: Data logger

Table 3.9: Description of the data logger

Manufacturer	Eto Electric Co. Ltd.
Model	Cadac 3
Specification	Mode：K-CA (Temperature module) 0~1372℃ Tolerance：K-CA (Temperature module) ±0.02%rdg±0.3℃

Hot Plate

In the downward-facing heater, a hot plate as shown in Fig. 3.13 is used to keep the temperature at the saturation temperature. The specification of the hot plate is given in Table 3.10.

Fig.3.13: Hot plate

Table 3.10: Description of the hot plate

Manufacturer	AS ONE
Name	Ceramic hot plate
Model	CHP-170DN
Specification	Maximum temperature：550℃ Heater power：900W

Transmission Electron Microscope (TEM)

A JEOL JEM-2010 high-resolution transmission electron microscope operating between 80 and 200 kV accelerating voltage is used in this study.

Fiber-Optics Particles Analyzer

The dispersion conditions of the nanoparticles in the fluids is measured by using the Dynamic Light Scattering (DLS) analysis machine in Fig. 3.14 with the description in Table 3.11.

Fig. 3.14: Fiber-optic Particles Analyzer

Table 3.11: Description of the fiber-optics particle analyzer

Maker	Otsuka Electronics Co. Ltd.
Product name	Fiber-Optics Particles Analyzer
Model	FPAR-1000
Specification	Particle diameter range：3nm ~5000 nm Concentration range：0.01%~10% Sample temperature range：10~70℃

3.4 General experimental procedure

3.4.1 Preparation of the nanofluids

Each experiment starts with the preparation of the nanofluids. In order to ensure stable and uniform dispersion conditions, ultrasonic excitation is performed for several hours by using an ultrasonic bath for each type of nanoparticles before the experimental investigation.

3.4.2 Heater surface preparation

Before each experimental run, the heater surface is prepared. First, the surface is polished using a metal polishing paste and further cleaned using acetone. After the surface cleaning, five water droplets of about 0.5 mm^3 in volume are placed on the heated surface to measure the static contact angle, θ from the side view of the droplets using a goniometer (PG-X, Fibro System AB). The value of θ was between 85º and 95º as shown in Fig. 3.15.

Fig. 3.15: Photograph of droplets placed on the heated after surface preparation.

3.5 Nanoparticles characterization

The nanoparticles size and aggregation conditions were verified by the transmission electron microscope (TEM) in Fig. 3.16. The size of the nanoparticles was fairly close to the specifications given by the manufacturer.

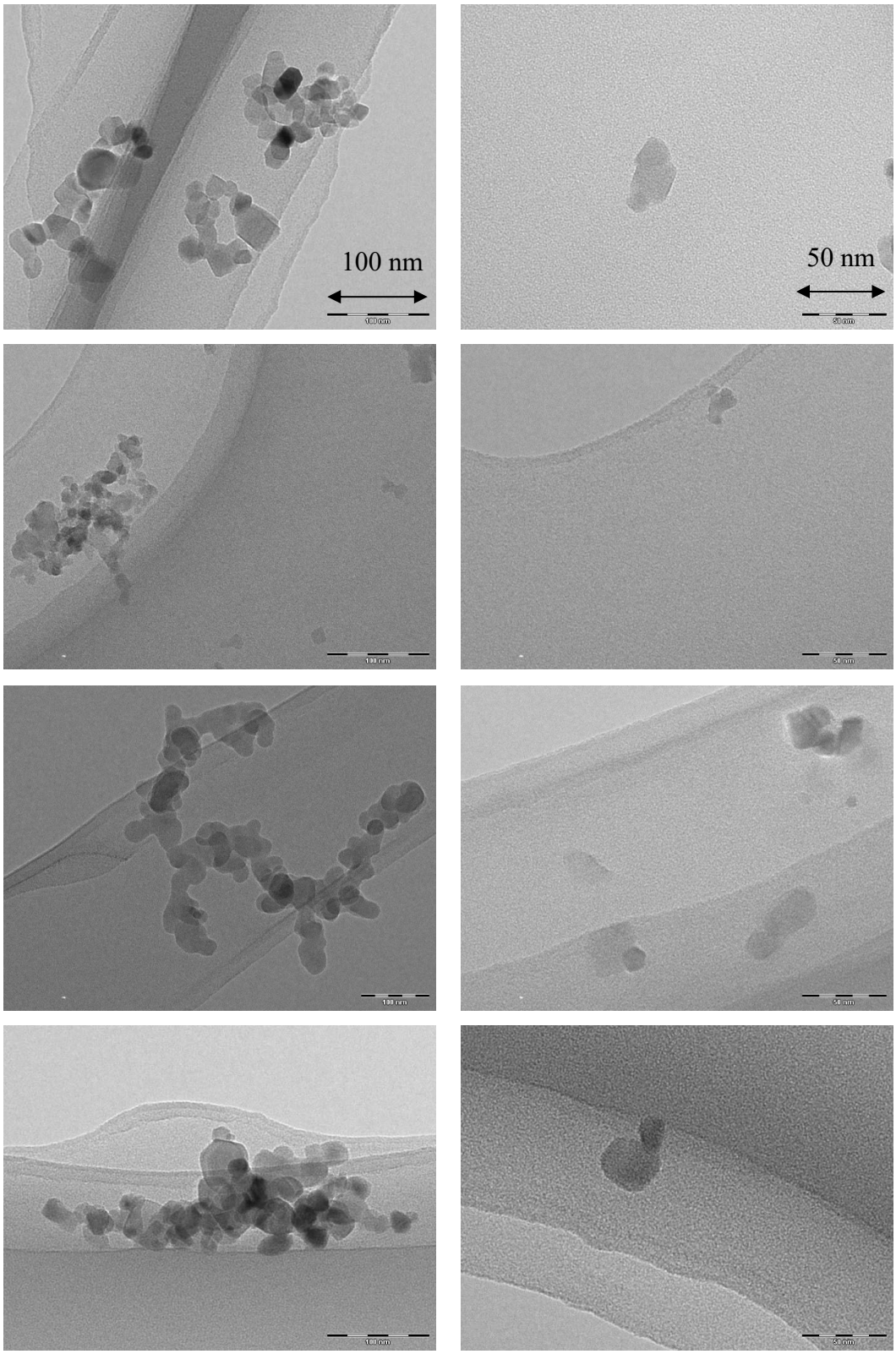

Fig. 3.16: TEM micrograph of nanoparticles observed at different scales; (a) TiO_2 (Type I), (b) Al_2O_3 (Type I), (c) SiO_2 (Type I), (d) TiO_2 (Type II)

3.6 Data analysis

In the present study, the heat flux is calculated by the Fourier law as shown in Figs. 3.17. Temperature measurements at different locations in a copper block were used to determine the heat flux through the heater.

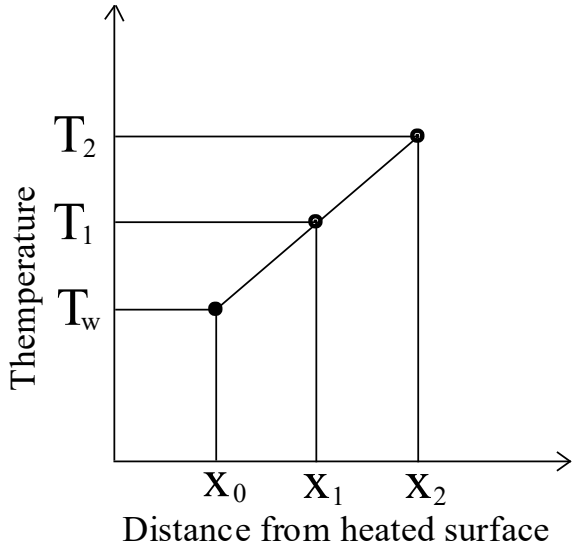

Fig. 3.17: Measurement of heat flux by the Fourier Law

The wall temperature is calculated based on

$$T_{\mathrm{W}} = T_2 - \frac{\delta T}{\delta x} x_2 = T_2 - 2(T_2 - T_1), \tag{3.1}$$

while, the wall superheat is calculated based

$$\Delta T_{\mathrm{W}} = T_{\mathrm{W}} - T_{sat}. \tag{3.2}$$

The wall heat flux q_{W} is calculated by using the value of thermal conductivity of copper k and the difference of the temperature gradient of the copper block as

$$q_{\mathrm{W}} = k\, dT/dx. \tag{3.3}$$

The precise value of the copper thermal conductivity corresponds to the temperature obtained from the correlation

$$k = 3.99\times10^{2} - 4.31\times10^{-2}\mathrm{T_W} - 2.02\times10^{-5}\mathrm{T_W^2}. \quad (3.4)$$

Hence, the heat transfer coefficient, α could be obtained by dividing ΔT_W with q_W as shown in Eq. 3.5.

$$\alpha = q_W/\Delta T_W. \quad (3.5)$$

3.7 Error analysis

The error in the heat flux measurement is estimated by using the method defined by Cooke and Kandlikar [95]

$$U_p = \sqrt{\sum_{i=1}^{n}\left(\frac{\partial p}{\partial a_i}u_{a_i}\right)^2},$$

where p is the calculated parameter, a_i is the measured parameter and u denotes the error of the subscripted parameter.

In the present study, the three possible sources of error are listed in Table 3.12.

Table 3.12: Parameters for the error determination

Parameters	Resolution
Thermocouple Precision Resolution [K]	1.5 K
Thermal conductivity of the material at different temperatures [W/m. K]	1 W/m. K
Length resolution of the equipment [m]	0.0001 m

From the error analysis method described, the measurement error of q_W and ΔT_W are less than 90 kW/m^2 and 3 K, respectively.

CHAPTER 4 EFFECT OF HEATER ORIENTATION ON CHF

4.1 Introduction

In nuclear power plants (NPPs), the reactor pressure vessel (RPV) is located in the containment. In the bottom part of the RPV's outer surface, the orientation is downward. As the nanofluid could be used during the loss of coolant accident (LOCA), information regarding the CHF in upward- and downward-facing conditions is important. Hence, this chapter discusses the result of the experimental work for the CHF enhancement in both upward- and downward-facing nano-coated heaters. In the present work, the mean contact angle of the heater surface for both orientations with various concentration are discussed in detail.

4.2 Experimental description

The main experimental parameters are shown in Table 4.1 for the upward-facing heater and in Table 4.2 for the downward-facing heater.

Table 4.1: Main experimental conditions for the investigation of the upward-facing heater

Run	q_w [kW/m^2]	C [kg/m^3]	t_b [s]	t_{us} [hrs]	Type
1-6	330	0.004	1,3, 10, 20, 40, 60	8	Type I (TiO_2)
7-12	330	0.04	1,3, 10, 20, 40, 60	8	Type I (TiO_2)
13-18	330	0.4	1,3, 10, 20, 40, 60	8	Type I (TiO_2)

Table 4.2: Main experimental conditions for the investigation of the downward-facing heater

Run	q_w [kW/m^2]	C [kg/m^3]	t_b [s]	t_{us} [hr]	Type
19 -24	330	0.004	1,3, 10, 20, 40, 60	8	Type I (TiO_2)
25-30	330	0.04	1,3, 10, 20, 40, 60	8	Type I (TiO_2)
31-36	330	0.4	1,3, 10, 20, 40, 60	8	Type I (TiO_2)

The experimental apparatus has been explained in Chapter 3. In the present work, titanium oxide nanoparticles (Aeroxide TiO_2 P 25, manufactured by Aerosil Corporation with a reported mean particles size of 21 nm) were selected. The nanoparticles were dispersed in distilled water and underwent sonication in the ultra-sonic bath for 8 hours to ensure an excellent dispersion stability. The experimental procedures are described as follows.

Following the surface preparation as discussed in Section 3.4.2 in Chapter 3, the distilled water was kept boiling in a separate vessel for 20 minutes for degassing. In the present experiment, test vessel I and test vessel II were used. After mounting the heating device on both test vessels, 1.8 and 3.0 liters of degassed distilled water were poured into Vessel I (upward facing heater) and Vessel II (downward facing heater). Then, electric power was applied to the cartridge heaters to heat up the water. The heat flux q_W was adjusted to 330 kW/m^2 for both the upward- and downward-facing heaters. At this particular stage, the temperature of the copper blocks increased gradually to generate vapor bubbles on the heated surface. Then, the fluid reached the saturation temperature, and the block temperatures approached asymptotic values. In the experiments for the

downward-facing heater, the hot plate was also used to ensure saturated boiling. After the steady state was reached, 0.2 respectively 0.3 liters of nanofluid were added to the boiling water depending on the configuration. The mixture was stirred with a stick to obtain a uniform spatial distribution of the nanoparticle concentration in the vessel; the stirring time was about 3 seconds. The concentration of nanoparticles C was defined as the total mass of TiO_2 nanoparticles divided by the total volume of the test liquid supplied to the experimental vessel. The particle concentration varied from 0.004±0.01 to 0.40±0.01 kg/m^3 in the present experiment depending on the configuration. The temperatures in the heating block were monitored to obtain information regarding the effect of the nanoparticle deposition on the nucleate boiling heat transfer. After waiting for a prescribed time t_b from the addition of nanofluid, the cartridge heaters were turned off, and the test liquid containing nanoparticles was poured off to eliminate the chance of further boiling in the nanofluid. It was supposed that the deposition of nanoparticles on the heated surface occurred during the waiting time in this experimental step. The waiting time was therefore used as the definition of the boiling time in the nanofluid, t_b. The boiling time t_b was set to 1, 3, 10, 20, 40, and 60 minutes. From the elapsed time during stirring and pouring off the test liquid, the accuracy of t_b was estimated within 10s. After the block temperature decreased until it was less than 40 degrees Celsius due to the heat transfer with ambient air, the contact angle was measured again to obtain the information concerning the change of surface properties. Then, the experimental vessel was cleaned and refilled with degassed distilled water. The electric power applied to the cartridge heaters was increased gradually, and the value at which a sudden increase in the block temperature was detected was regarded as the CHF. An analog-to-digital converter attached to a personal computer was used to record the temperatures measured in the copper block, and test liquid and the electric power were upplied to the heaters every second.

4.3 Results and Discussion

4.3.1 Critical heat flux and mean contact angle

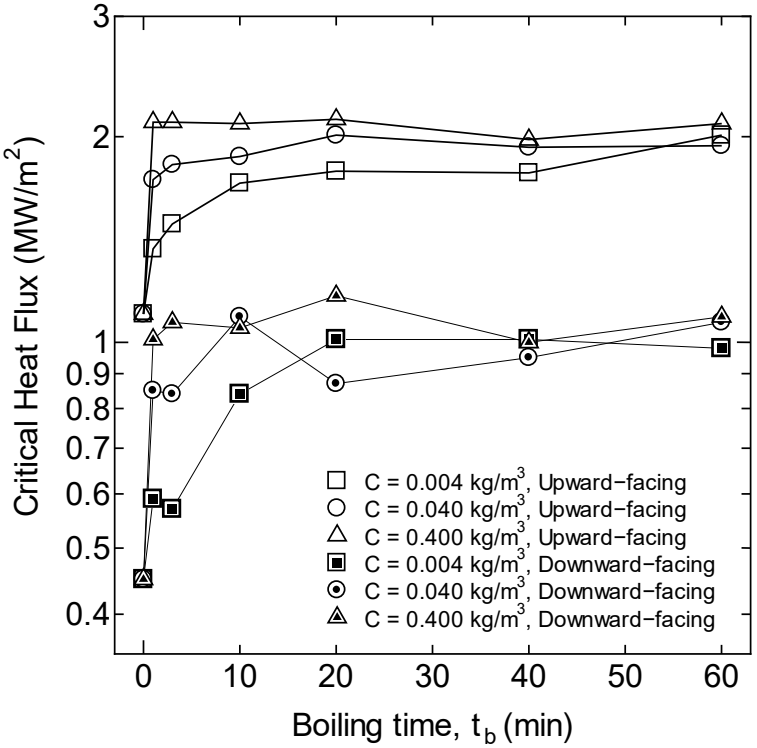

Fig. 4.1: Relation between boiling time and CHF

For the surfaces that did not experience boiling with nanofluid (t_b = 0), the CHF value was 0.47 MW/m^2 for the downward-facing heater was, 58 % less than for the upward-facing surface (1.14 MW/m^2). Also, the CHF value increased asymptotically with an increase in t_b in both the cases. The asymptotic CHF values for upward-facing and downward-facing heater obtained were 2.2 and 1.1 MW/m^2, respectively. Furthermore, the observed improvement varied depending on the nanofluid concentration and boiling time used.

The measured CHF value for the upward-facing and downward-facing heated surfaces at various concentrations and boiling time are shown in Fig. 4.1. From the figure, it can be comprehended that the downward-facing nanofluid-coated-heater had an approximately 50 percent lower CHF value compared to the upward-facing heater. Also,

the asymptotic critical heat flux enhancement is achieved after a boiling time of 10 minutes in both configurations (earlier in high concentration and slightly later for lower concentration).

In the upward-facing region, the buoyancy force removes the vapor from the heater surface in vertical direction. However, for the downward-facing heater, the vapor repetitively stratified and accumulated on the heater surface; the upward-facing heater did not experience these effects. The accumulation of a bubble layer upon the heater surface in downward-facing reduced the heat dissipation; thus, the heater absorbed the heat from the vapor. This consequentially contributed to the degradation of the critical heat flux.

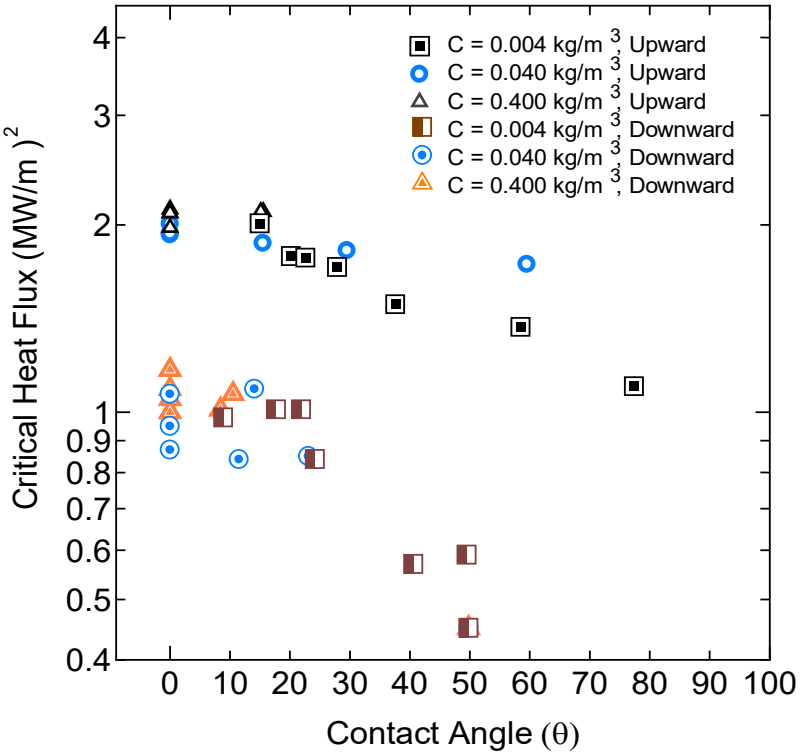

Fig. 4.2: Relation between contact angle and CHF

Fig. 4.2 shows the relation between the critical heat flux and the mean contact angle of the nanofluid-coated-surface for both upward- and downward-facing heaters. In the present study, the tabulated CHF data for both, the downward- and upward-facing heated surfaces show a strong relationship between the mean contact angle and CHF enhancement. One may infer that the heater surface could have changed due to the

deposited nanoparticles. The changes in the morphology of the heated surface are one of the primary factors for the critical heat flux enhancement. However, the CHF enhancement reached the asymptotic maximum value when the contact angle reduced to below 20° for all concentrations and orientations. Meanwhile, at lower contact angles, the reduction in wettability showed a positive effect respective to the CHF enhancement.

4.4 Conclusion

The CHF of nucleate boiling in titanium oxide nanofluid pool boiling under various concentrations in upward- and downward-facing heaters has been extensively investigated. The reduction of the CHF in the downward-facing heater compared to the upward- was by 50% in the bare heater surface condition. The CHF enhancements were observed faster for the higher concentration (C = 0.4 kg/m^3), slower for the low concentrations. The CHF was enhanced with nanofluids concentration as low as C = 0.004 kg/m^3. The higher concentrations led to faster CHF enhancement for both orientations. The maximum CHF enhancements in the nanofluid in various concentration for CHF for upward- and downward-facing heaters were 2.1 and 1.9 times, respectively. Both orientations of the heater surface demonstrated a similar magnitude of the CHF enhancement rate in nanofluids.

The reduction of the mean contact angle showed an enhancement of the critical heat flux for both upward-facing and downward-facing heaters. For the asymptotic CHF values, the mean contact angle was below 20° for both the upward-facing and downward-facing heaters.

CHAPTER 5 EFFECT OF NANOPARTICLE-MATERIALS, CONCENTRATIONS AND DISPERSION CONDITIONS

5.1 Introduction

This chapter deals with the effects of the nanoparticles' material, concentration and dispersion condition on the heat transfer characteristics of nucleate pool boiling in water-based nanofluids. For the boiling heat transfer, the time-variation of the wall superheat, the boiling curve and the critical heat flux are discussed. Some peculiarities during the experimental work, the detachment of layers of nanoparticles as well as abnormal temperature spikes are also explained in detail.

5.2 Description of the preparation of the experimental

In the present study, TiO_2, Al_2O_3 and SiO_2 were used as nanoparticle materials. The following three types of nanoparticles of (all white color, manufactured by Aerosil Corporation) were used to prepare the nanofluids:

(1) Aeroxide TiO_2 P 25, TiO_2 particles that are a mixture of anatase (80%) and rutile (20%) crystal structures with average primary particle diameter d_p of 21 nm),

(2) Aeroxide Alu C (Al_2O_3 (Alumina) particles with d_p of 13 nm),

(3) Aerosil 90 (SiO_2 (Silica) particles with d_p of 20 nm).

Two different sonication times were used to prepare the dispersion, 1 hour and 5 hours for coarse and fine dispersion, respectively. Three variations of the concentration, C of 0.04, 0.4 and 1 kg/m^3 were used. The experimental setups are summarized in Table 5.1.

Table 5.1: Main experimental conditions and parameters

Run	Particle material	Boiling time t_b [hour]	Concentration, C [kg/m^3]	Dispersion condition t_{us} [hour]	Base fluid used during the CHF measurement
1	TiO_2	1 hr	0.04	1 hr	Nanofluid
2				5 hr	Nanofluid
3			0.4	1 hr	Nanofluid
4				5 hrs	Nanofluid
5			1	1 hr	Nanofluid
6				5 hrs	Nanofluid
7	Al_2O_3	1 hr	0.04	1 hr	Nanofluid
8				5 hr	Nanofluid
9			0.4	1 hr	Nanofluid
10				5 hrs	Nanofluid
11			1	1 hr	Nanofluid
12				5 hrs	Nanofluid
13	SiO_2	1 hr	0.04	1 hr	Nanofluid
14				5 hr	Nanofluid
15			0.4	1 hr	Nanofluid
16				5 hrs	Nanofluid
17			1	1 hr	Nanofluid
18				5 hrs	Nanofluid
19	TiO_2	1 hr	0.4	1 hr	Distilled water
20	SiO_2	1 hr	0.4	1 hr	Distilled water
21			1	1 hr	Distilled water

Table 5.2: Experimental condition for the detachment investigation

Run	Particle material	Concentration, C [kg/m^3]	Dispersion condition t_{us} [hour]	q_W, [MW/m^2] (Maximum q_W applied)
1	TiO_2	0.4	1 hr	1.1
2				1.4
3	SiO_2	0.4	1 hr	1.4
4				1.6

The nanoparticles were mixed with 100 ml of distilled water in a cup and placed in the ultrasonic bath (CPX2800H-J, Branson) to perform ultrasonic excitation to obtain a uniform dispersion of nanoparticles. The particle concentration in the bath was set to 0.8, 8 and 20 kg/m^3. As will be described later, 75 ml of this nanofluid were injected into 1425 ml of boiling water in the test vessel to measure the heat transfer characteristics. As a result, the particle concentration C was reduced to 1/20 in the vessel and the final concentration obtained was 0.04, 0.4 and 1 kg/m^3, respectively.

5.3 Dispersion condition

In nanofluids, the primary particles commonly aggregate into larger agglomerates. The excitation time in the ultrasonic bath t_{us} was set to 1 respectively 5 hrs to obtain different dispersion conditions. The distribution of the aggregate size was measured using the fiber-optics particle analyzer (FPAR-1000, Otsuka Electronics). Figs 5.1 (a)-(i) compare the aggregate size distributions for short (1 hr) and long (5 hrs) excitation times for different materials and concentrations of nanoparticles. The values of the Sauter mean diameter d_{sm} is also presented in the figures. For the results of t_{us} = 5 hrs, all the aggregate size distributions have single peaks in the size dispersion except for Fig. 5.1 (f) in which a second peak of small magnitude is found (at 20 nm); the range of d_{sm} is slightly greater in SiO_2-water nanofluids than in TiO_2- and Al_2O_3-water nanofluids (95-119 nm for TiO_2 and Al_2O_3 and 127-188 for SiO_2). No clear dependence of d_{sm} on the particle

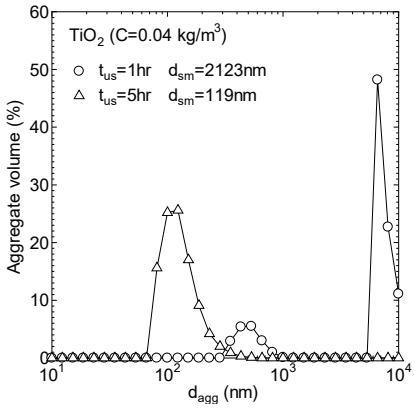

(a) TiO_2; $C = 0.04$ kg/m^3

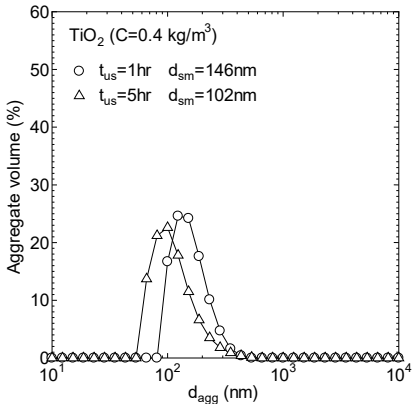

(b) TiO_2; $C = 0.4$ kg/m^3

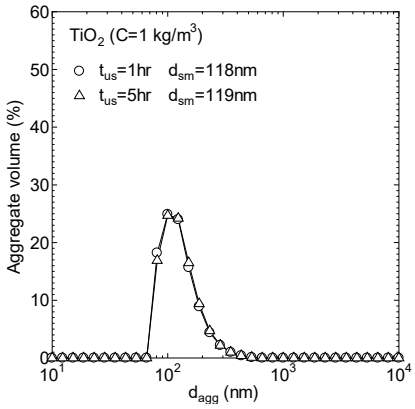

(c) TiO_2; $C = 1$ kg/m^3

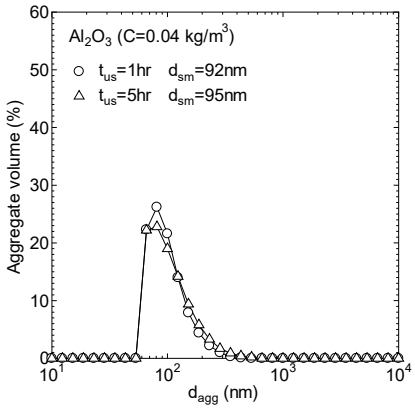

(d) Al_2O_3; $C = 0.04$ kg/m^3

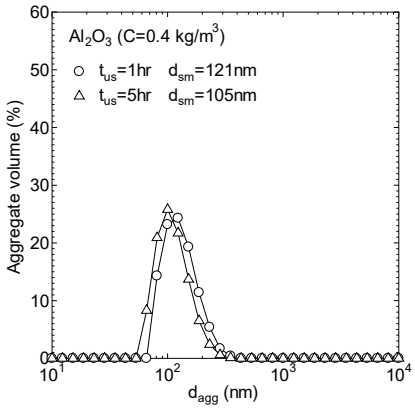

(e) Al_2O_3; $C = 0.4$ kg/m^3

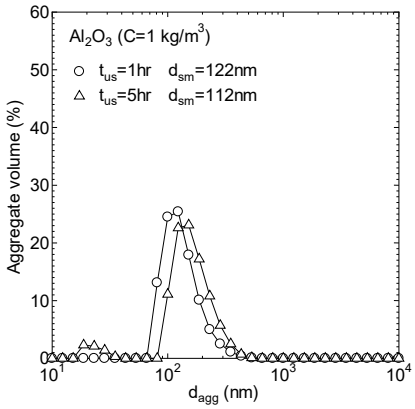

(f) Al_2O_3; $C = 1$ kg/m^3

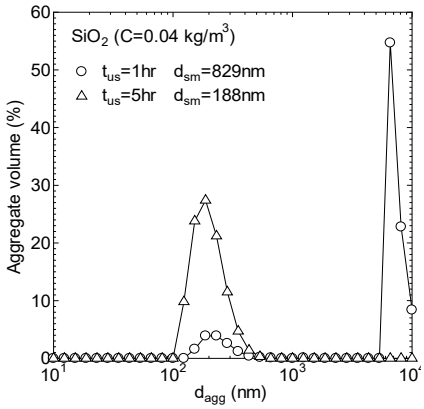

(g) SiO_2; $C = 0.04$ kg/m^3

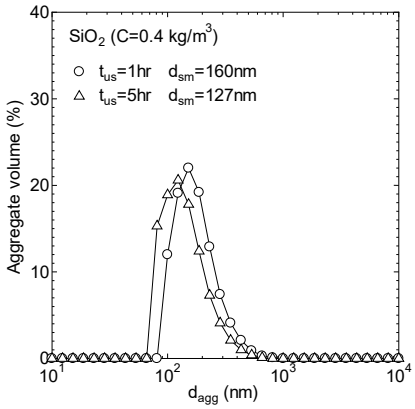

(h) SiO_2; $C = 0.4$ kg/m^3

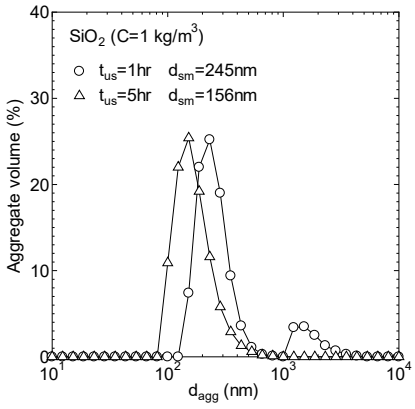

(i) SiO_2; $C = 1$ kg/m^3

Fig. 5.1: Fractional aggregate volume vs. aggregate size

concentration C is found. The distributions for t_{us} = 1 hr are similar to those for t_{us} = 5 hrs in Figs. 5.1 (c), (d) and (f) but are slightly shifted to the right in Figs. 5.1 (b), (e) and (h). In particular, the signature of considerably large aggregates of 1-10 μm in size can be seen in Figs. 5.1 (a), (g) and (i). This implies that 1 hr is not enough to obtain a stable particle dispersion, and the particle dispersion condition is fairly different in nanofluids boiled for 1 and 5 hrs. The dispersion conditions obtained when t_{us} was 1 and 5 hrs were hence regarded as the coarse and fine dispersions, respectively, to preliminarily investigate the effect of the particle dispersion condition on the heat transfer characteristics in saturated pool boiling of nanofluids.

5.4 Experimental procedure

The experiment began with the surface preparation as described in Section 3.4.2 of Chapter 3. In the present work, the test vessel III was used. After mounting the heating device on the test vessel, 1425 ml of distilled water was poured into the vessel, and electric power was applied to the cartridge heaters in the copper block; the heat flux q_W was adjusted to 600 kW/m^2. At this stage, electric power was also applied to the immersion heater to boil and degas the water. At the same time, the reflux condenser was used to return the vapor to the test vessel as liquid water. After about 15 minutes of degassing, the power to the immersion heater was reduced to the optimum level to keep the bulk fluid temperature at the saturation temperature. Then, the fluid temperature and the copper block temperatures changed asymptotically to the steady state. When the equilibrium state was reached, the value of the wall superheat, ΔT_W was calculated from the thermocouple data. Although the same experimental procedures were kept as in the other experiments, the scattering of ΔT_W was not negligible since the condition of the heated surface could not be kept unchanged. Hence, we moved to the next step only when wall temperature ΔT_W was within a range of 20±3 K to reduce the influence of the scattering of the initial wall superheat before adding the nanofluid.

When ΔT_W was within the desired range, 75 ml of nanofluid were added to the boiling water from a syringe in the hole of 15 mm in diameter on the top plate. Here, prior

to the addition of the nanofluid, the cup with the nanofluid was heated up in hot water to about 90 °C in order to reduce the temperature difference. After the addition of the nanofluid, the hole was closed again with the rubber plug, and the heating using the cartridge heaters was continued for 1 hr to record the time-variation of ΔT_W. After this, q_W was increased step by step to accumulate the data of ΔT_W to draw the boiling curves. The increment of q_W was within 50-100 kW/m^2 and q_W was maintained for 400 to 600 s in each step to obtain the steady state. The experimental run was finished when a sudden increase of the block temperature was detected or the block temperature reached the maximum allowable limit. The value of q_W just before the sudden increase of the block temperature was regarded as the CHF.

The electric power applied to the cartridge heaters and the immersion heater were controlled and monitored using voltage transformers and digital multimeters, respectively. An analog-to-digital converter (CADAC 3, Eto Denki) attached to a personal computer was used to record the copper block temperatures, the liquid temperature and the electric power supplied to the cartridge heaters every second.

5.5 Results and discussion

5.5.1 Time-variation of wall superheat

The time variation of wall superheat after adding the nanofluid is presented in Figs. 5.2 (a)-(i). Here, $t_b = 0$ denotes to the time at which the nanofluid was added. As the base case, 75 ml of distilled water was added to the boiling water. Although the temperature of the added water was about 10 K lower than the saturation temperature, the addition of the distilled water caused no noticeable variation of ΔT_W. However, ΔT_W varied significantly after the addition of the nanofluid. The trend of the time-variation of ΔT_W is similar for the coarse and fine dispersions (t_{us} = 1 and 5 hrs), while the effects of the nanoparticles' material and concentration are significant. In most cases in the present experiments, ΔT_W decreased rapidly immediately after the addition of the nanofluid and then increased asymptotically, see Fig. 5.2 (d) for a typical case. The amounts of initial decrease and asymptotic increase are however different depending on the material and

concentration of nanoparticles. In particular, the initial decrease is not observed for SiO_2 in high particle concentration in Figs. 5.2 (h) and (i) while the asymptotic increase in the later stage is negligibly small for Al_2O_3 of high particle concentrations in Figs. 5.2 (e) and (f). The initial decrease is more significant than the asymptotic increase for Al_2O_3 but less significant for SiO_2. In consequence, for all nanoparticle concentrations, the value of ΔT_W in the steady state is lower than the initial value before the addition of nanofluid for Al_2O_3 but higher for SiO_2 (Figs. 5.3 (g)-(i)). It can therefore be said that under the present experimental conditions, the boiling heat transfer is enhanced by Al_2O_3 but deteriorates with SiO_2. For TiO_2, the amount of asymptotic increase of ΔT_W in the later stage varies considerably depending on the nanoparticle concentration. Consequently, the equilibrium value of ΔT_W is higher than the initial value at the lowest concentration in Fig. 5.2 (a) but lower at the higher concentrations in Figs. 5.2 (b) and (c).

Since ΔT_W decreased immediately after the addition of the nanofluid, it is possible that the deposition of a small amount of nanoparticles on the heated surface contributed to increase the number of active nucleation sites and enhanced the boiling heat transfer. A further support of this hypothesis is an extra experiment that was performed using a different apparatus to visualize the bubble nucleation process. The description and result of this experiment are presented in the Chapter 7. As already mentioned, in most cases in the present experiment, ΔT_W increased asymptotically after the initial decrease and reached the steady state. This indicates that the deposition of a larger amount of nanoparticles causes the deterioration of boiling heat transfer. It is plausible that the nanoparticle layer acted as a thermal insulation material or the nucleation sites were deactivated by the sedimentation of nanoparticles.

The present results show that the same nanofluid leads to competing effects which depending on the circumstances either enhance or decrease the nucleate boiling heat transfer. This can be considered to be one of the reasons why small changes in experimental conditions may cause a significant difference in the effect the nanofluid has on the boiling heat transfer. It is also noted that a long time was needed to reach the steady state for ΔT_W in several experimental conditions. For example, in the cases shown in Fig. 5.2 (b), ΔT_W kept increasing even after 1 hr from the addition of nanofluid. This would be another reason of the scattering in the boiling heat transfer data of nanofluids reported in the literature.

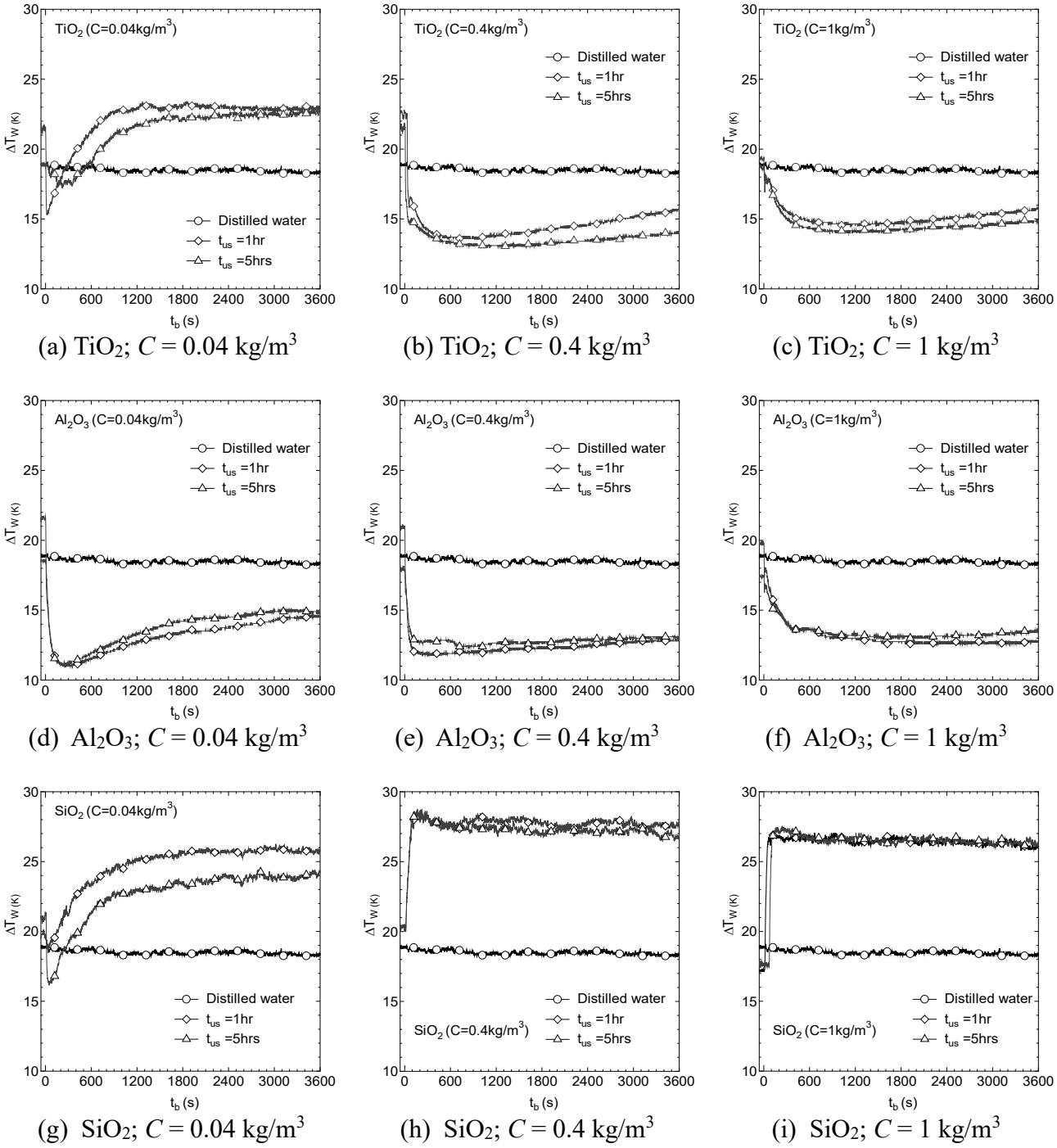

(a) TiO_2; $C = 0.04$ kg/m^3 (b) TiO_2; $C = 0.4$ kg/m^3 (c) TiO_2; $C = 1$ kg/m^3

(d) Al_2O_3; $C = 0.04$ kg/m^3 (e) Al_2O_3; $C = 0.4$ kg/m^3 (f) Al_2O_3; $C = 1$ kg/m^3

(g) SiO_2; $C = 0.04$ kg/m^3 (h) SiO_2; $C = 0.4$ kg/m^3 (i) SiO_2; $C = 1$ kg/m^3

Fig. 5.2: Time-variation of wall superheat after adding the nanofluids (q_W= 600 kW/m^2)

5.5.2 Boiling curves

Figs. 5.3 (a)-(f) show the boiling curves for the nanofluids of different materials, concentrations and dispersion conditions (t_{us}); the measured CHFs are indicated with double line symbols. In the figures, the Stephan-Abdelsalam (S-A) correlation [14] and the boiling curve for distilled water are also given for comparison. It can be seen that for the distilled water, the boiling curve is in fairly good agreement with the Stephan-Abdelsalam (S-A) correlation and the value of CHF is about 0.7 MW/m^2.

First, it can be seen that as in the case of the time-variation of ΔT_W, the boiling curves are not influenced significantly by the dispersion condition of the nanoparticles within the range tested in this work. For Al_2O_3 and SiO_2 (Figs. 5.3 (c)-(f)), the boiling curves are roughly parallel to the S-A correlation for all the nanoparticle concentrations except for the results of SiO_2 in the high heat flux range. In consequence, for all values of the heat flux, the boiling heat transfer is increase in comparison with the S-A correlation for Al_2O_3 while it decreased for SiO_2. For TiO_2, see Figs. 5.3 (a) and (b), however, the slope of the boiling curve is steeper at the lowest concentration of 0.04 kg/m^3. In consequence, although the value of ΔT_W is higher at the lowest concentration in the low heat flux range, it becomes higher when the heat flux reaches about concentrations of 0.4 and 1 kg/m^3 at the heat fluxes higher than 1.4 MW/m^2. It can hence be said that the boiling heat transfer enhancement by nanofluid depends on various parameters including the material of the nanoparticles, the concentration, the boiling time and the heat flux.

It should be noted that peculiar boiling curves were obtained in several experimental conditions. In most experiments with SiO_2, ΔT_W increased remarkably when q_W exceeded about 1.5 MW/m^2. Since not the whole boiling curves could be fitted into Figs. 5.3 (e) and (f), the whole curve was shown with extended axes in Figs. 5.4 (a) and (b), respectively. These figures indicate that when C was 0.4 kg/m^3, ΔT_W reached the particularly high value of 175 K before the onset of CHF condition (the CHF could not be measured in these cases since the copper block temperature had reached the maximum allowable limit). The conditions during the experiment under which the peculiar boiling curves were obtained, i.e. the time-variation of the electric power applied to the cartridge heaters Q and the copper block temperature measured at 5 mm below the heated surface

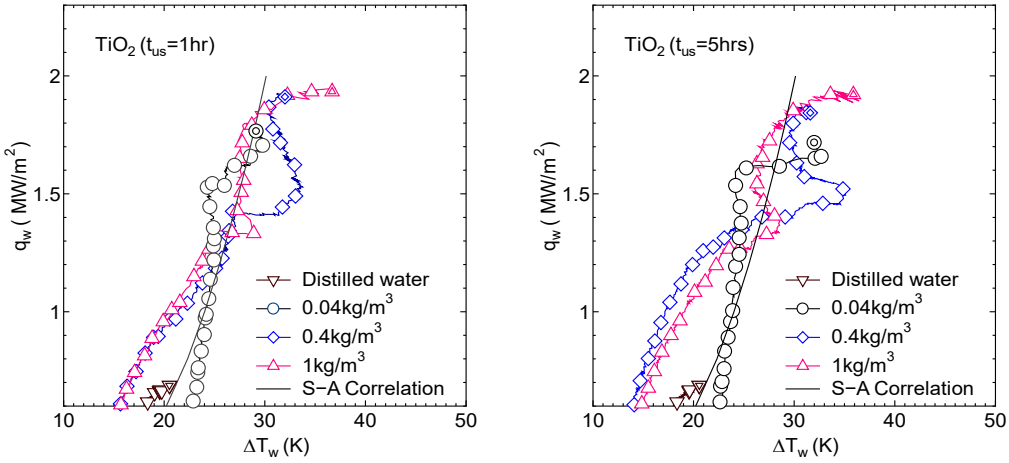

(a) TiO_2; t_{us} = 1 hr

(b) TiO_2; t_{us} = 5 hrs

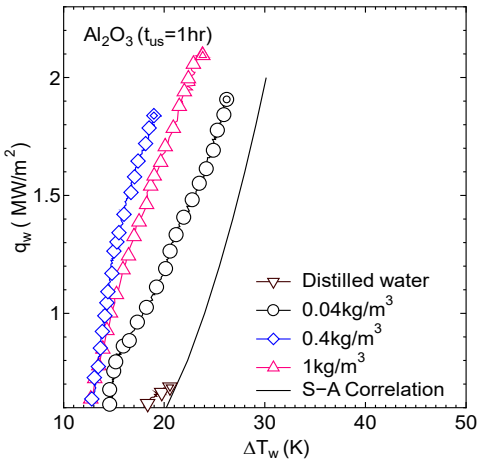

(c) Al_2O_3; t_{us} = 1 hr

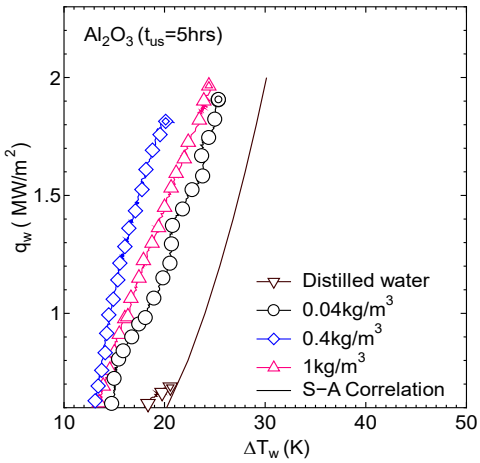

(d) Al_2O_3; t_{us} = 5 hrs

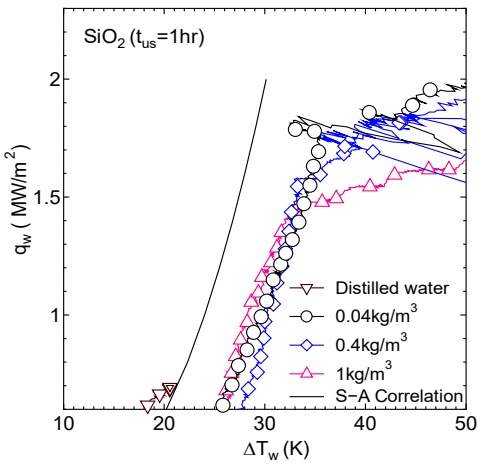

(e) SiO_2; t_{us} = 1 hr

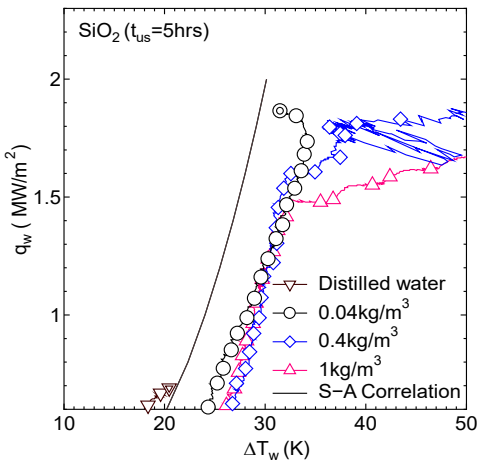

(f) SiO_2; t_{us} =5 hrs

Fig. 5.3: Boiling curves: the double lined symbols correspond to the CHF

T_1, are displayed in Figs. 5.5 (a) and (b). Here, the experimental conditions are C = 0.4 kg/m^3 and t_{us} = 1 hr for SiO_2 nanoparticles. It can be seen that until 6000s, T_1 rises asymptotically after the stepwise increase of Q as expected. At 6000s, however, T_1 rises sharply to about 192°C despite the fact that Q is held constant as shown in Fig. 5.5 (a). The abnormally high value of T_1 is kept for more than 1 min and then T_1 drops asymptotically to the ordinary value within about 6100-6300s. This is the situation when the peculiar trend marked '(A)' in Fig. 5.4 (a) appears. After this, T_1 is unstable but increases to a higher temperature range before a steady state for each stepwise increment of Q is achieved. When T_1 reaches 310°C, the experiment was terminated to avoid damage to the experimental apparatus. This point is indicated as '(B)' in Fig. 5.4 (a). A peculiar trend is also seen for the TiO_2 nanofluids for which typical results at C = 0.4 kg/m^3 and t_{us} = 1, as well as 5 hrs, are shown in Fig. 5.3 (a) and (b). In this case, the boiling curve is fairly similar to the S-A correlation in the intermediate heat flux range of 1.1-1.4 MW/m^2. However, ΔT_W rises sharply within the range of 1.4-1.5 MW/m^2 and then returns to the previous range within 1.5-1.9 MW/m^2; ΔT_W increases slightly before the CHF condition is reached.

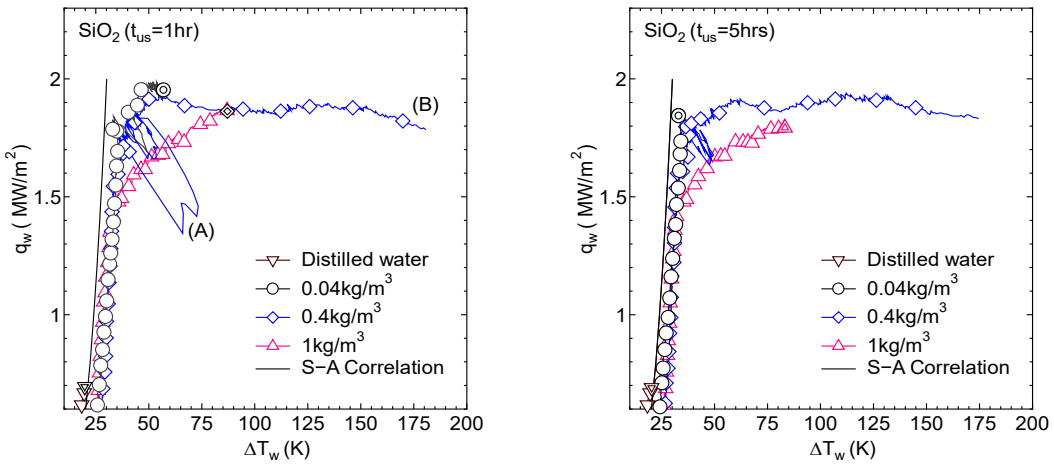

(a) SiO_2; t_{us} = 1 hr (b) SiO_2; t_{us} =5 hrs

Fig. 5.4: Boiling curves for the SiO_2-water nanofluids (the horizontal axes are extended; the double lined symbols correspond to the CHF)

(a)

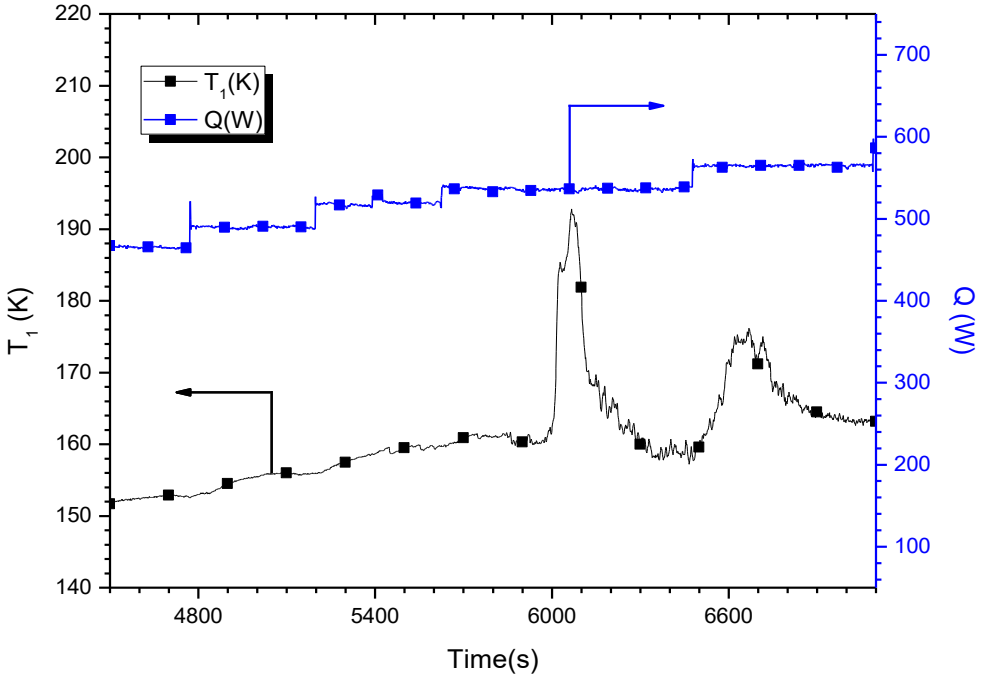

(b)

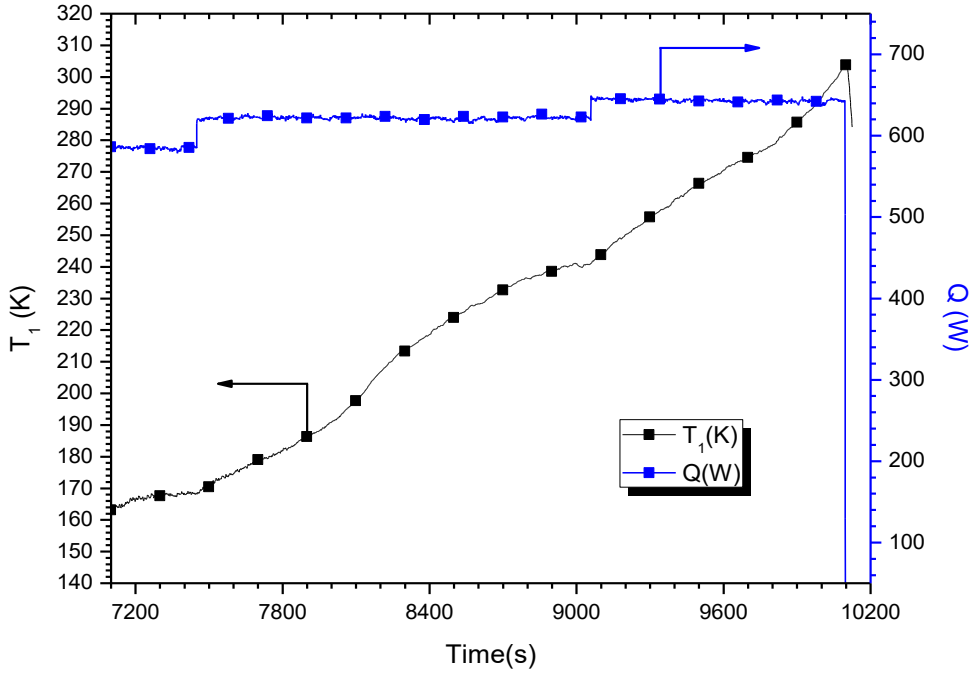

Fig. 5.5: Extracted time variation of SiO_2 wall superheat at high heat flux; (a) abnormal spike of T_1,(b) large scale stepwise increment of T_1 at constant Q

5.5.3 Nanoparticle layer detachment from the heated surface

To explore the mechanisms which cause the various peculiar trends in the boiling curves, the boiling heat transfer was measured for the nanoparticle-coated surface immersed in distilled water. In this experiment, nucleate boiling at 600 kW/m^2 was kept up for the nanofluid during 1 hr as described in Section 5.5.1 to enable the nanoparticle deposition on the heated surface. Then, the nanofluid in the vessel was exchange with distilled water. After the distilled water had been degassed with the immersion heater, the heat flux was increased step by step to accumulate the data for the boiling curves. The resulting boiling curve for TiO_2 of C = 0.4 kg/m^3 and those for SiO_2 of C = 0.4 and 1 kg/m^3 are presented in Figs. 5.6 (a) and (b), respectively. For comparison, the boiling curves the nanofluids are also shown in the figures. It can be seen that the boiling curves for the nanoparticle-coated surface in the distilled water are fairly parallel to the S-A correlation for all the three cases tested in this work. It can therefore be concluded that nucleate boiling in nanofluids at high heat flux is necessary so that the peculiar temperature rise can occur.

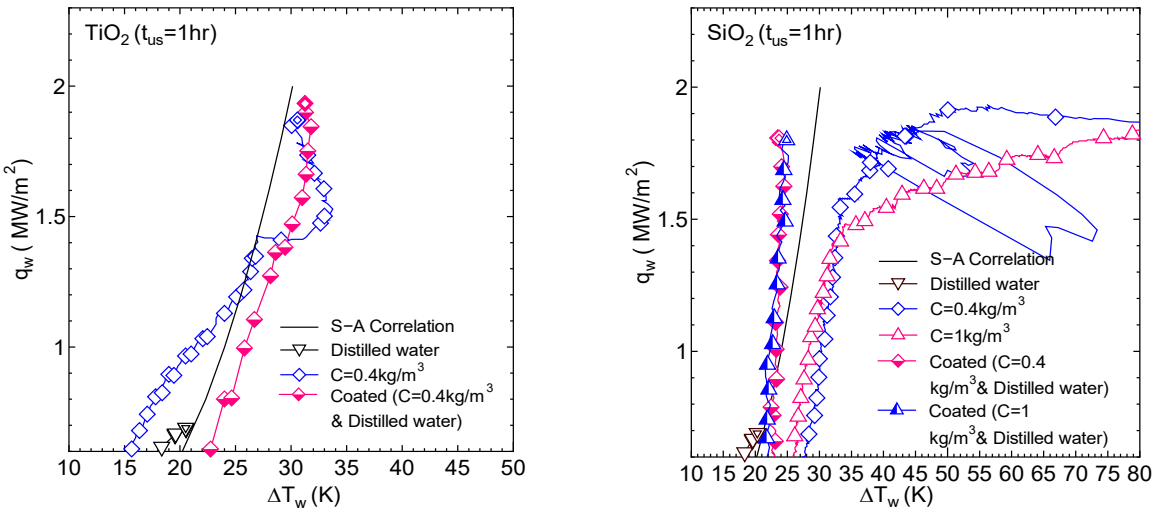

(a) TiO_2; C = 0.4 kg/m^3 (b) SiO_2; C = 0.4 and 1 kg/m^3

Fig. 5.6: Comparison of the boiling curves performed in nanofluids and nanoparticles-deposited heated surface (experiment were performed using nanoparticle-deposited heated surface with nucleate boiling time, t_b = 1hr), (double lined symbols correspond to the CHF)

The photos of the heated surface taken at several experimental stages for the TiO_2 and SiO_2 nanofluids of moderate particle concentration (C = 0.4 kg/m^3) are depicted in Figs. 5.7 and 5.8, respectively. Fig. 5.7 (a) indicates that the heated surface was totally covered by the nanoparticle layer after the nucleate boiling in the TiO_2 nanofluid at 600 kW/m^2 for 1 hr. As depicted in Fig. 5.7 (b), the surface condition before the onset of the peculiar temperature rise at q_W = 1.1 MW/m^2 is not significantly different from that in Fig. 5.7 (a). In the photo taken after the peculiar temperature rise at q_W = 1.4 MW/m^2 (Fig. 5.7 (c)), several defects are found in the nanoparticle layer on the heated surface, however, in the surface condition after the CHF measurement shown in Fig. 5.7 (d), no such defects are found. The photos in Figs. 5.7 (b) and (c) were taken after the separate experiments in which heating was terminated when q_W reached 1.1 and 1.4 MW/m^2, respectively. These results indicate that the nanoparticle layer was partly detached from the heated surface when q_W was within 1.4-1.5 MW/m^2 but the defects were repaired when q_W was further increased. Fig. 5.7 (e) indicates that a small number of defects were present also after the CHF measurement in the distilled water.

In the case of SiO_2 nanofluids, the nanoparticle deposition occurred only around the nucleation cavities after nucleate boiling at 600 kW/m^2 for 1 hr (Fig. 5.8 (a)). After several stepwise increases of q_W to 1.4 MW/m^2, the surface was totally covered by the nanoparticle layer (Fig. 5.8 (b)). However, after the peculiar temperature rise at about 1.6 MW/m^2, the detachment of a significant layer of nanoparticles was detected which is shown in Fig. 5.8 (c). It can be seen that the detached nanoparticle layer was not repaired even when the copper block temperature reached the maximum allowable limit (Fig. 5.8 (d)). On the other hand, the surface condition after the CHF measurement in distilled water (Fig. 5.8 (e)) is similar to the initial condition shown in Fig. 5.8 (a).

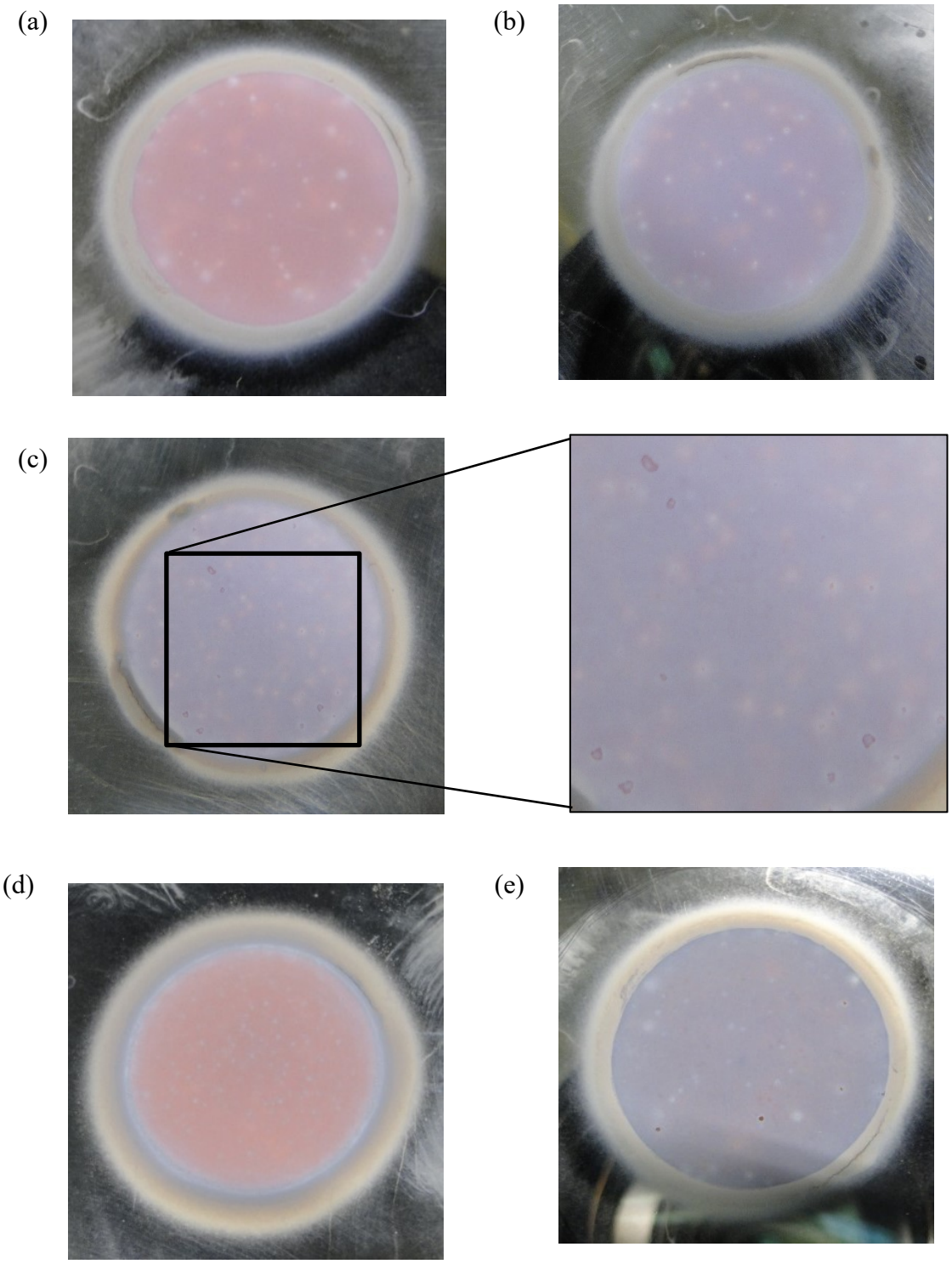

Figs. 5.7: Photos of heated surfaces deposited with TiO_2 (C=0.4 kg/m^3 and t_{us} = 1 hr); (a) After the surface preparation with q_W = 600 kW/m^{2}and t_b = 1 hr, (b) before the onset of the peculiar temperature rise, (c) after the onset of the peculiar temperature rise, (d) after the CHF measurement in nanofluid, and (e) after the CHF measurement in distilled water.

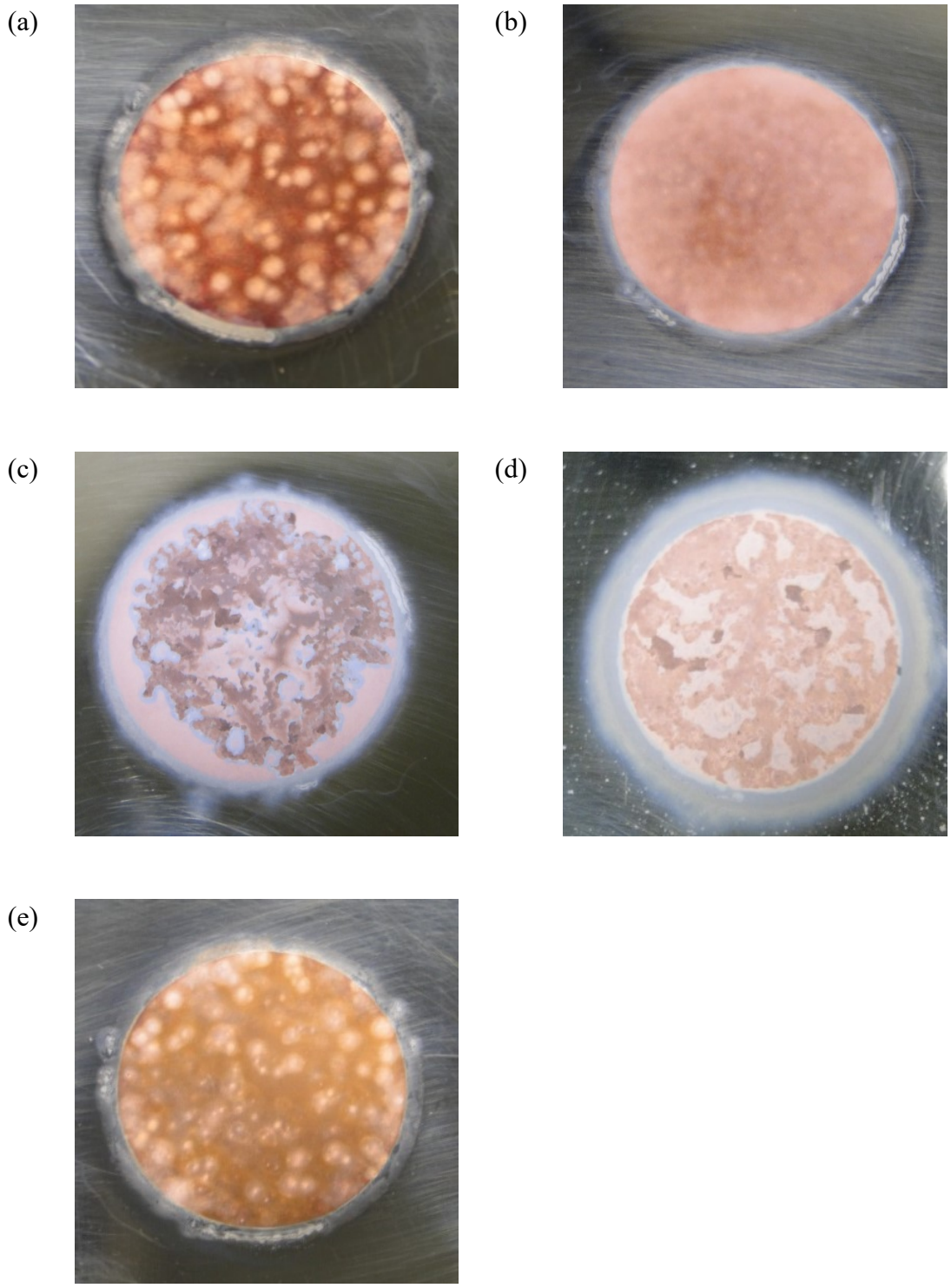

Figs. 5.8: Photos of heated surfaces deposited with SiO_2 (C=0.4 kg/m^3 and t_{us} = 1 hr); (a) After the surface preparation with q_W = 600 kW/m^{2}and t_b = 1 hr, (b) before the onset of the peculiar temperature rise, (c) after the onset of the peculiar temperature rise, (d) after the CHF measurement in nanofluid, and (e) after the CHF measurement in distilled water.

In the observation of the heated surface presented above, the detachment of the nanoparticle layer was always detected when the wall superheat was abnormally high (Figs. 5.7 (c), 5.8 (c) and (d)) while no such defect was found before the peculiar temperature rise and after the return to normal temperatures. One exception can be seen in Fig. 5.7 (e). The photo was taken after the CHF measurement in distilled water for a surface on which a TiO_2 layer had been deposited. In this case, the peculiar temperature rise did not occur, but several defects were found after the experiment. Obviously, further studies are needed to clarify the mechanism of the significant deterioration of boiling heat transfer in nanofluids. The present results however indicate that the significant rise of the wall superheat is likely to occur when a partial detachment of the nanoparticle layer occurs. We conclude that the formation of the defects in the nanoparticle layer may lead to the deterioration of the nucleate boiling heat transfer.

5.5.4 Critical heat flux

The measured CHFs are plotted against the particle concentration in Fig. 5.9. It is noted that in this figure, the highest heat flux during the experiment was plotted for the SiO_2 nanofluids of C = 0.4 kg/m^3 since the block temperature reached the maximum allowable limit before the CHF condition was reached. The values of CHF measured in the nanofluids are within 1.74-2.1 MW/m^2 and therefor 2.5-3 times higher than that in distilled water (0.7 MW/m^2). The highest CHF was measured for the Al_2O_3 nanofluid of C = 1 kg/m^3 and t_{us} = 1 hr. It seems that the CHF tended to increase slightly with an increase in C, but no clear dependence of CHF on the material and concentration of nanoparticles is found. It is interesting to note that although a significant nanoparticle layer detachment as shown in Fig. 9 (d) was observed, after all CHF measurements in the SiO_2 nanofluids the CHFs for SiO_2 nanofluids are comparable to those for TiO_2 and Al_2O_3 nanofluids. We conclude that the detachment of the nanoparticle layer may deteriorate the boiling heat transfer significantly but its influence on the CHF is not noticeable.

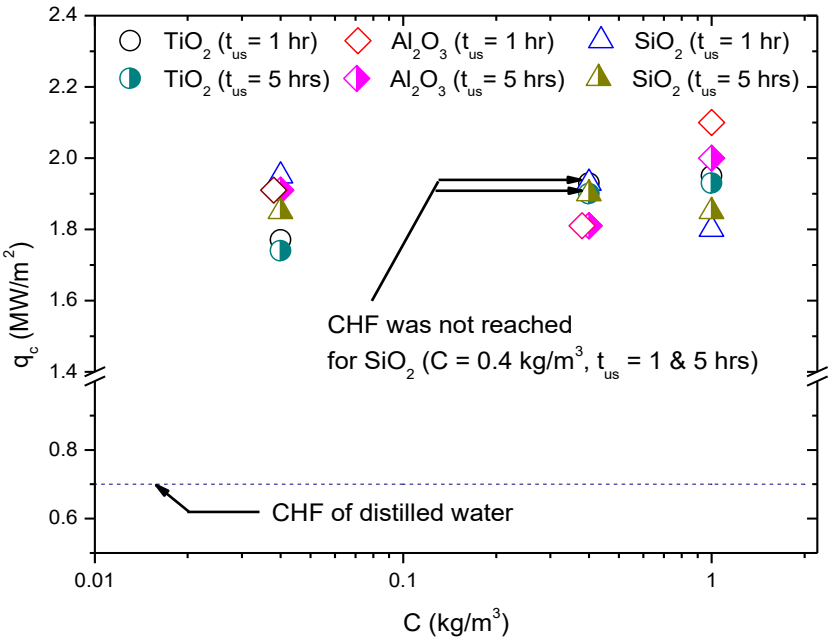

Fig. 5.9: Critical heat flux vs. nanoparticle concentration for different materials and dispersion conditions of nanoparticles (the data for both t_{us}= 1hr and 5hrs of SiO_2 at C = 0.4 kg/m^3 are not for the CHF but for the heat flux at which the copper block temperature reached the maximum allowable limit)

5.6 Conclusions

Experiments were performed to investigate the effects of the nanoparticles' material, concentration and the dispersion condition on the boiling heat transfer characteristics in saturated pool boiling of water-based nanofluids. The heat transfer characteristics studied in this work were the time-variation of the wall superheat during nucleate boiling, the boiling heat transfer (boiling curve) and the CHF. The main conclusions of this work are summarized as follows:

In most cases in the present experiment, the wall superheat first dropped rapidly and then rose asymptotically with the increase of the boiling time of the nanofluid. It can hence be said that the same nanofluid can increase or decrease the boiling heat transfer depending on the boiling time. The temperature drop was greater than the temperature rise for Al_2O_3 nanofluids but smaller for SiO_2 nanofluids. In consequence, the Al_2O_3 nanofluids increase while the SiO_2 nanofluids decrease it. The effect of the TiO_2 nanofluid

on the boiling heat transfer in the equilibrium state was depended on the nanoparticle concentration. The effect of the nanoparticles' dispersion was not noticeable in the experimental range tested in this work. It was also found that extremely long times may be necessary that the wall superheat reached the steady state, which is probably one of the main reasons for the inconsistencies in the boiling heat transfer data reported in the literature.

An abnormal increase of the wall superheat was observed for the TiO_2 and SiO_2 nanofluids when the heat flux was sufficiently high. It can be concluded that this phenomenon is related to the partial detachment of the nanoparticle layer formed on the heated surface since the defects of the nanoparticle layer could be always detected when such a temperature rise took place.

The CHF in the nanofluid was several times higher than that in distilled water in all the experimental conditions tested in this work. The maximum CHF was measured for the Al_2O_3 nanofluid of the highest particle concentration. Although significant cases of detached nanoparticle layers were found after the CHF measurement for the SiO_2 nanofluids, the value of CHF was not significantly different from those for the TiO_2 and Al_2O_3 nanofluids.

CHAPTER 6 EFFECTS OF HEAT FLUX ON THE CRITICAL HEAT FLUX AND BOILING HEAT TRANSFER IN TiO_2 POOL BOILING

6.1 Introduction

In this chapter, the effect of heat flux density on the heat transfer characteristics (HTC) and critical heat flux (CHF) were investigated. Since the enhancements in nanofluid pool boiling depend on the nucleated bubbles, the influence of the CHF enhancement rate on the heat flux is significant. In view of the importance of the heat flux effect in Loss of Coolant Accidents (LOCA), experiments were performed to elucidate the effect of the heat flux on the boiling heat transfer enhancement in nanofluids. Thus, the emphasis of the present study is on the boiling time in nanofluids at the corresponding heat flux density. The CHF enhancement and boiling heat transfer with respect to heat flux are discussed in detail.

6.2 Experimental description

In the present experimental setup, a similar surface preparation method has been employed as described in Chapter 3 (Section 3.4.2) and some other experimental steps were similar to those described in Chapter 5. However, in the present experiment, four different levels of heat flux were applied, from low to high heat flux in the saturated pool boiling. The heat flux applied was at 150, 300, 450 and 600 kW/m^2. The boiling time, t_b varied between 1, 3, 10, 20, 40 and 60 minutes. The concentration of nanofluids was selected based on the findings in Chapter 4: When the boiling with the nanofluids was performed with a higher concentration of 0.4 kg/m^3, the effects of CHF enhancement were instantly observed, in contrast to a lower concentration of 0.004 kg/m^3 which showed slower CHF enhancement. Therefore, the medium concentration of C = 0.04 kg/m^3 was selected as it could be expected to be the ideal concentration for the heat flux investigation. The primary experimental conditions are shown in Table 6.1.

Table 6.1: Main experimental conditions for the investigation of heat flux density effects

Run	q_W [kW/m^2]	t_b [min]	C [kg/m^3]	Type
1	150	1	0.04	Type II
2		3		(TiO_2)
3		10		
4		20		
5		40		
6		60		
7	300	1	0.04	Type II
8		3		(TiO_2)
9		10		
10		20		
11		40		
12		60		
13	450	1	0.04	Type II
14		3		(TiO_2)
15		10		
16		20		
17		40		
18		60		
19	600	1	0.04	Type II
20		3		(TiO_2)
21		10		
22		20		
23		40		
24		60		

The first step in the experimental procedure was the preparation of the nanofluids by the one-step method in order to have a stable and uniform dispersion of TiO_2. The TiO_2 nanofluids used were from Aerosol Corporation (Aeroxide AERO DISP W 740 X, 40 wt. %) and diluted in distilled water. For each experiment, 15 ml of nanofluid were prepared and added to the vessel with a syringe. The mean particle diameter reported by the manufacturer was 21 nm and the size was confirmed with a TEM micrograph from dried samples of the nanofluid. Further, in order to determine the dispersion stability of nanoparticles before and after the experiment, a device (ELSZ-1000 series) that is capable of measuring the Zeta Potential and particle size provided by Photal Otsuka Electronics was used.

The next step of the experiment was the preparation of the heated surface (similar to the preparation method discussed in Chapters 3, 4 and 5. Following the surface preparation, the heating device was mounted on the test vessel. Next, 1.485 liters of distilled water were supplied to the vessel. The distilled water was degassed with an immersion heater of power 1 kW power for 15 minutes. At a later stage, the power supplied to the immersion heater was reduced to the optimum level, sufficient to keep the bulk liquid in the saturated condition. Then, the cartridge heaters were powered up to the prescribed heat flux. In this experiment, the heat flux q_W was adjusted to 150, 300, 450 and 600 kW/m^2 for the measurement of the data series. After it could be confirmed that the heater block had reach a steady state, the nanofluid was added to the boiling water. A particle concentration of $C = 0.040 \pm 0.01$ kg/m^3 was used in the present experiment. The temperatures at several locations in the heating block were monitored to obtain the information regarding the effect of the nanoparticle deposition on the nucleate boiling heat transfer. After waiting for a prescribed boiling time following the addition of the nanofluid, the cartridge heaters and immersion heaters were turned off, and the test liquid containing the nanoparticles was poured off to eliminate further deposition of nanoparticles by boiling. It can be supposed that the deposition of the nanoparticles on the heated surface occurred during the prescribed boiling time in this experimental step. The waiting time was therefore used as the boiling time in the nanofluid. The boiling times t_b were set to 1, 3, 10, 20 40 and 60 minutes. After the block temperature decreased below 40 degrees Celsius due to the cooling in ambient air, the contact angle was measured again to obtain the information concerning the change of surface properties.

Then, the vessel was cleaned and refilled with degassed distilled water. The electric power applied to the cartridge heaters was increased gradually, and the value at which the sudden increase in the block temperature was detected was treated as the CHF. An analog-to-digital converter attached to a personal computer was used to record the temperatures measured in the copper block and the test liquid every second.

6.3 Results and Discussion

6.3.1 Critical heat flux enhancement and heat flux densities

Fig. 6.1 represents the CHF enhancement with respect to the boiling time in nanofluids at four different values for the heat flux. The CHF value of the heater surface without experiencing nucleate boiling in the nanofluid was 0.7 MW/m^2.

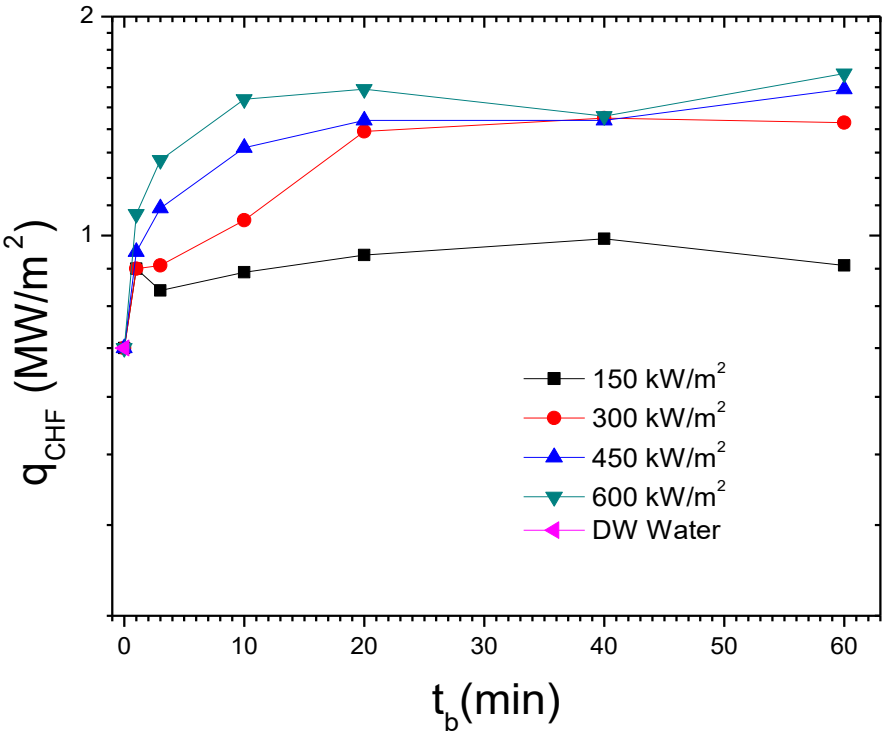

Fig. 6.1: Relation between CHF value and boiling time t_b at different heat flux density

The data for critical heat flux enhancement after experiencing boiling in the nanofluid for a prescribed time and heat flux are shown in Fig. 6.1. Here, the heater surface was coated with a nanofluid bath at a concentration of C = 0.01 kg/m^3, and four different levels of heat flux were applied within prescribed times, at 1, 3, 10, 20, 40 and 60 minutes. Later, the CHF value of the heated surface was successively measured by using distilled water. Fig. 6.1 shows that the CHF enhancement significantly depended on the heat flux, especially for the smaller boiling times in a nanofluid. However, the enhancement rate decreased gradually until it reached the asymptotic steady state value of approximately 1.7 MW/m^2. Here, the highest applied heat flux, q_W = 600 kW/m^2, shows faster CHF enhancement compared to the moderate applied heat flux (q_W = 450 kW/m^2 and 300 kW/m^2) and subsequently reached the asymptotic steady state in most cases. For instance, the applied heat flux of 600 kW/m^2 shows a significant increase in the CHF which reached the asymptotic steady state value after 10 minutes, while for 450 kW/m^2 and 300 kW/m^2 it occurred within 20 minutes. However, an exception can be seen for the minimum applied heat flux, with the lowest boiling intensity of q_W = 150 kW/m^2 which exhibits a relatively low CHF enhancement, and stochastic behavior. In this case, the asymptotic steady state could not even be reached after boiling in the nanofluid for 60 minutes.

Based on the previous study by Okawa et al. [86], empirical correlations were proposed to relate the dimensionless CHF enhancement, q_c^* and the amount of deposited nanoparticles with the heater surface in nanofluid boiling, Ct_b. However, that study [86] had used a single value of applied heat flux. Therefore, in the present study, an additional dimensionless applied heat flux had to be incorporated together with the amount of the deposited nanoparticles Ct_b, in order to account for the effect of the differing heat flux on the CHF enhancement.

The dimensionless CHF enhancement was defined by

$$q_c^* = \frac{q_c - q_{c0}}{q_{C,asy} - q_{c0}} \tag{6.1}$$

where $q_{C,asy}$ is the asymptotic value of CHF, q_c is the CHF value of the coated heater at the respective heat flux and boiling time and q_{c0} is the CHF value of the uncoated heater

(t_b = 0 min). The variable q_c^* was plotted against $q_w^* Ct_b$. The q_w^* is dimensionless heat flux is defined by

$$q_W^* = \frac{q_{hf}}{q_{max}} \tag{6.2}$$

where q_{hf} is heat flux applied during nanofluid boiling for the coated surface preparation, and q_{max} is the highest applied heat flux) and the results are shown in Fig. 6.2.

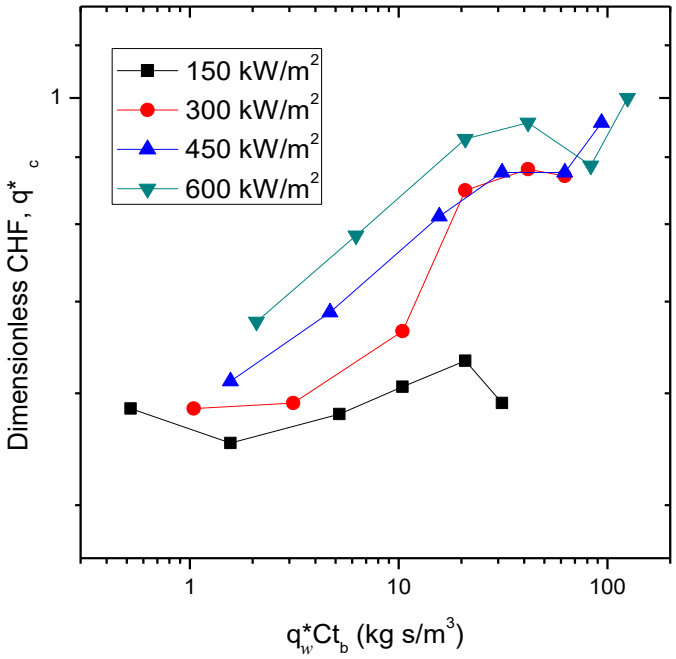

Fig. 6.2: Relation between the dimensionless CHF and the dimensionless heat flux q_w^* with boiling time and concentration C.

From Fig. 6.2, the relation between q_c^* and $q_w^* Ct_b$ for q_W at 450 and 600 kW/m^2 show a similar, parallel and linear trend. The highest heat flux q_W = 600 kW/m^2, demonstrates the highest dimensionless CHF value at all times before reaching the asymptotic dimensionless CHF value. However, for q_W = 300 kW/m^2 the trend for the dimensionless CHF enhancement demonstrates a parabolic curve before reaching the asymptotic value. For all these heat fluxes, the asymptotic CHF values were observed when the $q_w^* Ct_b$ value was higher than 30 kg s/m^2. Nevertheless, for the lowest heat flux

of q_W = 150 kW/m^2, a minimal increase in q_c^* was observed, even though the value for $q_w^* Ct_b$ reaches 29 kg s/m^3. In the present experiment, the maximum dimensionless CHF enhancement for all heat flux values occurred at a value of $q_w^* Ct_b \approx 29$ kg s/m^3 (except for weak boiling) and that value is close to the empirical correlation proposed by Okawa et al. [86].

6.3.2 Surface characteristics and the critical heat flux

The CHF enhancement, as discussed by several previous researchers [63,83,96] is mainly caused by the surface deposition of the nanoparticles. The modified surface structure changes the surface properties and affects several essential parameters for the bubbling activities in the boiling system. Several parameters which are believed to be of primary importance to the CHF enhancement were varied, i.e., the surface wettability, the surface porosity, and the capillarity. In the present study, the images of gradual modification of the surface morphology produced by boiling in nanofluids for a prescribed time are shown in Fig. 6.3. Here, all heated surfaces experienced a gradual change in the surface structure after the nanofluid injection into the base liquid at the respective heat flux. The deposition of nanoparticles started to take place at the vicinity of the nucleation sites, modifying the surface characteristics that affect several factors that favor the CHF enhancement.

The changes of corresponding gradual surface morphology of each surface condition after experiencing boiling with the respective heat flux and prescribed boiling times are shown in Fig. 6.3 (a) to (d). Here, the heated surfaces were gradually covered by the deposited nanoparticles during boiling for the prescribed boiling time. In most cases, the surface was fully covered with the deposited nanoparticles, especially for high heat flux. For example, faster changes in the surface characteristics could be clearly seen for the highest heat flux of q_W = 600 kW/m^2 where the nanoparticles covered the whole heated surface after 10 minutes of boiling time. For heat flux values of q_W = 450 kW/m^2 and 330 kW/m^2 , this effect occured after 20 and 40 minutes, respectively. At this particular state, the CHF reached the asymptotic value, consistent with the CHF enhancement discussed in the previous section.

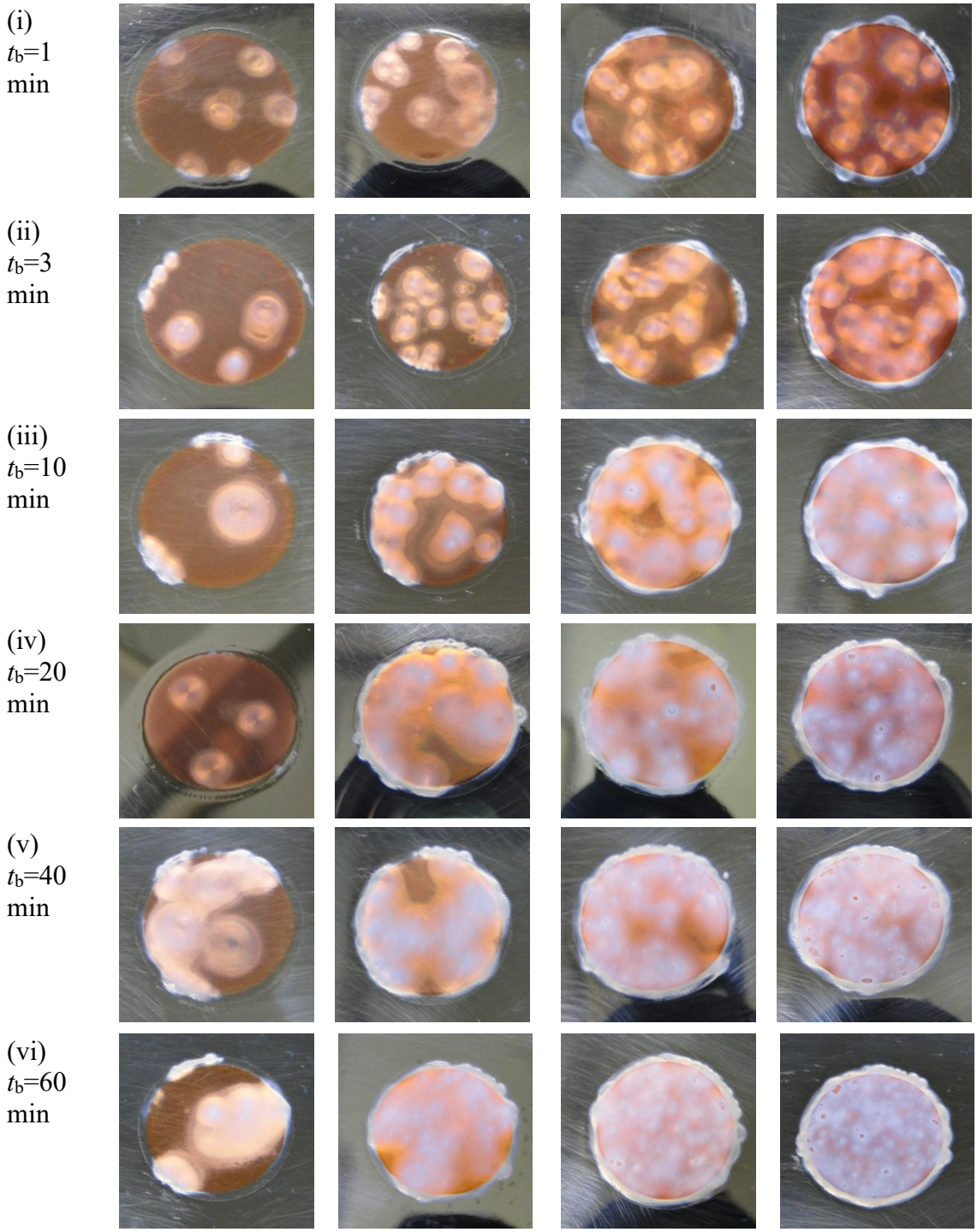

Figs. 6.3: Photographs of the heater surfaces with deposited nanoparticles after boiling in nanofluid between t_b = 1 to 60 min and C = 0.04 kg/m^3 with values of the heat flux; (a) 150 kW/m^2, (b) 300 kW/m^2, (c) 450 kW/m^2 and (d) 600 kW/m^2

However, for the lowest boiling intensity of qw = 150 kW/m^2, the heated surface was still not fully covered after 60 minutes of boiling, as shown in Figs. 6.3 (a) from (i) to (vi).

In the case of high heat flux, the nucleation site densities and the frequency of the release of bubbles were high which resulted in a faster deposition of the nanoparticles near the bubbles at the vicinity of the surface at a number of nucleation sites. As a result, the heated surface was rapidly fully covered with deposited nanoparticles so that it reached the asymptotic CHF value. For the lowest heat flux of q_W = 150 kW/m^2, minimal nucleation sites could be seen, as depicted in Figs. 6.3 ((a) – (i-iv)) and the surface was never covered fully. Apparently, the reason that the maximal CHF value was not reached at the lowest heat flux was due to the fact that heated surfaces underwent less modifications since on the bare heater surface, only minimal spots of nanoparticles were observed. This lack of change in the structure could be the causes for the early occurrence of the local CHF. However, it could be inferred that the CHF under low heat flux during nanofluid boiling did have a noticeable small enhancement while the maximum CHF enhancement was still not achieved in the present boiling time of 1 hour.

Surface wettability is one of the critical surface characteristics of the boiling system, especially in the case of CHF. In the present study, the surface wettability properties of the heater surface were measured after boiling in the nanofluid for a prescribed time. The results and conditions after boiling in nanofluids for 1 hour for several applied heat flux are shown in Fig. 6.4.

The data series for the surface wettability in the present experiment were plotted against the CHF, and compared to the experimental study by Wang and Dhir [97] and the theoretical study by Kandlikar [19]

$$q_{\mathrm{CHF}} = h_{\mathrm{fg}}\rho_{\mathrm{v}}^{0.5}\left(\frac{1+\cos\beta}{16}\right)\left[\frac{\pi}{2}+\frac{\pi}{4}\left(1+\cos\beta_r\right)\cos\phi\right]^{0.5}\left[\sigma g\left(\rho_{\mathrm{l}}-\rho_{\mathrm{v}}\right)\right]^{0.25}. \qquad (6.3)$$

The detailed explanation of Kandlikar's correlation was described in Section 2.1.2.

(a)

(b)

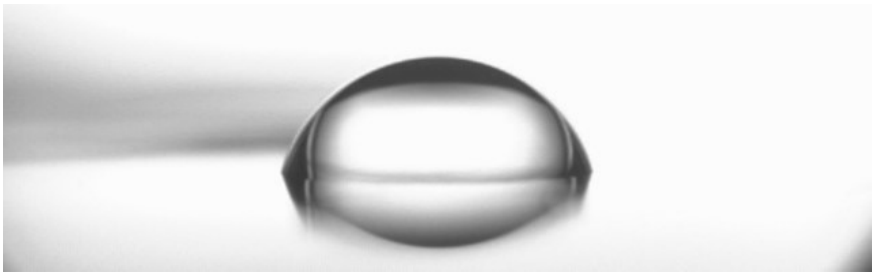

(c)

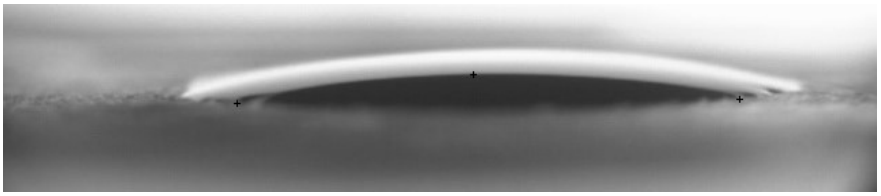

(d)

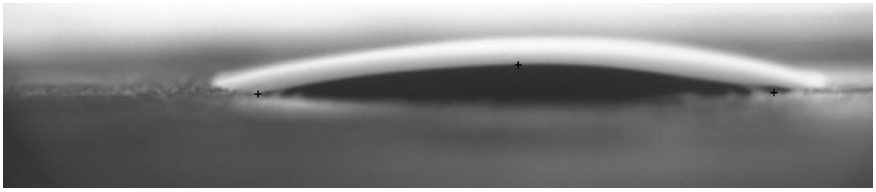

(e)

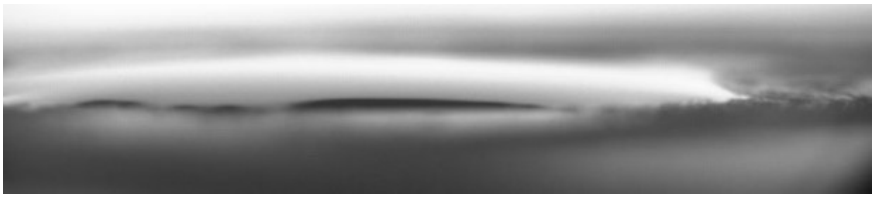

Figs. 6.4: Photographs of droplets on the heater surface after surface preparation (a), and after boiling in nanofluids $C = 0.04$ kg/m^3 for 60 minutes at $q_W = 150$ kW/m^2 (b), 300 kW/m^2 (c), 450 kW/m^2 (d) and 600 kW/m^2 (e)

The correlation equation formulated by Kandlikar incorporates the effect of the surface wettability on the CHF enhancement. It is widely used and has been shown reasonably successful in predicting the CHF enhancement with respect to the effect of the surface wettability from the range of hydrophobic surface conditions (high contact angle) to the fully wetted surface condition (small contact angle).

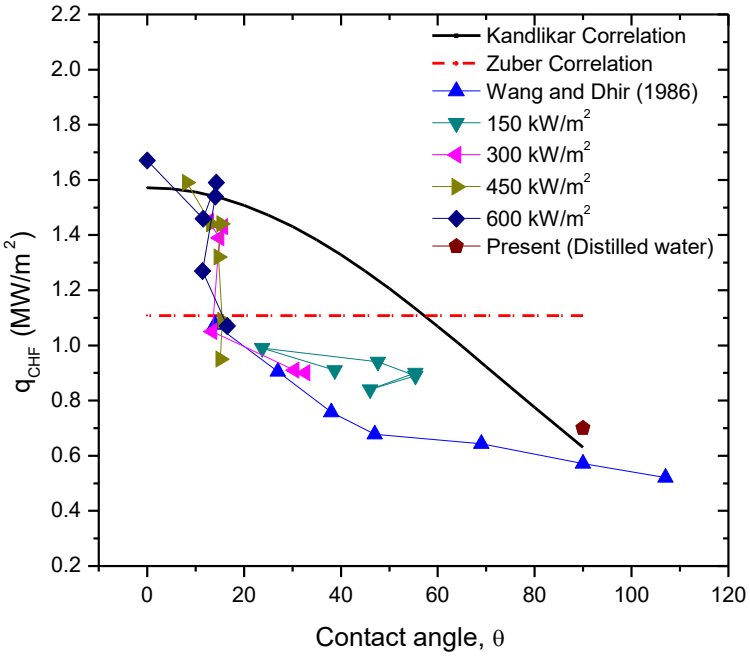

Fig. 6.5: Relation between the mean contact angle and the critical heat flux at q_W = 150, 300, 450 and 600 kW/m^2

Fig. 6.5 shows the experimental and theoretical relations for the enhancement of the CHF and the mean contact angle for the heated surface experiencing nanofluid boiling at q_W = 150, 300, 450 and 600 kW/m^2 for boiling durations. Here, the initial CHF value for the uncoated heated surface with θ = 90° was in good aggrement with Kandlikar's correlation and Wang and Dhir experimental data, but slightly lower than the Zuber correlation. In the present case, the CHFs increased as the surface wettability decreased. After boiling in the nanofluid for 1 minute, the value for the surface wettability changed for all applied heat flux values and the mean contact angle was immediately reduced to

below 20°, except for the weak heat flux of 150 kW/m^2, where the angle decreased to the value of between 55° to 22°. For low values of the heat flux, although the mean contact angle was reduced, the CHF enhancements were still minimal.

An interesting finding in the present results was the CHF enhancement at similar values of the surface wettability condition. For example, one can notice in Fig. 6.5 that the CHF enhancement for q_W = 300 kW/m^2, 450 kW/m^2 and 600 kW/m^2 showed a sequentially sharp increase at the mean contact angle of about 15°, and eventually reached the asymptotic CHF value. At the particular point where the mean contact angle was about 15°, the CHF increased sharply in the vertical direction, independent of the changes in the surface wettability. The asymptotic CHF value for the present experiment was comparable to that of the Kandlikar correlation for the lower average contact angle when $\theta < 15°$.

Here, it could be deduced that instead of the surface wettability, another factor of the surface structure (respectively the surface porosity) was probably modified. In addition, recent studies have also suggested that the porosity may be a dominant factor, in nexus the surface wettability properties for the CHF enhancement [81,98]. Hence, the increase of the CHF in the low wettability region is most probably due tof the buildup of a porous layer at the base of the vapor column that increases the capability of wetting. It is expected that the contact angle measured by Wang and Dhir [97,99] on the oxidation of copper also was related to porosity effects, compared to the nanofluid coated surface. The gradual build-up of the porous layer in nanofluid boiling was a continuous process which improved the ability of the surface structure to favor CHF enhancement. This gradual build-up of the porous layer could be observed qualitatively in Fig. 6.3, as discussed previously.

6.3.3 Time variation of the wall superheat for different heat flux values

The time variation of the wall superheat for all heat flux values during the prescribed boiling time is shown in Fig. 6.6 (a) to (b). The initial ΔT_W for distilled water was maintained at 20±2 °C. In the present work, upon the addition of the nanofluid, the ΔT_W was slightly reduced from the original ΔT_W of the distilled water, but at a later stage,

it increased monotonically to reach a fairly asymptotic steady state condition with a higher ΔT_W. This shows that the HTC slightly increased at first and later decreased. The present condition was similar to that described in Section 5.5.1 (Fig. 5.2) for the concentration of $C = 0.04$ kg/m^3 at $q_W = 600$ kW/m^2. In the present case, the final asymptotic ΔT_W increase compared to the case with distilled water for all the applied heat flux densities.

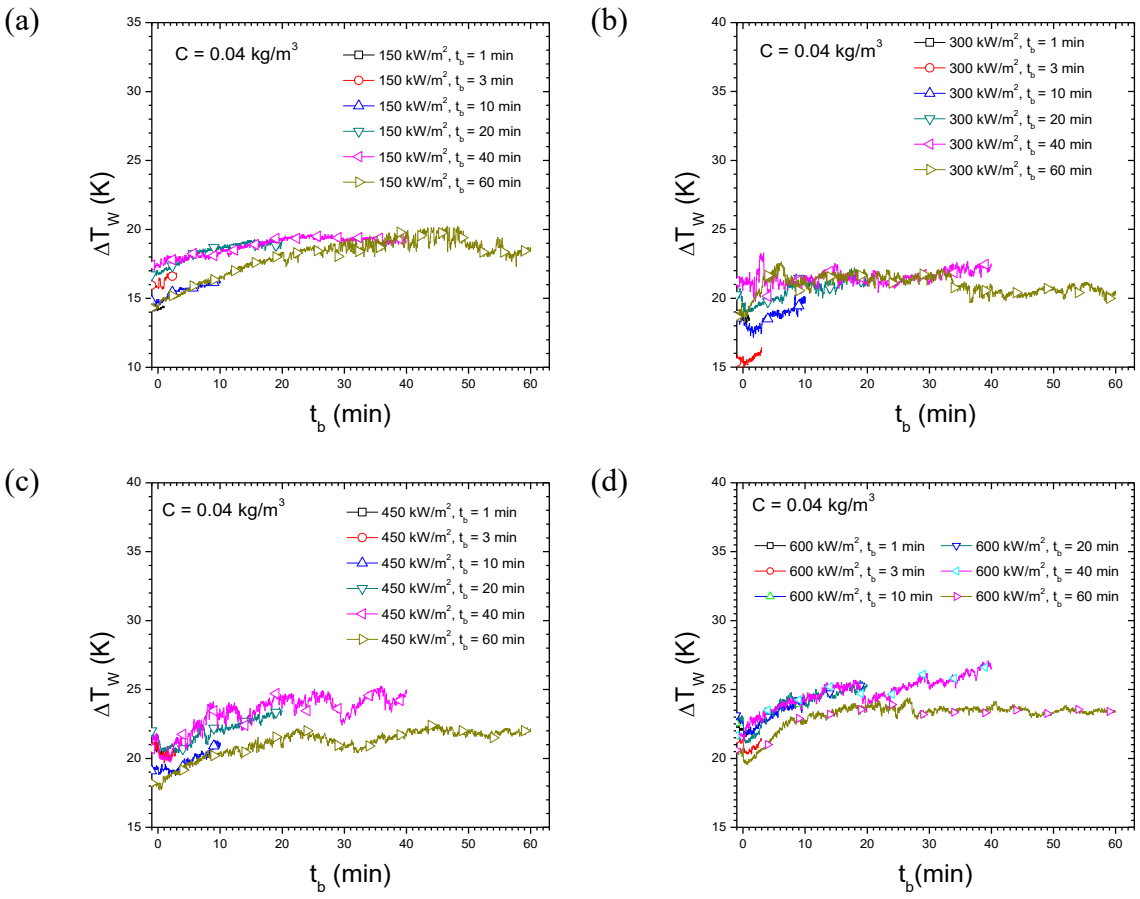

Fig. 6.6 Time variation of the wall superheat after the addition of nanofluid into the test vessel at (a) q_W = 150 kW/m^2, (b) q_W = 300 kW/m^2, (c) q_W = 450 kW/m^2 and (d) q_W = 600 kW/m^2

6.3.4 Boiling curves

Fig. 6.7 depicts the boiling curves (BCs) measured from the pre-coated heater for a prescribed heat flux and boiling time. The boiling curve measurements were performed with distilled water.

Here, the BC values for all heat flux values at a boiling time of t_b=1 min were close to the Stephen Abdelsalam (S-A) correlation, see Fig. 6.7 (a). After continued boiling until t_b=3 min, the BCs at the lower heat flux region were shifted towards the right indicating that the boiling heat transfer deteriorated for all heat flux values (see Fig. 6.7 (b)). Here, ΔT_w was increased, and the onset of nucleate boiling (ONB) was delayed. A similar condition for the lower heat flux BCs could be observed for all conditions (Figs. 6.7 (a)-(b)). After t_b=10 minutes, as shown in Fig. 6.7 (c), the CHF was gradually increased, especially for high heat flux with q_W = 600 kW/m^2. During this stage, the BC for the higher heat flux region became steeper and shifted towards the left, away from the S-A correlation, especially when the BC was at q_W > 800 kW/m^2. This indicates that the HTC was increased. Similar steeper BCs trends could be observed after 20 minutes for q_W = 300, 450 and 600 kW/m^2, as shown by Fig. 6.7 (d). However, after t_b = 40 min, the BCs at the high heat flux region for the heater surface which had been coated at q_W = 600 kW/m^2 were shifted towards the right, approaching the S-A correlation, as can be seen in Fig. 6.7 (e). At a later stage, when t_b = 60 min, the BC for the heated coated surface at q_W = 450 kW/m^2 was shifted to the right and approached the S-A correlation as shown in Fig. 6.7 (f). At this stage, the BC of the heated surface coated at q_W = 600 kW/m^2 was slightly shifted to the right of the S-A correlation. The shifted trend towards the right indicates that the heat transfers was decreased after further boiling in the nanofluid.

This could be interpreted in such a way that the surface modification has a significant influence on the heat transfer rate in distilled water and that the HTC depends on heat flux density and the boiling time in the nanofluids. Several possibilities could be associated with the reduction of the BHT in the region with the lower heat flux for boiling curve. The first possibility concerns the reduction of the number of nucleation sites which are affected by the reduction of the surface wettability. Prior to this study, a study by Wang and Dhir [97] has shown that the reduction of the heater surface wettability resulted

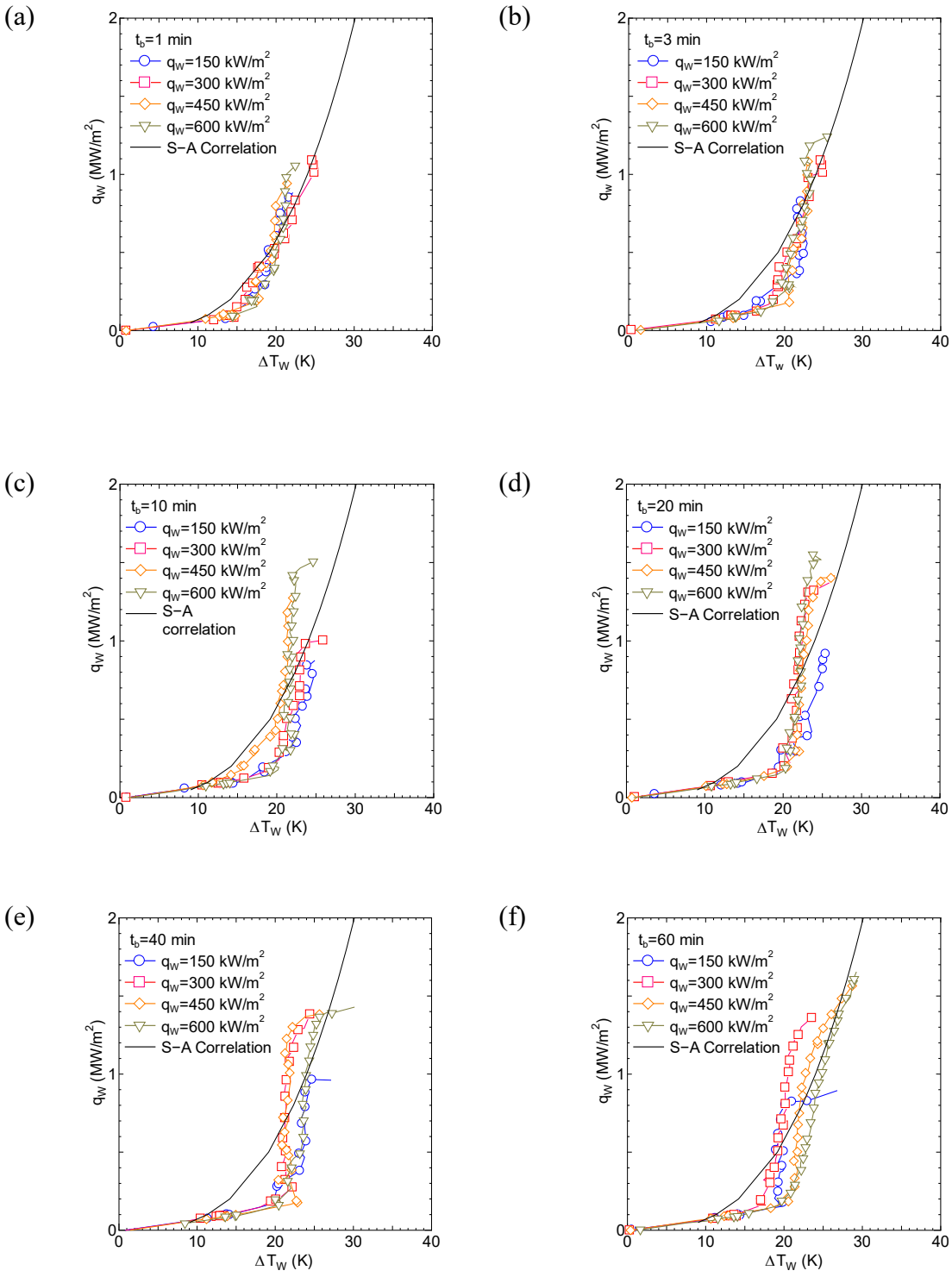

Fig. 6.7: Boiling curves measured with distilled water for the nano-coated surface

in a dramatic reduction in the number of cavities which allowed nucleation of bubbles and consequently deteriorated heat transfer. This is similar to the present experiment where the surface contact angle was also reduced. Related to this, the change in the size of the size of the cavities which act as nucleation site cavities for the bubbles could also be another possible reason. Micro-sized cavities have been shown to be the ideal size for bubble nucleation. However, since the material deposited from the nanofluid is of nanometer size, it could be deposited onto the heater surface and the newly changed cavity after the deposition becomes smoother compared to the original rougher surface condition and possibly deactivates the nucleation site. In fact, several researchers, Hegde et al. [100] and Stutz et al. [47] reported that the heated surface with deposited nanoparticles resulted in smaller than the original surface roughness values. In addition, the shifted trends at high heat flux for the BC of the heated surface coated at $q_W = 600$ kW/m^2 at longer boiling times was most probably caused by thermal insulation due to the deposited nanoparticles, as explained by Kwark et al. [52]. This is due to the fact that in the present case, the magnitude of the thermal conductivity of deposited TiO_2 nanoparticles was approximately ten times lower than copper heater surface.

Nevertheless, the reason for the increase of the heat transfer in the high heat flux region in the BC is still unknown. A number of new nucleation sites at high heat flux could possibly activate due to the increase in micro-cavities from the deposited nanoparticles, as suggested by the studies of Kim et al. [46]. Apparently, further studies are needed to clarify the reasons for HTC increases in this particular region.

6.4 Conclusions

In the present work, experimental investigations have been carried out to explore the effects of various values for the heat flux on the BHT and the CHF in TiO_2-water nanofluids for pool boiling. The essential conclusions from in the present experiments are as follows:

Nucleate boiling was the most crucial for the nanoparticle deposition on the heated surfaces. Higher heat flux leads to faster modification of the properties of the heater

surface properties such as surface wettability and porous structure which lead to a faster enhancement of the CHF.

For a particles concentration of C = 0.04 kg/m^3, the required time of nucleate boiling to achieve the maximum CHF enhancement was 10 minutes for heat flux of q_W = 600 kW/m^2, while 20 minutes were necessary for q_W = 300 and 450 kW/m^2. Weak boiling at q_W = 150 kW/m^2 does not lead to a the maximal CHF value, even after 60 minutes of boiling in nanofluids.

The CHF enhancements were independent of the mean surface wettability when the contact angles were at θ = 18 degrees. It is possible that another parameter responsible for the CHF enhancement is the porosity at the surface.

For the boiling curve, the HTC exhibits different trends for different heat fluxes: While at lower heat flux of the BC, all the HTC decreased, for higher heat flux in the BC, a stochastic trend manifested itself. During shorter to moderate boiling times in the nanofluid, the HTC increased at higher heat flux of the BC, but as the boiling time increased further, the HTC started to decrease.

CHAPTER 7 VISUALISATION OF NUCLEATE BOILING IN THE TiO_2 NANOFLUID

7.1 Introduction

As discussed in the previous Chapter 5 in section 5.5.1, the wall superheat dropped after the addition of the nanofluid in the present experiment in most cases. To preliminarily investigate the enhancement the heat transfer during boiling, a visualization of nucleate boiling was performed using another experimental apparatus.

7.2 Experimental description

To allow direct observation, a transparent and thin rectangular vessel was used (test vessel IV). The vessel was made of polycarbonate, and its inside cavity was 20 mm width, 230 mm length and 98 mm depth. An ITO film was deposited on the glass substrate was used as the heated surface as shown in Fig. 3.4 and Fig. 3.6 in Chapter 3, respectively. The size of the heated surface was 10 mm width and 170 mm length, and this region was heated ohmically using a DC power supply. The ITO film-deposited glass plate was used as the bottom face of the experimental vessel, and the vessel was fixed to the holder as shown schematically in Fig. 3.4. A small black tape was put at the center of the underside surface of the glass plate to measure the superheat of the glass plate ΔT_{BW} using an infrared thermometer.

Prior to the experimental work, the test section was cleaned to remove any contamination that could affect the experimental results. Then, 247.5 ml of distilled water was poured into the test vessel. The DC power was regulated to fix the wall heat flux at q_W = 230 kW/m^2. This rather low value for the heat flux value was selected to allow a clear observation of individual bubble nucleation. The values of q_W and ΔT_{BW} were recorded every second, and the bubble nucleation was visualized using a high-speed

camera after the steady state had been reached. After that, 2.5 ml of TiO_2 with a concentration of $C = 4$ kg/m^3 were added to the distilled water in the vessel; the resulting concentration was 0.04 kg/m^3. The boiling inside the vessel was further recorded with the high-speed camera to explore the effect of nanofluids on the bubble nucleation. The wall superheat ΔT_W of the transparent heater surface was calculated and described in Appendix A.

7.3 Experimental results and discussion

The time variation of T_{BW} is shown in Fig. 7.1. Though q_W was kept constant, ΔT_{BW} decreased from 11 K to 8 K asymptotically and reach a steady state after the addition of the nanofluid. It could be therefore be confirmed that the boiling heat transfer was enhanced immediately after the addition of the nanofluid as in the most cases in Fig. 7.1. The snapshots of the bubbles before and after the addition of nanofluid are shown in Figs. 7.2 (a) and (b). A comparison of these photos reveals that after the addition of nanofluid, the number of bubbles increased dramatically and the bubbles were distributed in a much wider region in the test vessel than before. From this observation, one can conclude that the formation of micro-cavities which had been caused by the nanoparticle deposition on the heated surface is one of the main mechanisms of the boiling heat transfer enhancement observed immediately after the addition of nanofluid.

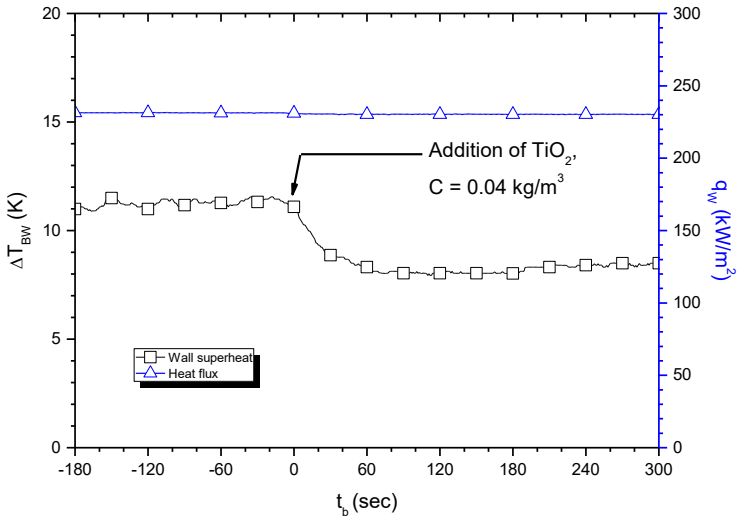

Fig. 7.1: Time variation of the wall superheat vs. boiling time

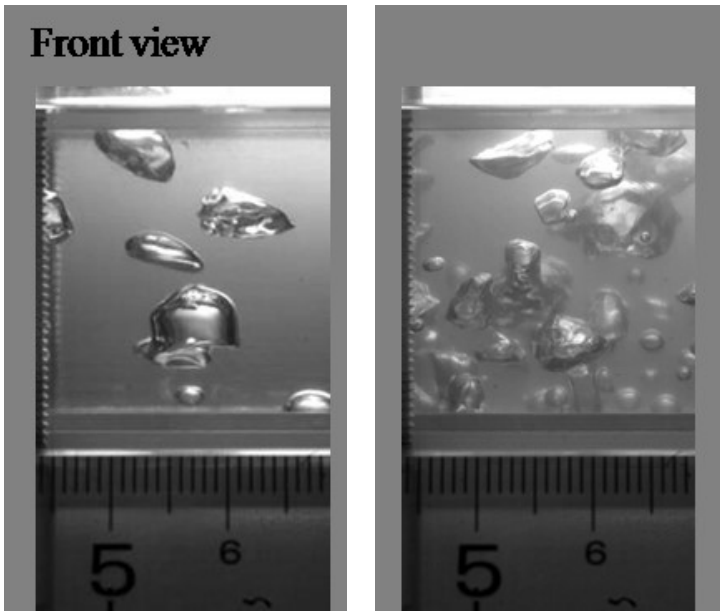

(a) $C = 0$ kg/m^3 (b) $C = 0.04$ kg/m^3

Fig. 7.2: Snapshots extracted from high-speed camera video for the bubbling of the distilled water in (a) and after addition of the nanofluid in (b).

7.4 Conclusion

In the present experiment, we concluded that the reduction of the ΔT_{BW} after the addition nanofluid addition was possibly due to the increase number of nucleation sites for the bubbling bubbles. Consequently, the latent heat transfer was increased to lowering wall superheat.

CHAPTER 8 CONCLUSION

8.1 Summary and conclusion

The effects of the nanofluid integration in nucleate pool boiling with various configurations have been studied and discussed in detail. Four experiments setups were designed and performed to investigate;

(a) the effect of the heater orientations on the critical heat flux (CHF),

(b) the effect of the nanoparticle-materials, concentrations and dispersion conditions;

(c) the effect of the heat flux density to the HTC and CHF.

(d) the visualizations of the nucleate boiling in nanofluid have also been performed.

It has been observed that the CHF increase significantly in nanofluid nucleate boiling compared to the distilled water. The heater orientation was also observed to affect the CHF. An improvement up to 200 percent in both upward-facing and downward-facing heaters' has been documented. Several other essential parameters related to the CHF enhancement rate, such as concentration and boiling time in nanofluids, was also investigated. The findings reveal that at higher concentration of TiO_2 nanofluid, the CHF enhances considerably and vice versa. Also, the CHF value for the downward-facing heater orientation is only half of that for the upward-ward facing heater. In addition, surface wettability measurements were also performed to explore the relation between surface properties and the CHF enhancement.

Moreover, the effects of nanoparticle materials, concentrations, and dispersion conditions on the HTC and CHF were also studied. The boiling heat transfer characteristics varied significantly depending on the nanoparticles material and concentration level. The higher TiO_2 and Al_2O_3 concentration, the higher was the heat transfer enhancement (except for the low concentration of TiO_2). Whereas, the SiO_2 showed deterioration in heat transfer for all concentrations in the time-variation of wall

superheat. However, no noticeable effect of dispersion condition was observed. Some peculiar boiling curves (BCs) were observed in TiO_2 and SiO_2 at the high heat flux compared to the simple BCs in Al_2O_3. The CHF enhancement was found to be in the range of 1.7 up to 2.1 MW/m^2 for all materials.

The effects of different heat flux density on the CHF enhancements was also investigated. The enhancement of the CHF depended significantly on the heat flux density; the heat flux at the higher densities shows considerably higher CHF enhancement rates compared to lower heat flux densities. However, the CHF enhancement value did not reach the asymptotic CHF value after boiling for 1 hour at the lowest heat flux in the present experimental investigation. Both the dimensionless CHF enhancement value with respect to the dimensionless heat flux for coated surface, concentration and boiling time was then correlated. The trend showed a linearity in the high heat flux especially for 450 and 600 kW/m^2. Nevertheless, for lower heat flux, non-linear trends were observed mainly at heat flux density of 300 kW/m^2 and more evident at 150 kW/m^2.

Heat transfer in nucleate boiling with nanofluids showed an enhancement in the CHF for both upward-facing and downward-facing conditions. However, the HTC performance was stochastic depending on materials and concentration of nanofluids, and nearly no noticeable dispersion condition effect was observed. The heat flux density affected the rate of CHF enhancements, where the high heat flux resulted in high enhancement rates, while nominal enhancements at the lowest heat flux.

In conclusion, experimental investigations on the boiling heat transfer in nanofluid pool boiling have been successfully performed. The findings are expected to contribute significantly towards high-density cooling, for example, in the passive cooling systems (PCS) during loss of coolant accidents (LOCAs) in nuclear power plants (NPPs). In the study, non-metallic nanofluid; metal oxide in water-based was used, and their performance was investigate and presented.

References

[1] S.U.S. Choi, Enhancing thermal conductivity of fluids with nanoparticles, Dev. Appl. Non-Newtonian Flows. FED-Vol. 2 (1995) 99–103.

[2] S.M. You, J.H. Kim, K.H. Kim, Effect of nanoparticles on critical heat flux of water in pool boiling heat transfer, Appl. Phys. Lett. 83 (2003) 3374.

[3] S.K. Das, N. Putra, W. Roetzel, Pool boiling characteristics of nano-fluids, Int. J. Heat Mass Transf. 46 (2003) 851–862.

[4] J. Buongiorno, L.W. Hu, G. Apostolakis, R. Hannink, T. Lucas, A. Chupin, A feasibility assessment of the use of nanofluids to enhance the in-vessel retention capability in light-water reactors, Nucl. Eng. Des. 239 (2009) 941–948.

[5] J.A. Beard, ESBWR Overview, 2006.

[6] S. Nukiyama, The maximum and minimum values of the heat Q transmitted from metal to boiling water under atmospheric pressure, J. Japan Soc. Mech. Engrs. 37 (1934) 367–374.

[7] A.E. Bergles, W.M. Rohsenow, The Determination of Forced-Convection Surface-Boiling Heat Transfer, J. Heat Transfer. 86 (1964) 365–372.

[8] W.M. Rohsenow, Heat transfer with boiling, Academic Press, 1966.

[9] S.S. Kutateladze, Boiling Heat Transfer, 1962.

[10] Y. Katto, S. Yokoya, Principle mechanism of boiling crisis in pool boiling, Int. J. Heat Mass Transf. 11 (1967) 993–1002.

[11] P.J. Berenson, Experiments on pool-boiling, Int. J. Heat Mass Transf. 5 (1962) 985–999.

[12] S.G. Kandlikar, A General Correlation for Saturated Two-Phase Flow Boiling Heat Transfer Inside Horizontal and Vertical Tubes, J. Heat Transfer. 112 (1990) 219.

[13] V.K. Dhir, S.P. Liaw, Framework for a Unified Model for Nucleate and Transition Pool Boiling, J. Heat Transfer. 111 (1989) 739–746.

[14] K. Stephan, M. Abdelsalam, Heat-transfer correlations for natural convection boiling, Int. J. Heat Mass Transf. 23 (1980) 73–87.

[15] I.L. Pioro, Experimental evaluation of constants for the Rohsenow pool boiling correlation, Int. J. Heat Mass Transf. 42 (1998) 2003–2013.

[16] N. Zuber, Hyrodynamic aspects of boiling heat transfer, University of California,

1959.

[17] C.L. Tien, Hydrodynamic model for nucleate pool boiling, Int. J. Heat Mass Transf. 5 (1962) 533–540.

[18] N. Zuber, Nucleate boiling. The region of isolated bubbles and the similarity with natural convection, Int. J. Heat Mass Transf. 6 (1963) 53–78.

[19] S.G. Kandlikar, A Theoretical Model to Predict Pool Boiling CHF Incorporating Effects of Contact Angle and Orientation, J. Heat Transfer. 123 (2001) 1071.

[20] J.M. Ramilison, P. Sadasivan, J.H. Lienhard, Surface factors influencing burnout on flat heaters, J. Heat Transfer. 114 (1992) 287–290.

[21] S. Lee, S.U.S. Choi, S. Li, J.A. Eastman, Measuring Thermal Conductivity of Fluids Containing Oxide Nanoparticles, J. Heat Transfer. 121 (1999) 280–289.

[22] P.E. Gharagozloo, J.K. Eaton, K.E. Goodson, Diffusion, aggregation, and the thermal conductivity of nanofluids, Appl. Phys. Lett. 93 (2008) 2006–2009.

[23] J. Lee, K. Sik, S. Pil, B. Ho, J. Ho, S.U.S. Choi, C. Jin, Effective viscosities and thermal conductivities of aqueous nanofluids containing low volume concentrations of Al 2 O 3 nanoparticles, Production. c (2008) 2651–2656.

[24] Y. Hwang, Y. Ahn, H. Shin, C. Lee, G. Kim, H. Park, J. Lee, Investigation on characteristics of thermal conductivity enhancement of nanofluids, Curr. Appl. Phys. 6 (2006) 1068–1071.

[25] MurshedS.M.S, K.C. Leon, C. Yang, Enhanced thermal conductivity of TiO2-water based nanofluids, Int. J. Therm. Sci. 44 (2005) 367–373.

[26] B. Tajik, A. Abbassi, M. Saffar-Avval, M.A. Najafabadi, Ultrasonic properties of suspensions of TiO2 and Al2O3 nanoparticles in water, Powder Technol. 217 (2012) 171–176.

[27] M. Emami-Meibodi, M. Vafaie-Sefti, A.M. Rashidi, A. Amrollahi, M. Tabasi, H. Sid-Kalal, A model for thermal conductivity of nanofluids, Mater. Chem. Phys. 123 (2010) 639–643.

[28] M. Hosseini, S. Ghader, A model for temperature and particle volume fraction effect on nanofluid viscosity, J. Mol. Liq. 153 (2010) 139–145.

[29] J. Avsec, M. Oblak, The Calculation of Viscosity and Thermal Conductivity for Nanofluids on the Basis of Statistical Nanomechanics, in: AIAA Thermophys. Conf., 2005: pp. 1–8.

[30] J. Garg, B. Poudel, M. Chiesa, J.B. Gordon, J.J. Ma, J.B. Wang, Z.F. Ren, Y.T. Kang, H. Ohtani, J. Nanda, G.H. McKinley, G. Chen, Enhanced thermal conductivity and viscosity of copper nanoparticles in ethylene glycol nanofluid, J. Appl. Phys. 103 (2008) 1–6.

[31] X.Q. Wang, A.S. Mujumdar, A review on nanofluids - Part II: Experiments and applications, Brazilian J. Chem. Eng. 25 (2008) 631–648.

[32] W. Yu, D.M. France, J.L. Routbort, S.U.S. Choi, Review and Comparison of Nanofluid Thermal Conductivity and Heat Transfer Enhancements, Heat Transf. Eng. 29 (2008) 432–460.

[33] I.M. Mahbubul, R. Saidur, M. a. Amalina, Latest developments on the viscosity of nanofluids, Int. J. Heat Mass Transf. 55 (2012) 874–885.

[34] Y. Hwang, J.-K.J.-K. Lee, Y.-M. Jeong, S. Cheong, Y.-C. Ahn, S.H. Kim, Production and dispersion stability of nanoparticles in nanofluids, Powder Technol. 186 (2008) 145–153.

[35] J. Veilleux, S. Coulombe, A dispersion model of enhanced mass diffusion in nanofluids, Chem. Eng. Sci. 66 (2011) 2377–2384.

[36] G.D. Parfitt, H.A.B. Unilever, The dispersion of fine particles in liquid media, Mix. Process Ind. (1997) 99–117.

[37] A. Nasiri, M. Shariaty-Niasar, A. Rashidi, A. Amrollahi, R. Khodafarin, Effect of dispersion method on thermal conductivity and stability of nanofluid, Exp. Therm. Fluid Sci. 35 (2011) 717–723.

[38] V. Penkavova, J. Tihon, O. Wein, Stability and rheology of dilute TiO2-water nanofluids., Nanoscale Res. Lett. 6 (2011) 273.

[39] Z. Haddad, C. Abid, H.F. Oztop, A. Mataoui, A review on how the researchers prepare their nanofluids, Int. J. Therm. Sci. 76 (2014) 168–189.

[40] J.M. Andersson, Controlling the Formation and Stability of Alumina Phases, 2005.

[41] P. Vassallo, R. Kumar, S.D. Amico, Pool boiling heat transfer experiments in silica – water nano-fluids, Int. J. Heat Mass Transf. 47 (2004) 407–411.

[42] I.C. Bang, S. Heung Chang, S.H. Chang, Boiling heat transfer performance and phenomena of Al2O3-water nano-fluids from a plain surface in a pool, Int. J. Heat Mass Transf. 48 (2005) 2407–2419.

[43] K. Park, D. Jung, Enhancement of nucleate boiling heat transfer using carbon

nanotubes, Int. J. Heat Mass Transf. 50 (2007) 4499–4502.

[44] S. Soltani, S.G. Etemad, J. Thibault, Pool boiling heat transfer of non-Newtonian nanofluids, Int. Commun. Heat Mass Transf. 37 (2010) 29–33.

[45] C.-K. Huang, C.-W. Lee, C.-K. Wang, Boiling enhancement by TiO2 nanoparticle deposition, Int. J. Heat Mass Transf. 54 (2011) 4895–4903.

[46] S.J. Kim, I.C. Bang, J. Buongiorno, L.W. Hu, Study of pool boiling and critical heat flux enhancement in nanofluids, Bull. Polish Acad. Sci. 55 (2007) 211–216.

[47] B. Stutz, C.H.S. Morceli, M.D.F. da Silva, S. Cioulachtjian, J. Bonjour, Influence of Nanoparticle Surface Coating on Pool Boiling, Exp. Therm. Fluid Sci. 35 (2011) 1239–1249.

[48] H.D. Kim, M.H. Kim, Effect of nanoparticle deposition on capillary wicking that influences the critical heat flux in nanofluids, Appl. Phys. Lett. 91 (2007) 14104.

[49] D. Wen, Y. Ding, Experimental investigation into the pool boiling heat transfer of aqueous based ??-alumina nanofluids, J. Nanoparticle Res. 7 (2005) 265–274.

[50] R.N. Hegde, R.P. Reddy, S.S. Rao, Behavioral Study of Alumina Nanoparticles in Pool Boiling Heat Transfer on a Vertical Surface, Heat Transf. Res. 40 (2011) 495–512.

[51] H.S. Ahn, J. Kim, M.H. Kim, Investigation of Pool Boiling Critical Heat Flux Enhancement on a Modified Surface Through the Dynamic Wetting of Water Droplets, J. Heat Transfer. 134 (2012) 71504.

[52] S.M. Kwark, R. Kumar, G. Moreno, S.M. You, Transient Characteristics of Pool Boiling Heat Transfer in Nanofluids, J. Heat Transfer. 134 (2012) 51015.

[53] X.-F.F. Yang, Z.-H.H. Liu, Pool boiling heat transfer of functionalized nanofluid under sub-atmospheric pressures, Int. J. Therm. Sci. 50 (2011) 2402–2412.

[54] R. Kathiravan, R. Kumar, A. Gupta, R. Chandra, Preparation and pool boiling characteristics of copper nanofluids over a flat plate heater, Int. J. Heat Mass Transf. 53 (2010) 1673–1681.

[55] S.K. Das, Pool boiling of nano-fluids on horizontal narrow tubes, Int. J. Multiph. Flow. 29 (2003) 1237–1247.

[56] E. Forrest, E. Williamson, J. Buongiorno, L.-W. Hu, M. Rubner, R. Cohen, Augmentation of nucleate boiling heat transfer and critical heat flux using nanoparticle thin-film coatings, Int. J. Heat Mass Transf. 53 (2010) 58–67.

[57] V. Trisaksri, S. Wongwises, Nucleate pool boiling heat transfer of TiO2–R141b nanofluids, Int. J. Heat Mass Transf. 52 (2009) 1582–1588.

[58] A. Suriyawong, S. Wongwises, Nucleate pool boiling heat transfer characteristics of TiO2–water nanofluids at very low concentrations, Exp. Therm. Fluid Sci. 34 (2010) 992–999.

[59] D.M. Vazquez, R. Kumar, Surface effects of ribbon heaters on critical heat flux in nanofluid pool boiling, Int. Commun. Heat Mass Transf. 41 (2013) 1–9.

[60] H.S. Ahn, M.H. Kim, The boiling phenomenon of alumina nanofluid near critical heat flux, Int. J. Heat Mass Transf. 62 (2013) 718–728.

[61] M. Kole, T.K.K. Dey, Investigations on the pool boiling heat transfer and critical heat flux of ZnO-ethylene glycol nanofluids, Appl. Therm. Eng. 37 (2011) 1–8.

[62] A. Mourgues, V. Hourtané, T. Muller, M. Caron-Charles, Boiling behaviors and critical heat flux on a horizontal and vertical plate in saturated pool boiling with and without ZnO nanofluid, Int. J. Heat Mass Transf. 57 (2013) 595–607.

[63] S.J.J. Kim, I.C.C. Bang, J. Buongiorno, L.W.W. Hu, Surface wettability change during pool boiling of nanofluids and its effect on critical heat flux, Int. J. Heat Mass Transf. 50 (2007) 4105–4116.

[64] M.-C. Lu, R. Chen, V. Srinivasan, V.P. Carey, A. Majumdar, Critical heat flux of pool boiling on Si nanowire array-coated surfaces, Int. J. Heat Mass Transf. 54 (2011) 5359–5367.

[65] J.H. Lee, T. Lee, Y.H. Jeong, Experimental study on the pool boiling CHF enhancement using magnetite-water nanofluids, Int. J. Heat Mass Transf. 55 (2012) 2656–2663.

[66] H. Kim, M. Kim, Experimental study of the characteristics and mechanism of pool boiling CHF enhancement using nanofluids, Heat Mass Transf. 45 (2007) 991–998.

[67] J. Jackson, Investigation into the pool-boiling characteristics of gold nanofluids, University of Missouri-Columbia, 2007.

[68] B. Truong, L. Hu, J. Buongiorno, T. McKrell, Modification of sandblasted plate heaters using nanofluids to enhance pool boiling critical heat flux, Int. J. Heat Mass Transf. 53 (2010) 85–94.

[69] P. Vassallo, Pool boiling heat transfer experiments in silica–water nano-fluids, Int. J. Heat Mass Transf. 47 (2004) 407–411.

[70] H. Kim, J. Kim, M. Kim, Experimental studies on CHF characteristics of nano-fluids at pool boiling, Int. J. Multiph. Flow. 33 (2007) 691–706.

[71] H. Kim, J. Kim, M. Kim, Effect of nanoparticles on CHF enhancement in pool boiling of nano-fluids, Int. J. Heat Mass Transf. 49 (2006) 5070–5074.

[72] R. Hegde, S.S. Rao, R.P. Reddy, Critical Heat Flux Enhancement in Pool Boiling Using Alumina Nanofluids, Heat Transf. Res. 39 (2010) 323–331.

[73] S.M. Kwark, R. Kumar, G. Moreno, J. Yoo, S.M. You, M. Amaya, R. Kumar, G. Moreno, S.M. You, J. Yoo, Pool boiling characteristics of low concentration nanofluids, Int. J. Heat Mass Transf. 53 (2010) 5199–5208.

[74] Y. Jeong, W. Chang, S. Chang, Wettability of heated surfaces under pool boiling using surfactant solutions and nano-fluids, Int. J. Heat Mass Transf. 51 (2008) 3025–3031.

[75] H. Peng, G. Ding, H. Hu, Effect of surfactant additives on nucleate pool boiling heat transfer of refrigerant-based nanofluid, Exp. Therm. Fluid Sci. 35 (2011) 960–970.

[76] A.H. Howard, I. Mudawar, Orientation effects on pool boiling critical heat flux (CHF) and modeling of CHF for near-vertical surfaces, Int. J. Heat Mass Transf. 42 (1999) 1665–1688.

[77] P. Vassallo, R. Kumar, S.D. Amico, Pool boiling heat transfer experiments in silica-water nano-fluids, Int. J. Heat Mass Transf. 47 (2004) 407–411.

[78] H. Seon, C. Lee, J. Kim, M. Hwan, H.S. Ahn, M.H. Kim, The effect of capillary wicking action of micro/nano structures on pool boiling critical heat flux, Int. J. Heat Mass Transf. 55 (2012) 89–92.

[79] G. Harish, V. Emlin, V. Sajith, Effect of surface particle interactions during pool boiling of nanofluids, Int. J. Therm. Sci. 50 (2011) 2318–2327.

[80] H.T. Phan, N. Caney, P. Marty, S. Colasson, J. Gavillet, Surface wettability control by nanocoating: The effects on pool boiling heat transfer and nucleation mechanism, Int. J. Heat Mass Transf. 52 (2009) 5459–5471.

[81] H. O'Hanley, C. Coyle, J. Buongiorno, T. McKrell, L.-W. Hu, M. Rubner, R. Cohen, Separate effects of surface roughness, wettability, and porosity on the boiling critical heat flux, Appl. Phys. Lett. 103 (2013) 24102.

[82] H. Seon, C. Lee, H. Kim, H. Jo, S. Kang, J. Kim, J. Shin, M. Hwan, Pool boiling

CHF enhancement by micro / nanoscale modification of zircaloy-4 surface, Nucl. Eng. Des. 240 (2010) 3350–3360.

[83] D. Wen, M. Corr, X. Hu, G. Lin, Boiling heat transfer of nanofluids: The effect of heating surface modification, Int. J. Therm. Sci. 50 (2011) 480–485.

[84] D. Wen, Influence of nanoparticles on boiling heat transfer, Appl. Therm. Eng. 41 (2011) 1–8.

[85] S. Vafaei, Nanofluid pool boiling heat transfer phenomenon, Powder Technol. 277 (2015) 181–192.

[86] T. Okawa, M. Takamura, T. Kamiya, Boiling time effect on CHF enhancement in pool boiling of nanofluids, Int. J. Heat Mass Transf. 55 (2012) 2719–2725.

[87] J. Barber, D. Brutin, L. Tadrist, A review on boiling heat transfer enhancement with nanofluids., Nanoscale Res. Lett. 6 (2011) 280.

[88] R. Kamatchi, S. Venkatachalapathy, Parametric study of pool boiling heat transfer with nanofluids for the enhancement of critical heat flux: A review, Int. J. Therm. Sci. 87 (2015) 228–240.

[89] T.G. Theofanous, S. Syri, T. Saimassi, O. Kym, H. Tuomisto, Nuclear and Design Critical heat flux through curved, downward facing, thick walls, Nucl. Eng. Des. 151 (1994) 247–258.

[90] T.G. Theofanous, On the proper formulation of safety goals and assessment of safety margins for rare and high-consequence hazards, Reliab. Eng. Syst. Saf. 54 (1996) 243–257.

[91] T.G. Theofanous, C. Liu, S. A, S. Angelini, Nuclear Engineering and Design In-vessel coolability and retention o f a core melt, Nucl. Eng. Des. 169 (1997) 1–48.

[92] A. Suriyawong, A.S. Dalkilic, S. Wongwises, Nucleate Pool Boiling Heat Transfer Correlation for TiO2-Water nanofluids, J. ASTM Int. 9 (2012).

[93] R.F. Gaertner, Photographic Study of Nucleate Pool Boiling on a Horizontal Surface, J. Heat Transfer. 87 (1965) 17–27.

[94] S.M. Kwark, R. Kumar, G. Moreno, J. Yoo, S.M. You, Pool boiling characteristics of low concentration nanofluids, Int. J. Heat Mass Transf. 53 (2010) 972–981.

[95] D. Cooke, S.G. Kandlikar, Pool Boiling Heat Transfer and Bubble Dynamics Over Plain and Enhanced Microchannels, J. Heat Transfer. 133 (2011) 52902.

[96] S.M. Kwark, G. Moreno, R. Kumar, H. Moon, S.M. You, M. Amaya, J. Yoo,

Nanocoating characterization in pool boiling heat transfer of pure water, Int. J. Heat Mass Transf. 53 (2010) 4579–4587.

[97] C.H. Wang, V.K. Dhir, Effect of Surface Wettability on Active Nucleation Site Density During Pool Boiling of Water on a Vertical Surface, J. Heat Transfer. 115 (1993) 659–669.

[98] S.G. Liter, M. Kaviany, Pool-boiling CHF enhancement by modulated porous-layer coating: theory and experiment, Int. J. Heat Mass Transf. 44 (2001) 4287–4311.

[99] C.H. Wang, V.K. Dhir, On the Gas Entrapment and Nucleation Site Density During Pool Boiling of Saturated Water, J. Heat Transfer. 115 (1993) 670.

[100] R.N. Hegde, S.S. Rao, R.P. Reddy, Experimental studies on CHF enhancement in pool boiling with CuO-water nanofluid, Heat Mass Transf. 48 (2012) 1031–1041.

Appendix A

Estimation of wall superheat temperature on glass heater surface.

A.1 Theory

Correlation for lower surface of the hot flat plate in natural convection of air is given by [1]

$$Nu = 0.27Ra^{0.25} \tag{A.1}$$

where

$$Ra = \frac{\rho\beta g\left(T_s - T_\infty\right)\left(L_c\right)^3}{\mu\alpha} \tag{A.2}$$

and

$$L_c = \frac{A_p}{P} \tag{A.3}$$

$$T_f = \frac{T_s + T_\infty}{2} \tag{A.4}$$

Rearrange equations (A.1) and (A.2) to obtain

$$Nu = 0.27\left[\frac{\rho\beta g\left(T_s - T_\infty\right)\left(L_c\right)^3}{\mu a_f}\right]^{0.25} \quad . \tag{A.5}$$

Note that the relation between T_W and surrounding fluid is given by

$$Nu = \frac{hL_c}{k_f}, \tag{A.6}$$

and the heat transfer coefficient h expressed in final form

$$h = \frac{Nuk_f}{L_c} = 0.27 \frac{\left(\frac{\rho\beta g \left(T_s - T_\infty\right)\left(L_c\right)^3}{\mu a_f} \right)^{0.25} \times k_f}{L_c}, \tag{A.7}$$

where T_s is equal to $T_{BW.}$

Given the relation between conduction and convection is

$$\frac{T_W - T_{BW}}{\delta} \times \lambda_{glass} = h\left(T_{BW} - T_\infty\right). \tag{A.8}$$

Rearranging Eq. (A.8) to obtain T_W as

$$T_W = \frac{h\left(T_{BW} - T_\infty\right) \times \delta}{\lambda_{glass}} + T_{BW}. \tag{A.9}$$

A.2 Parameters

Table A1: Parameters

ρ	1.034 kg/m^3	Density
T_s	111 °C	Surface temperature
T_f	68.15 °C	Film temperature
T_∞	25 °C	Fluid temperature
β	0.00293 1/K	Volume expansion coefficient
μ	2.044 x 10^{-5} kg/m.s	Viscosity
a_f	2.75 x 10^{-5} m^2/s^2	Thermal diffusivity
k_f	2.7526 x 10^{-5} W/m.K	Thermal conductivity
L_c	0.00472 m	Characteristic length
A_p	1.7 x 10^{-3} m^2	Area
P	0.36 m	Perimeter

λ_{glass}	1.4 W/m.K	Glass thermal conductivity
δ	0.005 m	Glass heater thickness
T_{BW}	111 °C	Bottom wall superheat

A.3 Calculations

The characteristic length is calculated using Eq. (A.3)

$$L_c = \frac{A_p}{P} = \frac{0.17 * 0.01}{(2 \times 0.17 + 2 \times 0.01)} = 0.00472 \text{ m.}$$

Then the heat transfer characteristic h is obtained using Eq. (A.7)

$$h = 0.27 \frac{\left(\frac{1.034 \times 2.93 \times 10^{-3} \times (9.81)(111-25)(0.00472)^3}{20.44 \times 10^{-6} \times 27.5 \times 10^{-6}} \right)^{0.25} \times 0.02868}{0.00472}$$

$$= 7.672 \text{ W/m}^2\text{.K.}$$

Finally, wall superheat of the heater surface T_W is calculated by Eq. (A.9)

$$T_W = \frac{7.672 \text{ W/m}^2\text{.°K} \times (111 - 25 \text{ °C}) \times 0.005 \text{ m}}{1.4 \text{ W/m.°K}} + 111 \text{ °C}$$

$$T_W = 113.4 \text{ °C}$$

Thus, the difference between T_W and T_{BW} is 2.4 K.

A.4 Nomenclature

ρ	Density [kg/m^3]
T_s	Surface temperature [°C]
T_f	Film temperature [°C]

T_∞	Fluid temperature [°C]
β	Volume expansion coefficient [1/K]
μ	Viscosity [kg/m.s]
α_f	Thermal diffusivity [m^2/s^2]
k_f	Thermal conductivity [W/m.K]
L_c	Characteristic length [m]
A_p	Area [m^2]
P	Perimeter [m]
λ_{glass}	Glass thermal conductivity [W/m.K]
δ	Glass heater thickness [m]
T_{BW}	Bottom wall superheat temperature of the glass heater [°C]
T_W	Wall superheat temperature of the glass heater [°C]

A.5 References

[1] Cengel, Y. A. (1998). *Heat transfer: A practical approach*. Boston, Mass: WBC McGraw-Hill.

PUBLICATIONS

Journals :

1) **Muhamad Zuhairi Sulaiman**, Masahiro Takamura , Kazuki Nakahashi, Tomio Okawa, "Boiling heat transfer and critical heat flux enhancement of upward- and downward-facing heater in nanofluids", *Journal of Engineering Gas Turbines and Power*, Vol. 135(7)-072901 (2013) ASME. (The contents of Chapter 4)

2) **Muhamad Zuhairi Sulaiman**, Daisuke Matsuo, Koji Enoki, Tomio Okawa, "Systematic measurements of heat transfer characteristics in saturated pool boiling of water-based nanofluids", *International Journal of Heat and Mass Transfer*, Vol. 102 264-276 (2016). (The contents of Chapter 5 and Chapter 7)

International Conferences:

1) **Muhamad Zuhairi Sulaiman**, Masahiro Takamura , Kazuki Nakahashi, Tomio Okawa, "Boiling heat transfer and critical heat flux enhancement of upward- and downward-facing heater in nanofluids", *International Conference on Nuclear Engineering (ICONE20-POWER2012)*, July 30 - August 3, 2012, Anaheim, California, USA.

2) Tomio Okawa, **Muhamad Zuhairi Bin Sulaiman**, Daisuke Matsuo, "Experimental study on the critical heat flux and heat transfer coefficient in nanofluid pool boiling", *10th International Topical Meeting on Nuclear Thermal Hydraulics, Operation and Safety (NUTHOS10)*, 14 – 18.

Local Conferences:

1) **Muhamad Zuhairi Sulaiman,** Tomio Okawa, "Heat flux effects on nanofluid boiling surface to the CHF enhancement", *The 18th National Symposium on Power and Energy Systems (SPES2013)*, 20-21 June 2013, Chiba, Japan.

2) Daisuke Matsuo, **Muhamad Zuhairi Sulaiman**, Tomio Okawa, "Effects of particle dispersion on boiling heat transfer in nanofluids", *The 63rd Japan National Congress for Theoretical and Applied*, 26 - 28 Sept 2014.